ROYAL ASTRONOMICAL SOCIETY

Volume 120 No. 6 1960

Published and Sold by the

ROYAL ASTRONOMICAL SOCIETY
BURLINGTON HOUSE
LONDON, W.1

Price £1 4s. 0d.; *in U.S.A.* $3.50

Subscription for volume: £6; *in U.S.A.* $18

The Geophysical Journal

OF THE

ROYAL ASTRONOMICAL SOCIETY

Editors

A. H. Cook
M.A., Ph.D., F.R.A.S., F.G.S.
National Physical Laboratory
Teddington

T. F. Gaskell
M.A., Ph.D., F.R.A.S.
British Petroleum Company
London

Price £1 per number; in U.S.A. $3. Annual Subscription £3; in U.S.A. $9

Volume 3 No. 2 June 1960

CONTENTS

P. J. Winter and H. D. Valliant, Relative gravity determinations in the Prairie provinces with Dominion Observatory bronze pendulum apparatus.

F. F. Evison, On the growth of continents by plastic flow under gravity.

D. E. Weston, The low-frequency scaling laws and source levels for underground explosions and other disturbances.

C. W. F. Everitt, Rock magnetism and the origin of the Midland Basalts.

C. Bull and E. Irving, The palaeomagnetism of some hyperbyssal intrusive rocks from South Victoria Land, Antarctica.

A. L. Hales and D. I. Gough, Isostatic anomalies and crustal structure in the Southern Cape.

E. C. Bullard, The automatic reduction of geophysical data.

J. Proudman, The condition that a long-period tide shall follow the equilibrium-law.

B. Gutenberg, PKIKP and pseudo-PKIKP phases at distances of less than 140°.

K. E. Bullen, A new method of deriving seismic velocity distributions from travel-time data.

Research Note

R. J. Donato, Seismic model experiments on the shape and amplitude of the refracted wave.

Notes on Progress in Geophysics

G. Jobert, Current research in geophysics in France.

Report of Meeting

Geophysical Discussion of the Royal Astronomical Society, 1960 January 22.

Orders should be addressed to:

The Assistant Secretary

Royal Astronomical Society, Burlington House, London, W.1

MONTHLY NOTICES
OF THE
ROYAL ASTRONOMICAL SOCIETY
Vol. 120 No. 6

THE USE OF A PENTAG WITH A TRANSIT-CIRCLE

R. d'E. Atkinson

(Communicated by the Astronomer Royal)

(Received 1959 December 2)

Summary

Preliminary work with a four-inch quartz pentag, mounted on the seven-inch Cooke T.C. to assess its usefulness for flexure determinations, showed that if the mounting is kept completely free of the telescope tube (as seems desirable), small orientation-errors are difficult to avoid. The second-order effects in declination which may be introduced by these errors, and by their interactions with any (permanent) error in the pentag-angle itself, are therefore all investigated; account is taken of the curvature of the diurnal circles, and of the need to observe off-axis in the telescope. It is found that of the three small angles which specify the pentag's mal-alignment, one has strictly zero effect. The second can readily be determined, at all pointings, by auto-collimation observations, and, with the Herstmonceux mounting, has been found to be so stable that these observations are not burdensome. If this angle is known, as a function of the pointing, the third one can be determined for each star by rough observations in R.A. The complete corrections for mal-alignment, to be added to the observational equation already published, are given explicitly.

It was shown in a previous paper (1) that there are serious deficiencies in all the methods so far used, or tried, for determining the flexure of a transit-circle; a new method was then proposed which involved the use of a "pentag". This is the name for a device consisting essentially of two plane mirrors, very rigidly connected so as to enclose an angle P say, which remains constant with high accuracy. It is easily verified that if a ray of light is incident on one mirror of the pair, in the plane containing both their normals, and is then reflected in the second, it is deviated through precisely $2P$ whatever the angle of incidence; this property has many important applications. Most commonly, P is designed to be 45°, so as to give a 90° deviation. If such a pentag is mounted in front of a transit-circle objective, with the plane of its normals vertical, stars observed in it will have declinations differing by 90° from those for which the circle is set; if the same star is observed (presumably on different nights) with and without the pentag, differencing the two observations leads to an equation of condition for the harmonic coefficients of the flexure as a function of zenith distance. This equation was given explicitly, as far as the pair of third harmonics.

After the 7-inch Cooke T.C. had been moved from Greenwich and brought into operation at Herstmonceux, a fused quartz pentag of four inches clear aperture was obtained and mounted on it for a trial period. The mounting, mainly of aluminium alloy angle-rods and plates, was carried entirely by thermoplastic shoes riding in the machined grooves, on the E–W axis, in which the lifting and reversing gear also engages when required; it had no direct contact with the telescope tube at all. It was counterpoised about the

E–W axis, so that it could be swung out of the beam and back again, and the pentag itself could rotate independently about a parallel axis (at A, in Fig. 1), this motion also being counterpoised. The complete dissociation from the telescope tube seemed necessary, because the "flexure" to be investigated is really differential flexure; if the tube, even though it did not carry the pentag's full weight, were used to constrain its orientation in any way, the reaction might perhaps double, or neutralize, the differential flexure even though the force involved was relatively small.

It is, however, somewhat difficult to preserve this independence and yet to guarantee that the plane of the pentag's normals is not displaced from the meridian, either by becoming inclined to the telescope-axis or by being rotated about it. If either of these faults occurs, second-order errors may be introduced; the square of sin 1′·72 (i.e. of sin 1/2000 radian) is sin 0″·05, and since 0″·05 would be somewhat objectionable as a random declination-error, and intolerable as a systematic one, either the mounting must orientate the pentag to appreciably better than one part in 2000 in all respects, or else the second-order terms must all be investigated and the orientation-errors determined experimentally, where this is shown to be necessary. The mounting actually made at Herstmonceux can keep one of the errors down to a few tenths of a minute, but not the others.

The present paper is therefore concerned with all the second-order errors which might, *a priori*, be involved; in addition to the two obvious orientation-errors, it considers the effect of varying the angle of incidence (irrelevant when the adjustment is otherwise perfect), and of having an "error of manufacture" in the pentag-angle P itself; the effects of curvature of the diurnal star-trails, and of observing at a number of points (and therefore off-axis) in the telescope field, are also investigated.

The investigation is confined to the case of the "hollow" pentag, i.e. one which really is fabricated from two plane mirrors; the "true" or "solid" pentag, an actual five-sided prism of optical glass in which the two reflections are internal, may possess additional errors of manufacture, and cannot be adjusted by the same auto-collimation method as the hollow one.

Fig. 1 shows a hollow pentag of 45° angle, mounted in front of the telescope objective in one of its two ideal operating positions (i.e. with the angle of incidence = 22½°, which results in symmetry and no vignetting); the other position can be obtained by rotating it clockwise through 90°, about an axis perpendicular to the plane of the figure, and this axis must pass through A if the beam is to be central on the objective in both positions. The rays marked T, N_1, I, N_2 and S represent the directions of the telescope-axis (looking outwards), the first normal, the "intermediate" ray, the second normal, and the ray to the star, respectively; in the ideal case these all lie in the plane of the figure; and (with the signs of the second and third reversed, as is here done) the angle between each one and the next is 22½°. The light is deviated through the angle TAS and not, of course, through its supplement (**2**).

Fig. 2 shows the intersections of the above ideal rays with the celestial sphere, and also the intersections T′, I′ and S′, of the actual telescope, intermediate, and star rays respectively, when these are not in the N_1N_2 plane and the angle of incidence $S'N_2$ is not $P/2$. (P also need not be 45°.) Since angles of incidence and reflection are always coplanar and equal, $T'N_1I'$ is a great circle, and $T'N_1 = N_1I'$. Similarly $I'N_2 = N_2S'$. If T′T″, I′I″ and S′S″ are drawn

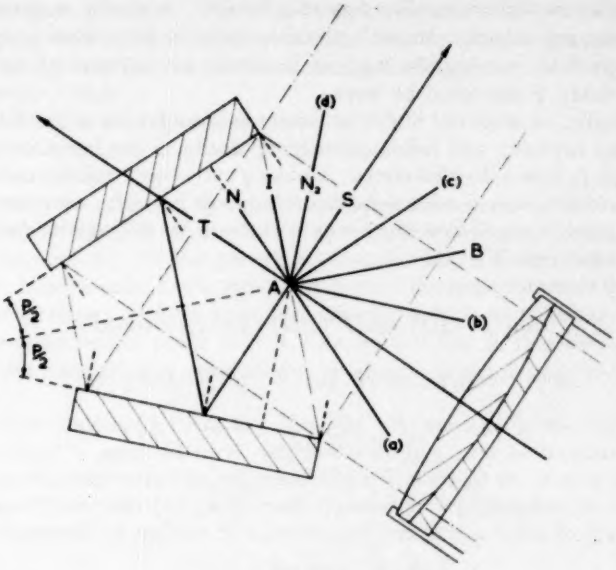

FIG. 1.

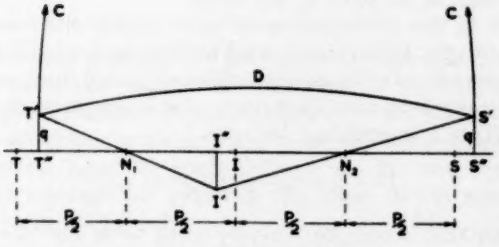

FIG. 2.

perpendicular to the great circle through N_1 and N_2, the triangles $T''T''N_1$ and $I'I''N_1$ are then equal in all respects, and similarly for the triangles $I'I''N_2$ and $S'S''N_2$. Thus $T''T'' = S'S''$; the point seen, S′, departs therefore by strictly the same amount, q say, from the plane of the normals (N_1N_2) as the telescope-axis T′ does. Also, $T''I'' = 2N_1I''$ and $I''S'' = 2I''N_2$, so that $T''S'' = 2N_1N_2 = 2P$. Since T″T′ and S″S′ if produced will meet at a pole, C, which is $90° - q$ from T′ and S′, the spherical triangle T′CS′ yields at once the relation

$$\cos D \equiv \cos T'S' = \sin^2 q + \cos 2P \cos^2 q, \qquad (1)$$

where D is the total (great circle) deviation produced by the pentag. This equation is rigorous, and shows that the magnitude of the deviation is completely independent of the angle of incidence, so long as changes in that angle do not alter q. If the pentag is rotated strictly in the plane of the normals, keeping the telescope T′ fixed, N_1 and N_2 will move along the line N_1N_2 but S′ will remain

fixed in both coordinates, to all orders of accuracy. Since this statement would also hold for any adjacent star S″, together with the associated image, T″, in the telescope-field, varying the angle of incidence (at constant q) will also not rotate the field; q may even be large.

Analytically, we shall not find it necessary to consider the angle of incidence, as such, any further; and instrumentally, it clearly is not necessary to fit the axis through A with a divided circle. Unless q varies very rapidly indeed as the pentag is rotated, any good mechanical stop will be quite adequate, and no correction need be applied for the position of the Z.D. micrometer (which does, of course, enter into T′).

We may re-write (1) as

$$2\sin(P-\tfrac{1}{2}D).\sin(P+\tfrac{1}{2}D)=\sin^2 q(1-\cos 2P) \tag{2}$$

or

$$\sin(2P-D)[1-\cot 2P.\tan(P-\tfrac{1}{2}D)]=\sin^2 q.\tan P \tag{3}$$

(since neither $\sin 2P$ nor $\cos(P-\frac{1}{2}D)$ will vanish). P, indeed, will never be at all near either 0 or $\pi/2$; and, as q will also never be large, $P+\frac{1}{2}D$ cannot be near either 0 or π, so that $\sin(P+\frac{1}{2}D)$ must be of order unity, very roughly, rather than of order $\sin q$. It follows, then, from (2) that $\sin(P-\frac{1}{2}D)$ must be not merely of order q (radians) but of order q^2, so that (3) becomes

$$2P-D=q^2\tan P+O(q^4) \tag{4}$$

with no terms of order q^3. Terms of order q^4 will in all cases be completely negligible, and may be dropped at this point.

We shall not in this investigation consider further any values of P except those very close to 45°. Other values would indeed be needed if it were proposed to investigate harmonics of order $4m$ in the flexure (3), and there is no real difficulty in extending the analysis to cover such cases; but it does make it more cumbrous. If $P=\pi/4+v$, where v is small, (4) becomes

$$D-\frac{\pi}{2}=2v-q^2(1+2v+\ldots), \tag{5}$$

showing explicitly that except for the very small term $2vq^2$ the effects of error of manufacture (v) and error of alignment (q) simply add; in particular, there is no interaction-term of order vq, and there are no higher powers of v that are not multiplied by q^2. A pentag designed for $P=\pi/4$ should result in $|v|<10^{-3}$, and if we also have $|q|<10^{-3}$, the term $2vq^2$ (0″·0004) can be neglected in all cases; dropping it, and writing $D-90°$ and v in seconds of arc, and q *in minutes*, (5) becomes

$$D-90°=2v-0''\cdot01745\,q^2. \tag{6}$$

The correction for the mal-alignment q is thus less than 0″·01 provided $|q|<0'\cdot757$, and less than 0″·001 if $|q|<0'\cdot240$.

One must clearly have a means of determining the value of q, in both of the positions in which the pentag will be used and in a variety of telescope-pointings for each. A number of unsatisfactory attempts to do this were made, before the possibility of the following simple procedure was noticed. It seems worthwhile, therefore, to describe this, as it is of general applicability.

With a hollow pentag there are four telescope-positions, necessarily all of them exactly in the plane of the normals, where auto-collimation in some part

of the pentag is possible. The vignetting is substantial, but the images are surprisingly good; much more than adequate for the present purpose. Taking them in order, these positions involve normal incidence on

(*a*) mirror 1 only
(*b*) mirror 2 as seen in mirror 1
(*c*) mirror 1 as seen in mirror 2
(*d*) mirror 2 only;

the angle between each and the next is 45°, and the successive directions to the *telescope* (180° from T′) are shown in Fig. 1 (and also in Fig. 3) as (*a*), (*b*), (*c*) and (*d*) respectively. If the pentag is rotated, with respect to the telescope, about the rotation-axis A, the successive auto-collimation images will appear at these four positions, though at a first attempt it may be necessary to search through a considerable range of R.A. settings in order to find them, since the plane of the normals may not initially be closely perpendicular to the axis of rotation.

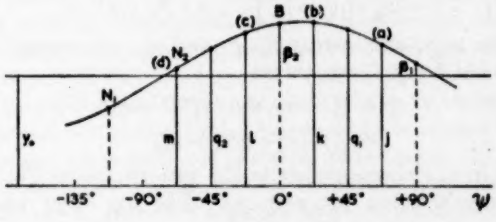

FIG. 3.

Fig. 3 is a Mercator projection of the equatorial region of that sphere whose poles are the rotation-axis through A; the plane of the normals thus defines a sine-curve (of some unknown phase and amplitude) if the adjustment is slightly imperfect. The abscissae, ψ, are angles of rotation, reckoned from the telescope tube to the bisector, B, of the angle between the mirrors; the ordinates are R.A. micrometer readings for points in the plane of the normals; and the equation of the curve is evidently

$$y = \beta_1 \sin\psi + \beta_2 \cos\psi + y_0. \tag{7}$$

If the four micrometer readings for auto-collimation are j, k, l and m respectively (minutes of arc) we readily obtain

$$\beta_1 = \frac{j-m}{2 \sin 67\tfrac{1}{2}^\circ} = \frac{k-l}{2 \sin 22\tfrac{1}{2}^\circ} \tag{8}$$

$$\beta_2 = \frac{(k+l)-(j+m)}{2(\cos 22\tfrac{1}{2}^\circ - \cos 67\tfrac{1}{2}^\circ)} \tag{9}$$

$$y_0 = \frac{(j+m)\cos 22\tfrac{1}{2}^\circ - (k+l)\cos 67\tfrac{1}{2}^\circ}{2(\cos 22\tfrac{1}{2}^\circ - \cos 67\tfrac{1}{2}^\circ)}. \tag{10}$$

A manufacturing error v will very slightly alter the nominal $22\frac{1}{2}^\circ$ and $67\frac{1}{2}^\circ$ angles, but the effect of this would be quite undetectable, for any reasonable values of v.

Since we have here four equations but only three unknowns, there is an identical relation between the coefficients; as is obvious from (8), this is

$$\frac{j-m}{k-l} = \tan 67\tfrac{1}{2}^\circ = 2{\cdot}41\ldots \tag{11}$$

and this may be used to throw the other equations into various equivalent forms.

The angle β_1 is that part of the pentag's maladjustment with respect to A which is anti-symmetrical about the bisector B; it may be made small by a rotation about this bisector, until $j-m$ and $k-l$ are both small, and the sign of the necessary movement will be readily seen in any trial. β_2, the symmetrical component, may be made small by moving the east end (say) of the pentag towards or away from the axis A; this affects k and l more than j and m, and the sign can be inferred from this. If the readings all reckon from the ordinary "collimation" reading as zero, y_0 is the angle by which the telescope-axis (so defined) departs from the equator of the pentag's rotation-axis; it can be made small by moving one end of the rotation-axis towards or away from the telescope, and this affects all four readings equally. Thus these four observations completely separate the three unknowns in question, and the adjustments can be made in any order.

In actual use on stars, one is concerned only with pentag-positions close to the two ideal operating ones, given by $\psi = \pm 45°$. We thus have

$$y = (q_1 \text{ or } q_2 =) \pm \beta_1/\sqrt{2} + \beta_2/\sqrt{2} + y_0. \tag{12}$$

Taking the upper sign, eliminating β_1, β_2 and y_0, and using (11) to make the coefficients of j and k equal, we obtain

$$q_1 = \tfrac{1}{2}[j+k+\tan 11\tfrac{1}{4}°(l-m)], \tag{13}$$

$$\approx \tfrac{1}{2}(j+k)+0{\cdot}1(l-m). \tag{14}$$

The upper sign in (12) corresponds to the case shown in Fig. 1, i.e. with the telescope half-way between (*a*) and (*b*). For the other positions we have similarly

$$q_2 \approx \tfrac{1}{2}(m+l)+0{\cdot}1(k-j). \tag{15}$$

Both equations will of course appear in other forms if (11) is applied differently; in particular, it might be preferred to eliminate m from (14) and j from (15), getting

$$q_1 = 0{\cdot}401j + 0{\cdot}740k - 0{\cdot}141l \tag{16}$$

and

$$q_2 = -0{\cdot}141k + 0{\cdot}740l + 0{\cdot}401m. \tag{17}$$

If ψ is incorrectly set (with individual stars), equations (12)–(17) will be slightly invalidated unless both β_1 and β_2 are zero; i.e. varying the angle of incidence (by rotation about the actual axis A) can have a slight effect on the deviation D, through its effect on q. But if ψ is in degrees, we have

$$\Delta q_1 = -0{\cdot}01745(q_2 - y_0)\Delta\psi, \tag{18}$$

$$\Delta q_2 = +0{\cdot}01745(q_1 - y_0)\Delta\psi, \tag{19}$$

and even a 1° error of setting will thus have negligible effects, for all reasonably small values of $q-y_0$.

If the mounting yields under gravity, the readings for auto-collimation may be different at different telescope-pointings; if they are repeatable over a reasonable period, at any one pointing, it is clearly permissible to plot q_1 and q_2 as functions of the circle-reading, and to read off the value appropriate for each star observed. It may be noted that although all fairly high *stars* can be observed in both positions of the pentag, there is no *telescope*-pointing in which both positions can be used. If circle-readings reckon from the zenith, positive to the north, with c_1 denoting (as in the previous paper) the value when the pentag is

in use, and if q_1 refers to the case when $c_1 \approx z + 90^\circ$ and q_2 to the case $c_1 \approx z - 90^\circ$, then q_1 will be required only for positive c_1-values, i.e. north pointings of the telescope; the stars observed will be south of the zenith if the pointing is above the horizon ($c_1 < +90^\circ$), and north if it is below. Similarly, q_2 will be required only for $c_1 < 0$. Near-zero values of c_1 involve near-horizon stars, i.e. no observations. It should thus be sufficient to observe only j, k and l at north pointings (assuming that Fig. 1 is drawn looking eastwards) and only k, l and m at south pointings, using (16) or (17) accordingly.

If (11) fails to hold, even though the readings are repeatable, errors involving higher harmonics of ψ are presumably present. They may be either pivot-errors of the axis A, or perhaps flexure between the pentag and A. Proper care in manufacture should keep the total pivot-errors below $0'{\cdot}1$, and flexure which is symmetrical (east–west) will not matter; if the failures of (11) are in fact significant, or if the measurements are seriously non-repeatable in any case, a complete re-design of the mounting may be necessary.

With the preliminary mounting made at Herstmonceux, it has been found possible to keep q_1 and q_2 within about $\pm 0'{\cdot}4$ for days on end, in spite of swinging the pentag out from the beam and back, and moving the telescope from one pointing to another. If the direct zenith-distance error due to q were the only one, (6) shows that this would then never reach $0''{\cdot}003$, and even though it would still be systematic in z it would hardly be necessary to correct for it at all; but in fact there are also cross-products of q with other errors.

The most troublesome maladjustment to prevent is rotation of the pentag, together with the axis A, about the telescope axis. It has been found very difficult to swing the pentag out of the beam and back without slewing the mounting so as to cause such a rotation, since the telescope itself interferes with almost any diagonal stays which one might wish to incorporate. Even variations of the pointing, without removing the pentag, are somewhat liable to result in the same trouble. Fortunately, however, it proves unimportant for this error to be constant, or repeatable, as long as q is so.

We consider the general case in which we have a small error of manufacture v (supposed precisely constant, but not necessarily known), a small alignment-error q (supposed sufficiently known from auto-collimation results), and a small rotation, p, about the telescope-axis (unknown as yet). For simplicity, we shall suppose the ordinary azimuth and level errors to be zero; their interactions with p, q and v need watching, but the interactions of p, q and v with each other (and with the curvature of the diurnal circles) should sufficiently illustrate the position. All R.A. micrometer readings are reckoned from the ordinary collimation-reading, which therefore does not appear explicitly; they will be defined as positive when they carry the micrometer to the east, and the point seen to the west. We also suppose, for the moment, that the flexure is zero and the zenith is therefore recognizable without ambiguity; this, however, is only for convenience in wording and does not affect the final equations. (The flexure is, in any case, less than $1''$.)

Let the telescope be pointed horizontally to the north, so that c_1 is $+90^\circ$; and let the pentag be set for stars at zenith-distance $z \approx c_1 - 90^\circ$, i.e. near the zenith. If the adjustment is perfect, the point seen is then on the meridian, at the distance $2v$ south of the zenith. If the telescope and pentag were now rotated as a unit, clockwise about the vertical (looking upwards), i.e. so that the eye-end moved east, through a small angle q, the point seen would move round the small circle

of radius $2v$, to a position $2vq$ east of the meridian, if all angles are in radians, and the star-field would appear to rotate, with respect to the wires, through the angle q, counterclockwise; the pentag, having an even number of reflections, does not reverse the field. (The opposite apparent rotation will be obtained if a single plane mirror at 45° is substituted for the pentag.) If q is small, the same net effect can be produced, without moving the telescope tube or objective, by rotating the pentag alone about the vertical, and then advancing the R.A. micrometer alone from zero through the angle $+q$, so as to place it again in the plane of the normals. Now let the micrometer alone be returned to zero; this evidently does not further rotate the field, and the point seen moves along the image of the Z.D. wire on the sky, eastwards through the angle $q\cos q$, or q to the second order, and northwards through the angle $q\sin q$, i.e. q^2, since the image of the Z.D. wire has been rotated clockwise. The distance of the point seen from the north point of the horizon is thus $\pi/2+2v-q^2$, in agreement with (5). Its distance from the meridian is $q+2vq$; from the plane of the normals it is of course q, the same as for the telescope-axis. If we repeat the argument, with the telescope pointed horizontally southwards ($c_1=-90°$) and the pentag set for $z\approx c_1+90°$, we find that a positive q again displaces the point seen to the east, but the wires are now rotated counterclockwise with respect to the field, i.e. negatively, if the former rotation was defined as positive. The distance east of the meridian is readily seen to be $q+2vq$ in this case also, and the distance from T′, now the south point, is $\pi/2+2v-q^2$, agreeing with (5) as before.

The argument is completely independent of the observer's latitude (in particular, of its sign) and can also be generalized immediately to stars at all zenith distances; it is merely necessary to replace "rotation in azimuth" by "rotation about a line which is in the meridian and perpendicular to the telescope", and to make other obvious minor changes. Thus we conclude that (with the above sign-conventions) a mal-alignment $+q$ and a pentag error $+v$ produce a total deviation from T′ of $\pi/2+2v-q^2$, a displacement to the east of $+q(1+2v)$, and a rotation $\pm q$, the upper sign being taken when c_1 is approximately $z+\pi/2$ (the same convention as in the previous paper).

We now superimpose a rotation of the pentag, through the small angle p, about the telescope-axis. We define the sign of p to be positive if it displaces the point seen towards the same side as a positive q does, i.e. towards the east, and it may then be verified in various ways that the field-rotation produced by a positive p is opposite to that produced by a positive q. If the point seen is at a distance D from T′ (the point seen without the pentag), a rotation p obviously produces a displacement $p\sin D$ along the "almost great" circle of radius D and centre T′, so that the magnitude of the distance from T′ is unchanged. Neglecting third-order quantities, it may then be shown as before that the total displacement east is now $p+q+2vq$, and the total rotation is $\pm(q-p)$, irrespective of whether p or q is performed first; there are no interaction terms of order p^2, pq, or pv. The second-order quantity $2vq$, which appears in E–W angles, but not in N–S ones, may be dropped at this stage; it will probably lie below the probable error of q, and it will in any case never be used except when multiplied by quantities comparable with p.

Fig. 4 represents a portion of the sky (looking outwards) which is viewed through a pentag orientated so that $c_1\approx z+90°$. T′, the point seen in the absence of the pentag, is distant $90°+2v$ from O, in the N direction, and all great circles

through T′ are parallel lines in this figure, which may be thought of as a Mercator projection with T′ as its pole. The projections of the micrometer wires are tangents to great circles, and practically coincide with them throughout the field of view. The displacement from Q to P, caused by the rotation p, is at right angles to the N-direction, as shown. The displacement q, from O to Q, is inclined, but all inclinations are of course enormously magnified here.

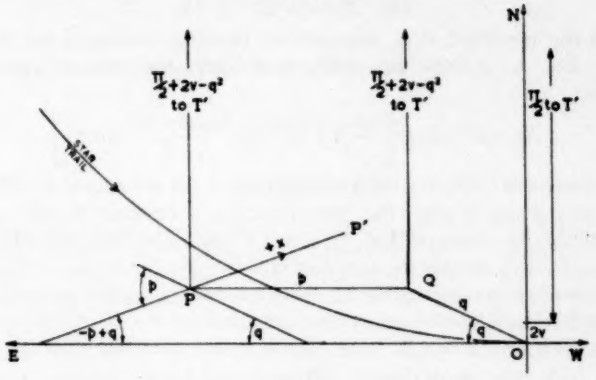

FIG. 4.

O is the point which would be seen, if the pentag were perfectly adjusted, when the circle-reading is c_1, and the R.A. micrometer-reading is zero. (The "circle-reading" includes that part arising from the Z.D. micrometer, and is adjusted to be zero at the zenith.) P is the point actually seen, with the R.A. micrometer still at zero, and it is north of the E–W great circle through O by $0''{\cdot}01745\ q^2$ if q is now in minutes once more. PP′ is the image of the Z.D. wire, inclined at the angle $+(q-p)$ to the east-west great circle through O; and points on this image, west of P by x (minutes of arc) are north of the great circle by $0''{\cdot}01745\ [q^2+(p-q)x]$. The declination-circle through O is north of the same great circle by $0''{\cdot}00872\ (p+q-x)^2 \tan\delta$; and the actual circle-reading, if the Z.D. wire bisects a star of the declination of O, when it is x minutes west of P, must therefore be increased by

$$\Delta c_1 = 0''{\cdot}01745[\pm q^2 \pm (p-q)x - \tfrac{1}{2}(p+q-x)^2 \tan\delta] \qquad (20)$$

in order to obtain the c_1 for use in eqn. (55) of the previous paper. The upper signs are those appropriate to the argument just given, i.e. to the case where the pentag is set for $c_1 \approx z+\pi/2$, and the lower ones correspond to $c_1 \approx z-\pi/2$, as in the previous paper. The term $2v$ is shown (**2**) explicitly in (55) and is therefore not included in Δc_1.

So far as the term in $\tan\delta$ is concerned, there is no need to determine p explicitly; the complete coefficient $p+q-x$ can be obtained directly, for each Z.D. bisection, by using the R.A. micrometer as well as the Z.D. one. It is not, of course, possible to bisect the star with both wires at once, but no real precision is required in R.A. and it is sufficient to set the R.A. wire slightly ahead of the star and to set the R.A. drive to the right speed as closely as practicable. The R.A. difference between star and wire will then be small and will vary linearly with time; if actual values are required at all, they can be estimated by eye at

known times before and after the set of Z.D. bisections, and interpolated. If, then, an audible signal is sounded at the times when the R.A. micrometer is recorded, the observer merely has to make his Z.D. bisections when he hears the signal. The star's distance east of the meridian is $\frac{1}{4}(\alpha-t)\cos\delta$ (in minutes of arc), at the true local sidereal time t, if α is its apparent right ascension and $\alpha-t$ is in seconds of time; we thus have

$$\tfrac{1}{2}(\alpha-t)\cos\delta = p+q-x, \tag{21}$$

where x is the recorded R.A. micrometer reading, corrected for the star–wire difference. For α, it will be sufficient to take the tabular apparent value. Accordingly,

$$\Delta c_1 = 0''\cdot01745\left[\pm q^2 \pm (p-q)x - \left(\frac{\alpha-t}{8}\right)^2 \sin 2\delta\right]. \tag{22}$$

Since this correction will in practice be averaged for a number of different Z.D. bisections at any one transit, the term which still contains p will vanish if the observations are so arranged that $\sum x = 0$. If the observing procedure does not permit this, it will probably be simplest and most accurate to evaluate a mean p for the transit from (21), using all the t and x values recorded (as well as the *mean* star–wire difference), and to insert this in (22).

At high declinations, small errors in the instants of bisection (or in the estimated star–R.A. wire separations) will tend to become serious, in spite of the coefficient $\sin 2\delta$, since $(\alpha-t)\cos\delta$ will be roughly independent of δ. It will also be necessary, if p is large and of unknown sign, to set for each star well before true transit time and perhaps observe well after it. For both these reasons, high declinations are disadvantageous. Fortunately, it is not necessary to include them, in order to obtain a sufficient separation of the unknowns in (55); the observations always give only the difference in flexure, as between two pointings 90° apart, and one should get exactly the same result from observing equatorial stars with and without the pentag as from observing near-polars with and without it. Incidentally, this means that we may somewhat further restrict the range of pointings over which auto-collimation readings are needed; within, say, ±15° either way from the equator, we may perhaps omit them altogether.

The pentag-mounting as used in this experimental work was inconvenient even when not in use, and was removed again to facilitate the AGK3R programme. When that has been completed, it is planned to make a sufficient series of flexure determinations, with a more fully engineered mounting. The use of tubing instead of angle-rods should diminish the tendency to slew, and so enable p to be kept small more readily.

Royal Greenwich Observatory,
Herstmonceux Castle,
Sussex:
1959 *November.*

References

(1) R. d'E. Atkinson, *M.N.*, **115**, 427, 1955.
(2) This point was overlooked in the previous paper, and wherever the quantity $2v$ occurs there (p. 440, l. 8, l. 19, and eqns. 52, 53, 54 (twice), and 55), its sign (or double sign) should be reversed.
(3) *L.c.*, p. 440.

ON THE DETERMINATION OF EPHEMERIS TIME: A CORRECTION

C. A. Murray

(Communicated by the Astronomer Royal)

(Received 1960 January 21)

Summary

This note contains a correction to a previous paper in which recommendations were made for the determination of Ephemeris Time. The statements in that paper on the equinox to be used in reducing the lunar observations are erroneous. A definite numerical formula for reducing modern observations, referred to the FK_3 system, to the system of Newcomb's Fundamental Catalogue is proposed.

In a previous paper (**1**) recommendations were given for the reduction of lunar observations and the determination of Ephemeris Time. Since that paper was published my attention has been drawn to a paper by Aoki (**2**) in which he concludes that the equinox to which the observed longitudes of the Moon, as derived by Spencer Jones (**3**), are referred, is that of Newcomb's Fundamental Catalogue (**4**) and not the ideal equinox as I argued in my paper. Aoki's conclusion is quite correct and the statements in Section 3 of my paper are erroneous.

As Aoki points out, the constant and linear terms of the Moon's mean longitude in the *Improved Lunar Ephemeris* (**5**) have been deduced from observations referred to Newcomb's system, and hence, in all determinations of ΔT, the observed longitudes of the Moon should be referred to that system.

The results from the annual discussions of occultations and of the Washington meridian observations are at present referred to the FK_3 system; it therefore seems desirable that a definite numerical formula for reducing longitudes observed with reference to the FK_3 system to that of Newcomb's Fundamental Catalogue should be agreed on. A comparison between the systems of FK_3 and Eichelberger is given by Nowacki (**6**). The straight mean of $\Delta\alpha_\delta$ and $\Delta\mu_\delta$ gives for $30^\circ > \delta > -30^\circ$

$$FK_3 - \text{Eichelberger} = +0^s{\cdot}0016 + 0^s{\cdot}00061t$$

where t is measured in years from 1925. Also, a comparison between Eichelberger and Newcomb is given in Eichelberger's catalogue (**7**). The weighted mean of $\Delta\alpha_\delta$ and $\Delta\mu_\delta$ for $30^\circ > \delta > -30^\circ$ gives

$$\text{Eichelberger} - \text{Newcomb} = -0^s{\cdot}0533 - 0^s{\cdot}00054t;$$

thus

$$\text{Newcomb} - FK_3 = +0^s{\cdot}0517 - 0^s{\cdot}00007t.$$

The equivalent correction in seconds of arc of longitude is obtained by multiplying by $15 \cos \epsilon$. Transferring the time origin to 1900 and the unit of time to centuries we have the following correction which should be applied to observations of the Moon's longitude which have been referred to FK_3 in order to reduce them to Newcomb:

$$+0''\cdot73 - 0''\cdot10T.$$

In particular, this correction should be applied to the observations since 1923 used by Brouwer (**8**) in place of the constant $0''\cdot6$ adopted by him.

Royal Greenwich Observatory,
Herstmonceux Castle, Hailsham,
Sussex:
1959 *December* 31

References

(1) C. A. Murray, *M.N.*, **119**, 612, 1959.
(2) S. Aoki, *A.J.*, *Publ. Astr. Soc. Japan*, **12**, No. 1, 1960.
(3) H. Spencer Jones, *Cape Annals* XIII, part 3, 1932.
(4) *Astr. Papers of A. E.* VIII, part 2, 1905.
(5) *Improved Lunar Ephemeris*, Washington 1951.
(6) H. Nowacki, *A.N.*, **255**, 301, 1935.
(7) *Astr. Papers of A. E.* X, part 1, 1925.
(8) D. Brouwer, *A.J.*, **57**, 125, 1952.

THE CALCULATION OF METEOR VELOCITIES FROM CONTINUOUS-WAVE RADIO DIFFRACTION EFFECTS FROM TRAILS

J. S. Mainstone

(Communicated by H. Bondi)

(Received 1959 September 23)

Summary

The theory of continuous-wave radio diffraction effects from meteor trails is reviewed and it is shown that the zone lengths corresponding to the pairs of maxima of the echo waveform used for velocity measurements depend on the phase relationship between the ground wave and the wave reflected from the trail. Large errors can arise if no account is taken of this phase relationship. A new method of analysis for c.w. echoes is proposed and a comparison is made with other methods. It is shown that with this method it is possible to measure meteor orbits with a c.w. system. A discussion of the factors affecting the accuracy of measurements made with new equipment at Adelaide is given, together with some preliminary results.

---

1. *Introduction.*—Radio measurements of the velocities of meteor particles have been carried out by observations of diffraction patterns from the ionized trails produced as the particles enter the Earth's atmosphere. Expressions for the intensity of the radio echo from a meteor trail for both pulse and continuous-wave systems have been given by McKinley (1). In the c.w. case, where a portion of the signal radiated by the transmitter reaches the receiver directly, via the ground wave, the echo intensity is given by

$$I = F_r^2(C^2+S^2) + F_d^2 + 2F_rF_d(C\cos\psi - S\sin\psi), \qquad (1)$$

where F_r and F_d are constants for a given meteor for the reflected and direct waves respectively, C and S are the Fresnel integrals and ψ is the phase difference between the ground wave and the wave reflected from the t_0 or specular reflection point of the trail. If R_0 is the range at the t_0 point, and D is the separation between transmitter and receiver, then

$$\psi = \frac{2\pi}{\lambda}(2R_0 - D). \qquad (2)$$

Except in the immediate vicinity of the t_0 point, algebraic expressions for the echo waveform may be obtained by substituting Cauchy's approximations for the Fresnel integrals C and S in equation (1). Prior to t_0 the echo is represented by

$$I_{(1)} = \frac{F_r^2}{\pi^2x^2} + F_d^2 + \frac{2F_rF_d}{\pi x}\sin\left(\frac{\pi x^2}{2} + \psi\right) \qquad (3)$$

and after t_0 by

$$I_{(2)} = F_d^2 + 2F_r^2 + \frac{F_r^2}{\pi^2 x^2} - 2\sqrt{2}F_r F_d \sin\left(\psi - \frac{\pi}{4}\right) + \frac{2F_r}{\pi x}\left[F_d^2 + 2F_r^2 - 2\sqrt{2}F_r F_d \sin\left(\psi - \frac{\pi}{4}\right)\right]^{1/2} \left\{\sin\frac{\pi x^2}{2} - \tan^{-1}\left[\frac{F_r - F_d \sin\psi}{F_r + F_d \cos\psi}\right]\right\} \quad (4)$$

where $\pi x^2/2 = 2\pi s^2/(R_0\lambda)$, s being the distance along the trail from the t_0 point. In terms of Cornu's spiral representing the reflected wave, x is the distance along the curve corresponding to the distance s along the trail.

The oscillatory term in each equation involves the phase angle ψ which is a constant for a particular meteor trail provided R_0 is constant, and serves to define the orientation of Cornu's spiral representing the reflected wave, relative to the vector representing the ground wave. The waveforms of the diffraction echoes, commonly called "whistles", for meteors with various values of ψ will vary considerably due to the product of the functions in $1/x$ and $\sin(\pi x^2/2 + \psi)$ in the last term of equation (3) and the corresponding functions in equation (4). This complication does not arise in the case of pulse systems, where the ground wave is not present, and hence the waveforms are always of the same shape.

It is now necessary to examine the implications of this change of the echo waveform with the value of ψ more closely, and in particular its effect on the measurement of velocities.

2. *Measurement of velocities from echo waveforms.*—Any method for determining the velocity of a meteor from its diffraction pattern echo ultimately depends on a knowledge of the separation along Cornu's spiral between points representing any two maxima or any two minima of the echo waveform. Two such points constitute a zone. The distance along the spiral between the points defines a line segment of the meteor path since $s^2 = (x^2/4)R_0\lambda$. The time δt taken to traverse this distance s is obtained directly from the recorded echo and in this way the velocity v may be found; i.e.

$$v = \frac{\nabla}{2} \cdot \frac{\sqrt{(R_0\lambda)}}{\delta t}, \quad (5)$$

where ∇ is the zone value, i.e. difference in x-values for the particular zone. With the pulse system this method presents no difficulties since the zone values for any sets of maxima or minima may be calculated accurately from the Fresnel integrals.

In the c.w. case the production of maxima and minima in the echo waveform is due to the vector addition of the ground wave and reflected wave as the end of the reflected wave vector moves along Cornu's spiral at a rate determined by the velocity of the meteor. For example, at the time represented by the conditions shown in Fig. 1 (*a*), the resultant signal is approaching a maximum. For the two maxima, say *m*th and *n*th, produced when the end point of the reflected wave vector has reached P and Q respectively, the zone value is given by $\nabla_{m,n} = x_P - x_Q$. In Fig. 1 (*b*) the ground wave has a different phase from that of Fig. 1 (*a*) and the resultant signal now approaches a maximum at Q'

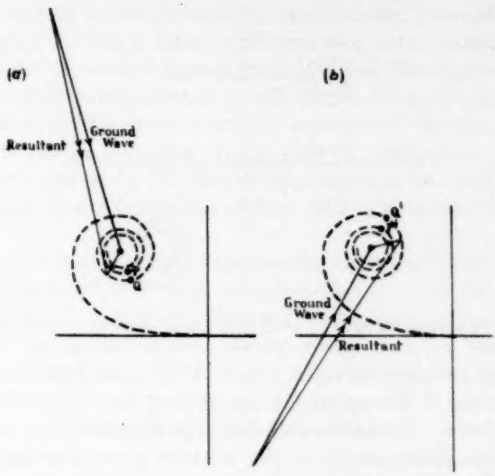

FIG. 1.—*Vector plots of ground wave and sky wave prior to the t_0 point, for two different values of the phase of the ground wave.*

and P'. For the same two maxima, the mth and nth counting from the t_0 point, the zone value is $\nabla_{m,n} = x_{P'} - x_{Q'}$. Since P, P', Q and Q' are points on a spiral, the zone values for the zone defined by the mth and nth maxima (or minima) will be seen to be different for the two cases considered. It is therefore necessary to establish the variation of zone length ∇ with the phase angle ψ before the c.w. waveforms can be used for velocity measurements.

3. *Variation of zone length ∇ with phase angle ψ.*—For zones of sufficiently high order prior to the t_0 point the loops of Cornu's spiral are very nearly circular so that little variation of zone length with ψ would be expected. However this is not the case for the lower order zones which are normally used for velocity measurement. In fact the closer a given zone is to the t_0 point, in general, the greater the possible variation in zone length with ψ, due to increasing departure of a loop of the spiral from a circle as the t_0 point is approached.

In Fig. 1, where two different phases of the ground wave are considered, the positions on the spiral of the 1st and 2nd maxima are shown for each case. Since the phase angle ψ may have any value between 0 and 2π it is possible to define the portions of the spiral on which the various maxima may lie. By starting with the 1st maximum prior to the t_0 point and working towards the higher order maxima it will be seen that the nth maximum may lie on a loop of the shape shown in Fig. 2 (actually the third loop is shown, i.e. $n = 3$). Having established this, we are in a position to examine the zone values for the zone defined by the mth and nth maxima.

In order to simplify the calculations McKinley used the 4th and 9th cycles of the whistle in the bulk of his reduction work (1). Now, with a plot of the 4th and 9th loops of Cornu's spiral it is possible to determine graphically the distribution of values for $\nabla_{4,9}$ for various values of ψ and different ratios of the ground wave amplitude to reflected wave amplitude. The resulting contour pattern is shown in Fig. 3. Except in cases where the amplitude of the total signal reflected from the trail is considerably greater than the amplitude of the

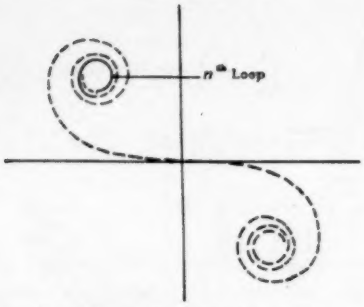

FIG. 2.—*Method of defining the nth loop of Cornu's spiral, prior to t_0, drawn for the case $n=3$.*

ground wave, the contours of equal values of $\nabla_{4,9}$ are seen to radiate from the negative focal point of the spiral, i.e. in general the value of the zone length depends directly on ψ. As can be seen from the diagram, $\nabla_{4,9}$ may vary between 2·00 and 2·19, the discontinuity in the contour pattern at the extreme values resulting from the shape of the loops.

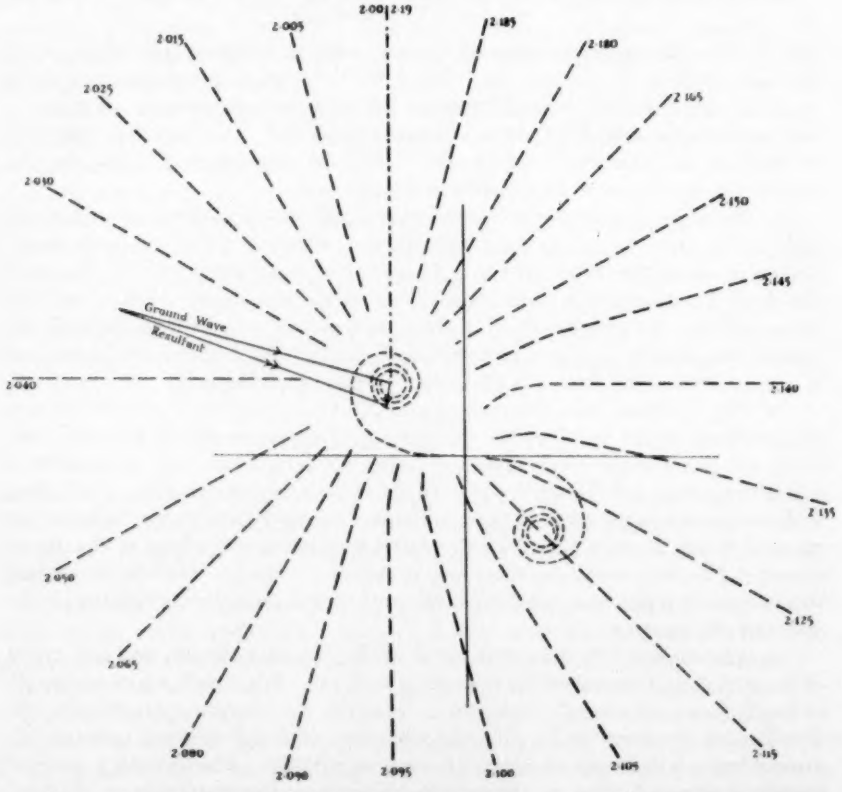

FIG. 3.—*Contour pattern showing distribution of values of $\nabla_{4,9}$ as a function of the amplitude and phase of the ground wave.*

The same procedure could be used to examine the variation in ∇ for the equivalent zone after t_0, but a rather different and more complicated contour pattern would result. It is sufficient to point out that the zone values found in this way for the whistle subsequent to t_0 will not be the same as those before t_0 for the same value of ψ. However, since the number of whistles occurring after the t_0 point which can be recorded satisfactorily is small (they rapidly tend to become lost in the larger body Doppler fluctuations due to wind drifts), a more detailed investigation is not warranted and we will confine the discussion to the zones prior to t_0.

By reasoning similar to that used to find the limiting values of $\nabla_{4,9}$ we can find the limiting values for any other zone length $\nabla_{m,n}$, e.g. for $\nabla_{2,5}$ the limits are 1·64 and 1·99, for $\nabla_{3,9}$, 1·83 and 2·07 etc. The range of possible values for the zone lengths for several typical zones which may be used for velocity measurement is indicated in Table I.

TABLE I

Values of zone lengths for typical zones

Zone m, n	Zone length $\nabla_{m,n}$
2, 4	1·17–1·45
2, 5	1·64–1·99
2, 6	2·07–2·46
2, 7	2·46–2·89
3, 5	1·01–1·17
3, 6	1·43–1·64
3, 7	1·83–2·07
4, 6	0·90–1·01
4, 7	1·29–1·43
4, 9	2·00–2·19
5, 7	0·82–0·90

4. *Determination of* ψ.—In order to make use of the appropriate zone values when calculating the velocity of a meteor, the value of ψ for the particular echo must be found. As can be seen from the range of values for the zone lengths given in Table I, very serious errors can arise if the value of ψ is not taken into account.

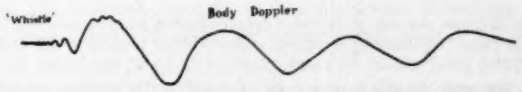

FIG. 4.—*A complete c.w. echo showing "whistle" and body Doppler.*

It is not possible to determine ψ with any certainty by inspection of the whistle waveform. However, it is shown in what follows that by using the complete c.w. echo waveform comprising both whistle and body Doppler beat pattern due to the effect of wind drift on the trail, together with the sense of this drift, the phase of the ground wave at the times represented by any maxima of the whistle which are used in the measurement of velocity can be found. This method of analysis was suggested in a preliminary report by Mainstone, Elford and Weiss (2).

Fig. 4 represents a complete c.w. echo. The body Doppler beat pattern results from the motion of the trail in the line of sight direction after formation, due to the changes in the phase of the wave reflected from the trail, relative to the ground wave. For a receding echo the reflected wave vector rotates in a

clockwise direction with respect to the ground wave vector with increasing time, and for an approaching echo the rotation is anticlockwise. This is equivalent to the ground wave rotating about the reflected wave in an anticlockwise direction for a receding echo and in a clockwise direction for an approaching echo. This latter concept is more useful for the purpose of the discussion which follows.

The minima of the body Doppler beats occur when the reflected and ground waves are exactly out of phase and the maxima when they are in phase. Hence the body Doppler record may be "calibrated" in terms of the angle ψ', where ψ' is the angle between the ground wave and the resultant reflected wave (see Fig. 5). When the sense of drift of the trail is known, e.g. as in the case of the echoes recorded by Robertson, Liddy and Elford (**5**), this calibration is unambiguous.

Provided that the body Doppler beat frequency is constant, we have the situation in which the ground wave vector is rotating at a constant rate relative to the reflected wave, and by extrapolation of this rotation into the region of the t_0 point and beyond, the phase relationship between the ground wave and the

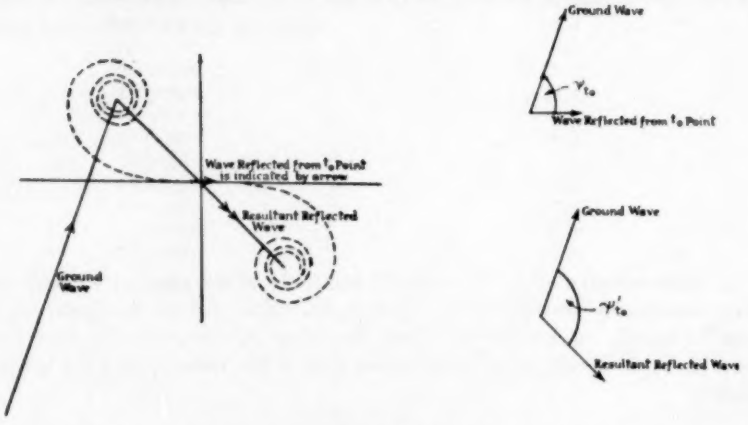

FIG. 5.—*Vector diagram showing relationship between ground wave vector, total sky wave vector and the vector representing the wave reflected from vicinity of the t_0 point.*

reflected wave at any instant may be found. In other words, during the formation of the trail the ground wave vector may be pictured as rotating continuously at a known rate about the negative focal point of Cornu's spiral, while at the same time the end of the reflected wave vector moves along the spiral at a speed determined by the rate of formation of the trail.

Since the vector representing the final intensity of the reflected wave lies along the line joining the focal points of Cornu's spiral, all phase angles ψ' found from the body Doppler beat in the manner described above are measured from the ground wave to this line in a clockwise direction, whereas the values of ψ as defined in equation (2) are measured from the ground wave to the vector representing the wave reflected from the t_0 point, in the same sense. This is shown in Fig. 5. It will be seen that $\psi_{t_0} = \psi_{t_0}' - \pi/4$. Extending this to the general case, the angle ψ_t, where $\psi_t = \psi_t' - \pi/4$, gives the direction of the ground wave relative to the x-axis of the spiral at time t.

5. *Determination of* ∇.—In order to apply the above method to the determination of the correct zone length ∇, certain rules must be observed. For the purposes of this discussion we shall assume that the whole process is carried out graphically using Cornu's spiral. In practice the reduction of data can be greatly simplified by the use of a table (see Section 7 (*a*)).

Let us suppose that we wish to find $\nabla_{4,9}$ for the echo of Fig. 4. The phase of the ground wave at the instant of the first maximum of the diffraction whistle, counting backwards from t_0, is measured according to the above method, and the points of intersection (x_4, x_9) of this vector (produced) with the 4th and 9th loops of Cornu's spiral are noted (Fig. 6). The points x_4, x_9 would then correspond to the positions of the 4th and 9th maxima if no drift of the trail had occurred before the first maximum.

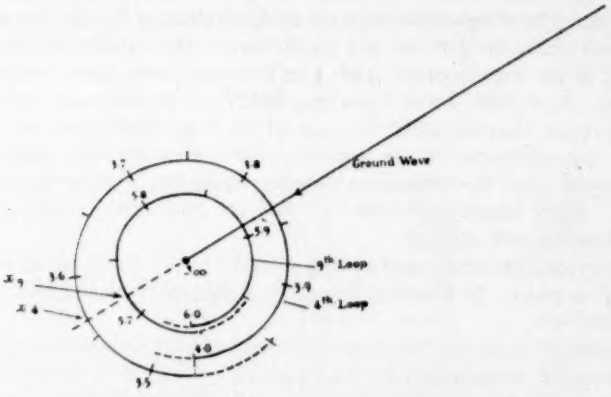

FIG. 6.—*Graphical solution for the values of* $\nabla_{4,9}=x_9-x_4$.

From the echo the changes in the phase of the ground wave between the 1st and 4th maxima and the 4th and 9th maxima can be obtained. If the Doppler beat indicates a receding echo then the phase shift of the ground wave vector between the 1st, 4th and 9th maxima is in a clockwise direction, and vice versa if the echo is approaching. It must be remembered that working from the 1st to the 4th and 9th maxima prior to t_0 is equivalent to working backwards in time.

Having established the directions of the ground wave vector at the 4th and 9th maxima it is necessary to find the correct intersections with the spiral for both of these maxima. This is best done by using the points x_4 and x_9 as reference points and applying the rule that if the echo is receding the positions of the maxima move along the spiral away from the t_0 point, i.e. in a clockwise direction, and vice versa for an approaching echo, when proceeding from the 1st to the 4th and 9th maxima. This method ensures that no ambiguity occurs, as could happen when the line of sight component of the drift velocity is very large and the meteor velocity relatively small, causing considerable rotation of the ground wave relative to the spiral, e.g. if $v=30$ km/sec at range $R_0=140$ km, and the body Doppler beat frequency $f=15$ cycles/sec, between the 4th and 9th maxima the ground wave vector rotates through an angle of about 250°. However, under the conditions generally encountered and for the zones normally used, the rotation is usually less than 30°.

The above method of analysing the echo therefore enables the x-values for the mth and nth maxima to be obtained accurately and hence the true value of $\nabla_{m,n}$ may be used to measure the velocity of the meteor.

6. *The significance of the method*

(*a*) *Velocity measurement.*—From a consideration of equations (3) and (4) and a similar expression for the pulse echo waveform (1), McKinley proposed the formula

$$v = \sqrt{R_0\lambda}\,\frac{(\sqrt{n}-\sqrt{m})}{\delta t} \tag{6}$$

for finding the velocity of a meteor if the time difference between the mth and nth oscillations, counting from t_0, is δt. Now by analogy with the expression given in equation (5) which is used for determining velocities from pulse echoes, the quantity $\sqrt{n}-\sqrt{m}$ of equation (6) must be equivalent to $\nabla/2$ for the same zone.

McKinley chose the 4th and 9th oscillations of the whistle for the reduction of the bulk of his data because $\sqrt{n}-\sqrt{m}$ becomes unity, thus simplifying the calculations. Now from Table I we find that $\nabla_{4,9}$ may have any value between 2·00 and 2·19, so that the value $\nabla_{4,9}=2$ which is in effect given by McKinley is actually the minimum of the possible zone values for this zone. Thus if equation (6) is used the calculated velocity could be in error by as much as 9 per cent. More significant is the fact that the calculated velocity will always be lower than the true velocity.

For the 4th and 9th maxima of a pulse echo the zone value given by the Fresnel integrals (3) is 2·113. In this case the use of equation (6) would lead to an error of 6 per cent.

If equation (6) is applied to zones other than that of the 4th and 9th maxima, the possible error is indicated by the range of values for ∇ given in Table I, since for each zone the quantity $\sqrt{n}-\sqrt{m}$ corresponds to the lower limit. From this it can be seen that quite large errors can be introduced for zones approaching the t_0 point.

However, by taking into account the phase relationship between the ground wave and reflected wave the accuracy of the method of velocity measurement becomes independent of the zone used.

(*b*) *Orbit measurements using a c.w. system.*—The fundamental measurements in meteor orbit determinations are the recording of the times of passage of the t_0 point relative to three spaced stations. With a knowledge of the velocity measured from one station, the time differences give the spatial orientation of the trail and hence the orbit can be determined.

Gill and Davies (4) have described a pulse system for orbit measurements by this method. In their case the time of passage of the 1st maximum of the diffraction pattern was observed at three stations. Since the 1st maximum of a pulse diffraction echo represents a fixed point on Cornu's spiral, the method is equivalent to measuring the time of passage of the t_0 point.

In the c.w. case the position of the 1st maximum on Cornu's spiral depends on the phase difference between ground wave and reflected wave, and in the absence of any knowledge of this phase difference an uncertainty of ± 60 per cent, compared with the pulse case, can arise for each station. If the complete echo waveform from each station is recorded, however, the method of echo analysis given above allows the appropriate points on Cornu's spiral corresponding to the

1st maxima of the three echoes to be identified. As the velocity is known, the corrections to be applied to the measurement of the differences between the times of occurrence of the three maxima may be readily calculated.

With this method, therefore, it should be possible to use a c.w. system to measure meteor orbits to at least the same order of accuracy as given by the pulse system of Gill and Davies.

7. *Adelaide equipment.*—In order to measure meteor velocities, and eventually orbits, an equipment has been constructed to operate in conjunction with the upper atmosphere wind measuring equipment described by Robertson, Liddy and Elford (**5**). Some slight modifications have also been made to the original wind equipment, resulting in an increase in overall sensitivity. A discussion of some preliminary results from this equipment is given in Section 9.

(*a*) *Table for data reduction.*—In order to facilitate data reduction a table has been prepared giving the x-values on Cornu's spiral at 10° intervals of ψ

TABLE II

Values of $\nabla_{m,n}$

ψ	x_2	x_3	x_4	x_5	x_6	x_7
°						
270	2·012	2·833	3·466	4·002	4·473	4·900
260	2·039	2·852	3·483	4·015	4·486	4·911
250	2·065	2·871	3·499	4·029	4·498	4·922
240	2·094	2·891	3·514	4·043	4·510	4·934
230	2·119	2·910	3·540	4·057	4·523	4·945
220	2·145	2·929	3·556	4·070	4·535	4·956
210	2·170	2·948	3·562	4·084	4·547	4·967
200	2·196	2·967	3·577	4·098	4·559	4·979
190	2·221	2·985	3·592	4·111	4·572	4·990
180	2·245	3·004	3·608	4·125	4·584	5·001
170	2·270	3·022	3·623	4·138	4·596	5·012
160	2·294	3·040	3·638	4·151	4·608	5·023
150	2·318	3·059	3·654	4·165	4·620	5·034
140	2·342	3·077	3·669	4·178	4·632	5·045
130	2·365	3·095	3·684	4·191	4·644	5·056
120	2·388	3·113	3·699	4·205	4·656	5·067
110	2·411	3·130	3·714	4·218	4·668	5·078
100	2·434	3·148	3·729	4·231	4·680	5·089
90	2·457	3·165	3·744	4·244	4·691	5·100
80	2·479	3·183	3·758	4·257	4·703	5·111
70	2·501	3·200	3·773	4·270	4·715	5·122
60	2·523	3·218	3·788	4·283	4·727	5·132
50	2·545	3·235	3·803	4·296	4·739	5·143
40	2·567	3·252	3·817	4·309	4·750	5·154
30	2·588	3·269	3·832	4·322	4·762	5·165
20	2·609	3·286	3·846	4·335	4·774	5·176
10	2·630	3·303	3·860	4·347	4·785	5·186
0	2·651	3·319	3·875	4·360	4·797	5·197
350	2·672	3·336	3·889	4·373	4·808	5·208
340	2·693	3·353	3·903	4·386	4·820	5·218
330	2·713	3·369	3·917	4·398	4·831	5·229
320	2·733	3·386	3·932	4·411	4·843	5·240
310	2·754	3·402	3·946	4·423	4·854	5·250
300	2·774	3·418	3·960	4·436	4·866	5·261
290	2·793	3·435	3·974	4·449	4·877	5·271
280	2·813	3·451	3·988	4·461	4·889	5·282

for that portion of the spiral covering the 2nd to the 7th loops. Pearcey's tables of the Fresnel integrals (**6**) were used for this purpose.

In Table II the x-values for each loop are tabulated under $x_2, x_3, \ldots$. It must be remembered, however, that since the spiral is a continuous curve it sometimes happens that, for example, the 5th maximum actually lies on the 6th loop or vice versa.

As the 9th loop of the spiral is not included in Table II (Pearcey's tables do not extend sufficiently far to include this loop), echoes for which the 4th and 9th maxima are used must still be solved graphically. However, if warranted, the table could be extended by other means to cover the 9th loop.

8. *Factors affecting velocity measurement.*—In addition to the inherent limitations of the equipment, three physical factors may lead to inaccuracy in velocity measurements by radio reflections, viz. non-uniformity of ionization along the trail, wind shear, and diffusion of the trail during formation.

(*a*) *Non-uniformity of ionization.*—Some meteors are known to produce bursts of ionization along their paths. The result is that there is local distortion of Cornu's spiral for the wave reflected from the trail which thus alters the diffraction pattern observed at the receiver. The effect is possibly more serious in the case of c.w. than pulse observations because of the vector sum involved in the production of maxima. However the number of meteors which show bursts of ionization is quite small, and in any case serious irregularities in ionization will be detectable in the c.w. system as distortion of the whistle amplitude, and these can be rejected during the reduction of the data. Another source of non-uniformity of ionization arises from the change in ionization along the trail as the meteor evaporates in the Earth's atmosphere. The worst case arises when the meteor enters the atmosphere at near vertical incidence, when the ionization along the trail may change by as much as 10 per cent per km. The effect of such an ionization gradient on the measurement of velocities requires further investigation since in the mathematical development of the Fresnel diffraction theory of meteor echoes a uniformly ionized trail is assumed.

The effect of both positive and negative ionization gradients of 10 per cent per km has been considered. By comparison with Cornu's spiral for a uniformly ionized trail, both the shape and focal point of the spiral are altered. However, the combined effect of these distortions of the spiral is such that for any particular maximum of the c.w. echo waveform the error in the phase of the reflected wave does not exceed 4°. Reference to Table II shows that the resulting error in the difference in "x-values" on the spiral for any two maxima is negligible.

(*b*) *Wind shear.*—Kaiser (**7**) has investigated the effect of a uniform wind shear on velocity measurements with pulse equipments. For a wind shear of 10 m/sec/km of trail length he finds that the difference between the apparent and true velocities for a meteor with a velocity of 40 km/sec is less than 1 per cent.

The effect of wind shear on c.w. measurements is to cause a non-uniform rotation of the ground wave vector relative to Cornu's spiral. We would therefore expect a linear extrapolation of the body Doppler beat into the region of the whistle to lead to an error in velocity measurement.

The error in neglecting the effect of wind shear depends on the ratio of the wind gradient to the line of sight component of the wind at the t_0 point. Thus the greatest error is likely to arise when the line of sight component of the wind is small, as indicated by a very low frequency body Doppler. The error will

also be greatest when the meteor velocity is low, as the extrapolation is then made over a longer period of time.

The highest wind gradient recorded at Adelaide is less than 10 m/sec/km, and the lowest frequency body Doppler which triggers the recording system is of the order of 1·5 cycles/sec, corresponding to a line of sight component of the wind of about 8 m/sec. An upper limit to the error may thus be found by assuming an actual wind speed of 8 m/sec at the t_0 point, towards or away from the observer and a wind shear of 10 m/sec/km. Since the aerial system is such that most of the trails which are detected are formed at a low inclination to the horizontal we shall consider the effect of the above conditions on a meteor of velocity 20 km/sec forming a trail inclined at 30° to the horizontal at a range of 100 km.

If the zone defined by the 2nd and 7th maxima is used, it is found that the measured velocity is in error by 1 per cent if the effect of wind shear is neglected. This error is even less if intermediate zones such as that of the 7th and 4th or 6th and 3rd maxima are used.

Since the wind gradient encountered above Adelaide only occasionally exceeds 2–4 m/sec/km the effect of wind shear on velocity measurement with the c.w. system may be neglected.

(*c*) *Diffusion of the trail during formation.*—Ellyett (**8**) has considered the effect of diffusion of the trail during formation and the consequent decay of the echo on the pulse diffraction pattern. He finds that the lengths of the zones immediately following the t_0 point are altered by 10–12 per cent under conditions of severe diffusion, but after the 3rd zone, the variation is much less than 1 per cent.

The effect is much less serious in the case of the zones before the t_0 point used in the c.w. measurements, owing to the time dependence of the diffusion and the vector sum involved in the production of the maxima of the echo, and may be neglected.

9. *Discussion of preliminary results.*—Fig. 7 shows the distribution of velocities of 65 sporadic meteors measured using the c.w. system at Adelaide. Fig. 7 (*a*) is the distribution (v_1) obtained by applying McKinley's formula, Fig. 7 (*b*) the distribution (v_2) for the same meteors when corrected for ground wave phase. The majority of echoes were analysed by using the zone defined by the 2nd and 5th maxima, the remainder by the zone of the 4th and 9th maxima, and the zone of the 2nd and 4th maxima.

Fig. 8 is a plot of the difference between v_1 and v_2 against v_2 for each meteor. From this diagram it is clear that the error is essentially negative as would be expected from the discussion in Section 6 (*a*). The same trend is indicated by comparison of the means of the two distributions of Fig. 7, viz. 34·5 km/sec for v_1 and 38·0 km/sec for v_2.

The broken line in Fig. 8 is the least squares fit for the plotted values. It will be seen that the average error increases with velocity in such a way that the average percentage error is constant at about −8 per cent. A constant average percentage error would be expected since the error involves only the x-values on Cornu's spiral which are independent of velocity. If the zone defined by the 2nd and 5th maxima had been used exclusively, an average error of about −10 per cent would be expected; if the 4th and 9th maxima had been used exclusively the expected average error would be about −5 per cent (see Table I).

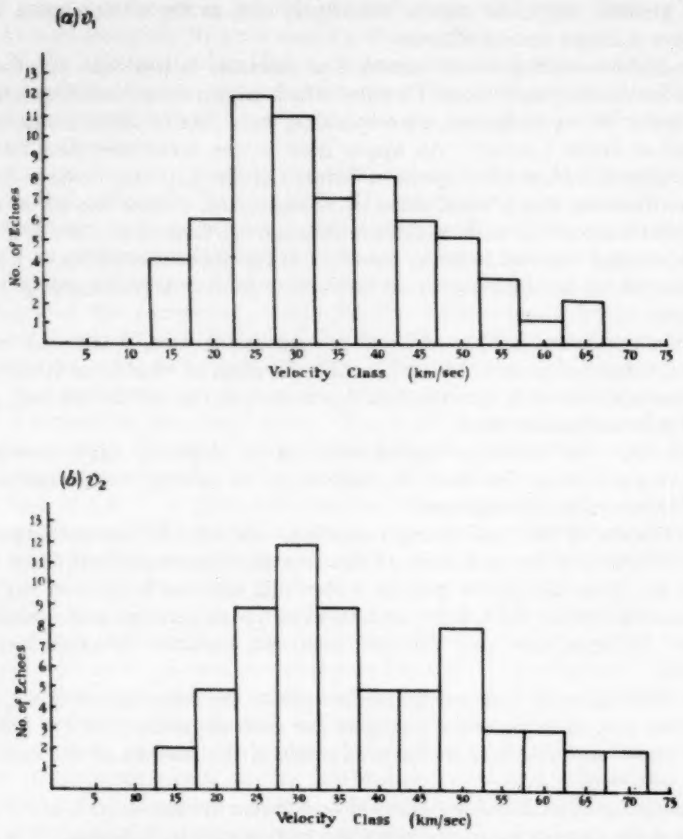

FIG. 7.—*Distribution of velocities of 65 sporadic meteors. (a) ground wave phase neglected, (b) velocities corrected for phase of ground wave.*

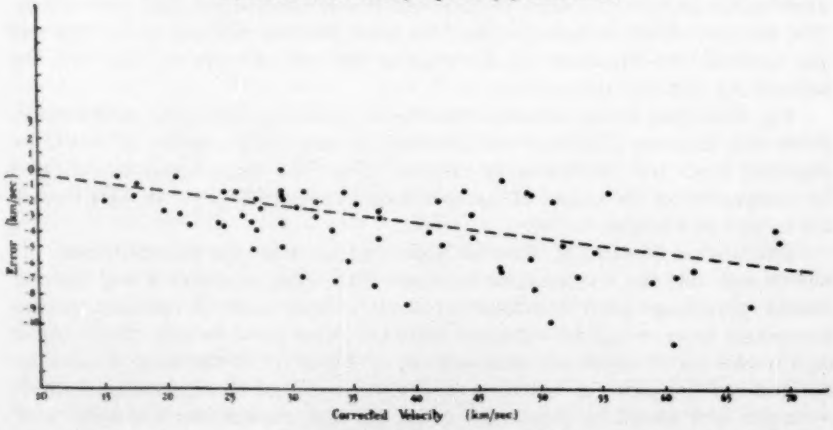

FIG. 8.—*Plot of error v. corrected velocity.*

This assumes that the effect of the rotation of the ground wave vector, being in opposite sense for receding and approaching echoes, tends to cancel over a large number of echoes. This assumption appears to be correct since an average error of -8 per cent is obtained after analysing the majority of echoes by using the 2nd and 5th maxima.

The correction involves a considerable increase in equipment complexity and film reading procedure. If this is not practicable, the systematic negative error can be eliminated by using the mean value for the zone length for each zone, e.g. $\nabla = 2{\cdot}10$ for the 4th and 9th maxima. However an uncertainty of ± 5 per cent for the 4th–9th zone and ± 10 per cent for the 2nd–5th zone etc. would remain, and it would appear that such large errors would be completely unacceptable for most applications of meteor velocities.

Acknowledgments.—The author wishes to thank Professor L. G. H. Huxley for the facilities to carry out this work, and Dr W. G. Elford and Dr A. A. Weiss for many helpful discussions. He also wishes to thank the University of Adelaide and Philips Electrical Industries Pty Ltd, for awarding scholarships which enabled this work to be undertaken.

Department of Physics,
University of Adelaide,
South Australia:
1959 *July.*
Now at the Cavendish Laboratory, Cambridge.

References

(1) D. W. R. McKinley, *Ap. J.*, **113**, 225, 1951.
(2) J. S. Mainstone, W. G. Elford and A. A. Weiss, *Aust. J. Phys.*, **11**, 277, 1958.
(3) J. G. Davies, *Jodrell Bank Ann.*, **1**, 58, 1954.
(4) J. C. Gill and J. G. Davies, *M.N.*, **116**, 105, 1956.
(5) D. S. Robertson, D. T. Liddy and W. G. Elford, *J. Atmos. Terr. Phys.*, **4**, 225, 1953.
(6) T. Pearcey, Table of Fresnel Integrals to 6 decimal places, Melbourne, C.S.I.R.O., 1956.
(7) T. R. Kaiser, *J. Atmos. Terr. Phys.*, Suppl. 2 on " Meteors ", 55, 1955.
(8) C. D. Ellyett, private communication.

THE STRUCTURE AND MAGNETIC FIELD OF THE SOLAR CORONA

J. A. Högbom

(Received 1959 December 10)*

Summary

Observations of the radio star Taurus-A when it passed close to the Sun in June 1958 have shown that the scattering of radio waves in the solar corona is highly anisotropic and this is interpreted in terms of irregularities aligned in the general magnetic field of the Sun. The direction of the field can thus be investigated, and has been found to be approximately radial between 10 and 30 solar radii. The scattering irregularities can be regarded as an extension of the fine structure seen on eclipse photographs. The anisotropic scattering also provides a possible explanation of the observed variations of integrated intensity from the radio star at closest approach.

It is suggested that the corona at maximum phase is expanding and that the observed radial field is the result of localized fields from the surface being carried out in the corona by the expanding gas The typical polar field at sunspot minimum could then be caused by a consistent N–S asymmetry in the localized fields during the preceding maximum phase.

When the extreme minimum corona of the 1954 eclipse is treated as a magneto-hydrostatically stable configuration, the surface field strength at the poles can be calculated. The result, 1·5 gauss, agrees well with the photospheric measurements by Babcock.

---

1. *Introduction.*—When the radio star Taurus-A passes close to the Sun it can be observed through the outer corona. Machin and Smith (1951) and Vitkevitch (1951) showed that this would cause refraction effects and that the electron density in the corona could be calculated if the effective occultation radius is known as a function of radio frequency. The main effect observed, however, proved to be an apparent broadening of the source due to the scattering of the radio waves by irregularities in the electron density of the corona (Machin and Smith 1952, Hewish 1955, Vitkevitch 1955). Hewish showed also that the size of the irregularities must be in the range $1–10^5$ km. This is much smaller than the mean free path for electrons and protons in these parts of the corona. If there are no forces keeping the irregularities together, they must diffuse with a speed comparable with the thermal velocity of the protons and be smoothed out in less than one hour. It is difficult to imagine any mechanism that can replace them at this rate and Hewish suggested that the irregularities represent an extension of the visible polar plumes, maintained by the general magnetic field of the Sun.

The path of a charged particle in a magnetic field is a spiral about a particular line of force which it cannot leave unless it suffers collision with another particle. In the corona, collisions are rare and mass motions and diffusion must take place almost entirely along the lines of force. The conditions along adjacent lines of force may be different; this is likely to be the explanation of the polar plumes (Alfvén 1941, van de Hulst 1950).

* Received in original form 1959 August 14.

This argument can be applied to the irregularities responsible for the scattering of the radio waves, but they must then be filamentary and lined up parallel to the magnetic field. Some evidence for this was obtained in 1956 when it was found that scattering, measured in a N–S direction, was greater than that measured E–W (Hewish 1958). Similar results were reported by Vitkevitch (1958) from observations of the same occultation as that described here. It is, however, necessary to make simultaneous observations in three different directions to determine the direction of maximum scattering uniquely. This is at right angles to the mean direction of the filaments and the magnetic field along the line of sight. Observations were made in Cambridge in 1958 June using three interferometers and the direction of the magnetic field could be determined out to a distance of $30R_{\odot}$.

A large reduction of integrated intensity from the radio star occurs at 38 Mc/s when it is observed near closest approach. Changes of integrated intensity have also been observed by Blum and Boischot (1958) at 169 Mc/s and by Slee (1959) at 85 Mc/s, and were by these authors ascribed to refraction effects. On the other hand, Hewish (1958) found that it is not possible to account for these changes on the basis of isotropic scattering and refraction unless the mean electron density is higher than that determined optically. The observed anisotropic scattering changes the situation, and it is even possible to understand the intensity variations without reference to refraction. This is shown in the Appendix. The observational material is, however, not yet enough to decide whether this mechanism is the main reason for the intensity variations.

2. *The observations.*—Four phase-switching interferometers were used at a frequency of 38 Mc/s. In three of these a 3300 ft E–W corner reflector was combined with smaller aerials to give two axes of length about 45λ SW–NE and SE–NW, and one about 3λ N–S. The latter system was designed to investigate changes of integrated intensity, but it also enabled the large scattering at closest approach to be determined directly from the broadening of the response of the 0°·8 fan beam. A 133λ E–W interferometer was also used which, when combined with the skew axis pair, made it possible to determine uniquely the direction of maximum scattering.

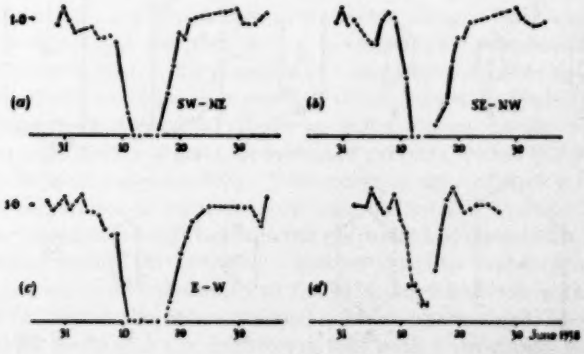

FIG. 1.—*The normalized response of the Crab nebula as observed with the three interferometers (a), (b), (c), and the integrated intensity as measured with the fan beam (d).*

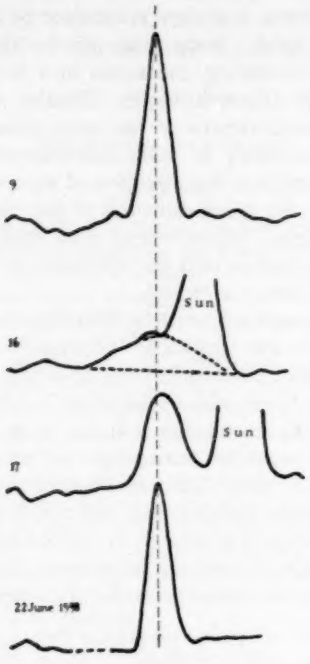

FIG. 2.—*Examples of fan beam tracings.*

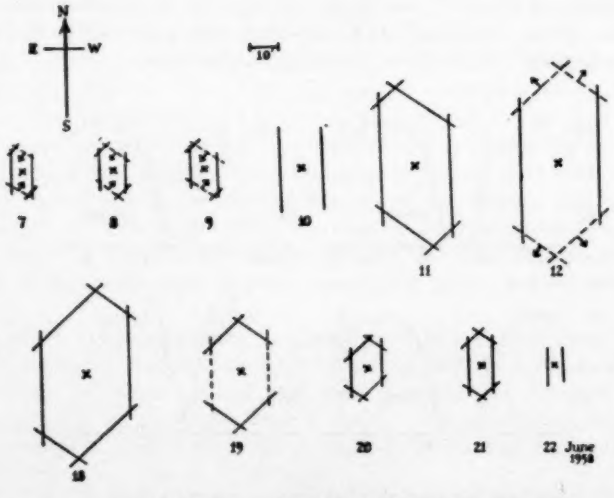

FIG. 3.—*The apparent dimensions of the Crab nebula.*

The four occultation curves are shown in Fig. 1, and some tracings from the 3λ total power system in Fig. 2. The corresponding diameters (Fig. 3) were calculated from these observations assuming Gaussian brightness distributions and refer to the widths between exp(−1) points. The direction of the magnetic field, i.e. that at right angles to the maximum scattering is plotted in Fig. 4. This is within the observational errors directed radially away from the Sun.

FIG. 4.—*The direction of the coronal magnetic field as indicated by the anisotropic scattering.*

Fig. 3 also shows that the scattered distribution as seen from the Earth cannot be purely linear at right angles to the radius vector from the Sun. A linear distribution can be expected only if all the filaments are lined up exactly parallel to each other. There is certainly some misalignment of the filaments along the line of sight which would cause a broadening; furthermore, radially orientated filaments can be regarded as parallel only where the scattered distribution occupies an angle which is small compared with the distance to the Sun (see Appendix).

3. *The structure of the maximum corona.*—The observations were made close to a maximum in the sunspot cycle and typical eclipse photographs at this phase show a spherically symmetrical corona with fine structure directed approximately radially away from the Sun. This structure can now be observed as far out as $30R_\odot$ by radio means. The configuration of the magnetic field, as outlined by the structural details, is such that it cannot be due to currents entirely inside the Sun (Gold 1955). This shows that the field is to a very great extent determined by the movements of the coronal electron gas.

There is, at sunspot maximum, a great number of localized photospheric fields all over the solar disk (Babcock and Babcock 1955) and these are presumably connected with the arches seen in the lower corona. The electron density and the temperature in these is higher than in the surroundings. Such a configuration is likely to be expanding and this gives a mechanism for transporting magnetic fields out into the corona. The presence of a magnetic field does not change the hydrostatic equilibrium along any one line of force (van de Hulst 1950). If a high gas pressure is maintained above an active region on the surface, it is necessary for equilibrium to have an increased pressure within the whole region occupied by its local magnetic field. The energy density of such a field falls off steeply with height, and at some distance from the surface, this will be less than the difference in kinetic energy between the gas inside and outside the field region. Thus, at some height, the structure becomes unstable and expands and the expansion may continue indefinitely as the field, stretched out in this way, will be too weak to contain the excess pressure. Many of the details seen on eclipse photographs certainly give the impression that such a process is going on (for instance the drawings of the corona communicated by the Astronomer Royal and published by the Society (1927)).

The radial magnetic field gives a strong indication that the corona as a whole is expanding, but the velocity does not have to be very high. The diffusion of the lines of force through the coronal gas is very slow because of its high electrical conductivity. The field will remain approximately radial as long as expansion velocities dominate those of this diffusion. A radial field does not necessarily require the very high velocities, 500–1000 km/s, proposed by Parker (1958).

Chapman (1957) made a detailed analysis of the corona, regarded as a quiet atmosphere. All heating is here supposed to be from the surface by thermal conduction. The inner parts of the corona are thus kept at a temperature T_0, and the corona is taken to be in gravitational equilibrium with the Sun. With $T_0 = 10^6$ °K, the computed electron densities agree very well with those measured. Chapman's model can be in equilibrium only if interstellar densities are very much higher than those observed (Parker 1958), and the influence of magnetic fields has been ignored. A static corona would have to rotate with the Sun as a rigid body and the centrifugal force then becomes important at distances $> 30R_\odot$. The thermal conductivity can also be changed by the presence of magnetic fields. It seems possible, however, that the real conditions can be described according to Chapman, if his theory is modified by the introduction of a moderate general expansion.

4. *The structure of the minimum corona.*—An extreme case of a quiet minimum corona was observed at the 1954 eclipse. It possessed a high degree of symmetry and seemed to be completely undisturbed by local fields from the sunspot belts. If this is a stable configuration, all mass motions must take place along the lines of force of a stationary magnetic field. The equatorial streamers, which are probably parts of an uninterrupted belt around the Sun, converge and break up into narrow spikes at about $5R_\odot$. The general expansion velocity inside this belt must be small, because it would otherwise lead to impossible velocities inside these spikes.

It would be interesting to know if this configuration satisfies the magneto-hydrostatic equations, but the calculations have not yet been made. It is, however, easy to calculate what the polar field must be if this corona were approximately in hydrostatic equilibrium. It is well known that the effect of a magnetic field is equivalent to a pressure $H^2/8\pi$ at right angles to the field together with a tension $H^2/8\pi$ along the lines of force. The latter term is important mainly where the lines of force are curved. The contours of the equatorial streamers were in 1954 practically straight at about $3R_\odot$ from the centre of the Sun, and if extrapolated to this distance, this would also hold for the polar plumes. In this case, the sum of the kinetic gas pressure $2kTN_e$ and the component of the magnetic lateral pressure at right angles to the radius vector, $(H^2/8\pi).\cos\kappa$, must be a constant on the surface $R = 3R_\odot$. Thus, if the magnetic field is known at any point on this surface it can be calculated everywhere else from the known gas densities and temperatures.

The general field is known to have had different polarity in the two hemispheres (Babcock and Babcock 1955) and the equatorial field can then be expected to be very weak; the absence of structural details inside the streamers supports this view. Assuming that the magnetic pressure on the equator is negligible one gets for the polar field at three solar radii:

$$H^2_{pol}/8\pi \approx 2k\,.\,T\,.\,\Delta N_e.$$

At this distance the equatorial density was $3{\cdot}4 \times 10^5$ cm^{-3} (Blackwell 1956). For the polar regions we shall use the value $1{\cdot}6 \times 10^5$ cm^{-3} (Michard 1954). The temperature in both regions is probably close to 7×10^5 °K (de Jaeger 1959). The polar field strength at $3R_\odot$ then becomes $3{\cdot}0 \times 10^{-2}$ gauss.

The polar rays show the configuration of the field out to about $2R_\odot$. If they are extrapolated to $3R_\odot$, it becomes possible to relate the coronal field to the surface field at the poles. This is then found to be about 50 times stronger or 1·5 gauss, in excellent agreement with measurements of the Zeeman effect in the photosphere (Babcock and Babcock 1955).

Gold (1956) showed that the existence of the polar rays requires a field of at least one gauss to balance the excess pressure, and Conway (1956) could set an upper limit of 2·5 gauss from the absence of detectable circular polarization of the radio waves from the quiet Sun. Three independent determinations give a value of about 1·5 gauss for the polar field strength in 1954:

(i) Photospheric Zeeman effect.

(ii) The large scale structure of the corona.

(iii) The pressure balance of the polar rays and the absence of detectable circularly polarized radio waves from the Sun.

This good agreement is not likely to be due to a coincidence, and the reasonable assumption that the three methods do in fact measure the same physical quantity leads to some important conclusions:

the photospheric Zeeman effect measures the mean flux through the photosphere, and Alfvén's (1956) objection to the method does not apply;

the polar field in the corona equals the mean field through the photosphere and there is no electromagnetic shielding;

the hypothesis that the corona of 1954 was a quiet atmosphere, subject only to the forces of gravity and a general magnetic field, has given the right value of the field strength; and

the surface field strength at the poles was approximately 1·5 gauss.

The energy density of the general magnetic field is comparable with the kinetic energy of the coronal gas, and there are certainly ways in which gas and fields interact. This points at a connection, and it seems easier to think of the gas movements as determining the field than the other way round. If there is any N–S asymmetry in the fields that are carried out in the corona during the maximum phase of the solar cycle, there will be a residual magnetism left over in the polar regions. The polar field should then change sign from one cycle to the other because this is known to be the case with the sunspot fields. Babcock (1959) has reported such a change from his magnetograph observations. It has recently changed to a S magnetic pole in the northern hemisphere; during the last cycle the following (northern) spot in a typical dipolar group had this polarity.

5. *The fine structure of the corona.*—Hewish (1955) found that the scale l of the scattering irregularities was in the region 1–10^5 km. At the upper limit the required variations in the electron density were about the same as the electron density itself and he suggested that the irregularities may represent an extension of the polar rays. The electron density in these is 5–10 times the mean density (Saito 1958) and, if extrapolated to the outer corona, their width would be about 10^5 km. They do not appear at sunspot maximum, but photographs show

a great number of other fine rays which may be the cause of the scattering. The theory of Chandrasekhar (1952) gives for the r.m.s. scattering angle ϕ:

$$\phi = \frac{2}{l} L.$$

Following Hewish we set L, the r.m.s. difference in electrical length for waves passing the corona, equal to the path difference introduced by one irregularity times the root of the number n of irregularities encountered:

$$L \approx \tfrac{1}{2} l . \Delta\epsilon \sqrt{n}.$$

ϵ is the dielectric constant.

$$\phi = \Delta\epsilon \sqrt{n} = 2{\cdot}8 \times 10^{-8} \Delta N_e \sqrt{n} \quad \text{radians at } 38 \text{ Mc/s}$$

when expressed in terms of the variations of the electron density. Assuming that the rays in the maximum corona, like the polar rays, have electron densities 5–10 times the mean density we find at $15 R_\odot$ with Blackwell's (1956) electron densities:

$$\phi = (0{\cdot}6\text{–}1{\cdot}1) 10^{-2} \sqrt{n} \quad \text{radians.}$$

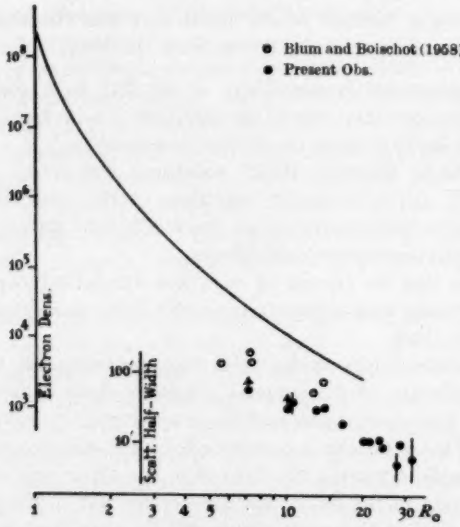

FIG. 5.—*The measured coronal scattering compared with the equatorial electron densities of Blackwell.*

The observed scattering at this distance is $30' = 0{\cdot}9 \times 10^{-2}$ radians. If the radio waves encounter only a few of these rays they will be scattered through an angle large enough to explain the observations. Thus it is possible to account for the observed scattering in terms of the known structure, provided this can be extrapolated to the outer corona. There is on present evidence no need to introduce any unknown small scale structure.

On the simplest possible model the diameter of the rays is set proportional to the distance from the Sun, and the ratio of the electron densities inside and between the rays assumed to be a constant. The scattering should in this case be directly proportional to the mean electron density. The present measure-

ments at 38 Mc/s and Blackwell's electron densities are compared in Fig. 5. Some measurements by Blum and Boischot (1958) at 169 Mc/s have been included to get points closer to the Sun. These have been scaled by a factor $(169/38)^2$ and the direction of maximum scattering assumed to be at right angles to the radius vector from the Sun. The points define a curve which, within the limits of error, is parallel to that of the electron density on the logarithmic scale.

Acknowledgments.—It is a pleasure to express my thanks to Dr A. Hewish for many valuable discussions and advice. I also want to thank Naturvetenskapliga Forskningsrådet (Swedish Natural Science Research Council) for a generous maintenance grant.

Stockholm,
Sweden:
1959 *December* 8.

(*Now at Leiden Observatory, The Netherlands*)

Appendix

The anisotropic scattering makes the situation complicated near closest approach. We shall here use an extremely simplified model of the coronal scattering in order to show the kind of effects that may occur. In this model refraction is ignored, the scattering is supposed to be only at right angles to the radius vector from the Sun and to obey a power law $\phi(\rho)=\phi_0\rho^{-s}$ for the half-width of the scattering angle.

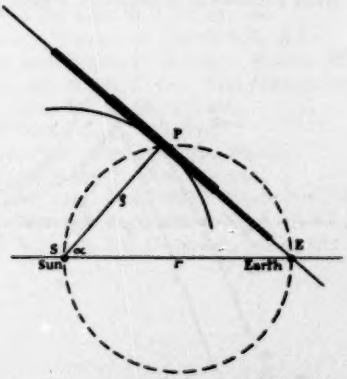

Fig. 6.—*Scattering by radially orientated filaments near closest approach.*

Fig. 6 shows the relative position of the Sun and the Earth as seen from the radio star. The rays incident on the corona at some point *P* will be scattered along a line *PE* at right angles to the radius *SP*. The locus of points from which some scattered radiation may reach the Earth is thus the circle *SPE*. This would also be the apparent shape of the source seen from the Earth, but the inner parts of the circle will contribute very little as the scattering here is very large and the

incident power spread over a large angle. We want to know the total flux received at the Earth. The waves will be regarded as scattered with equal intensity through the angle $2\phi(\rho)$. A Gaussian power distribution will be approximated later, using the results obtained for three values of $\phi(\rho)$, namely $\frac{1}{2}\phi_0\rho^{-s}$, $\phi_0\rho^{-s}$ and $\frac{3}{2}\phi_0\rho^{-s}$. Of the flux incident on the corona at the distance ρ (Fig. 6) a fraction

$$\frac{dr}{\phi(\rho)\sin\alpha}$$

appears between r and $(r+dr)$. For unit power density, the total power available from the annular region of radius ρ is $2\pi\rho\,d\rho$. The area of the region at r is $2\pi r\,dr$. The intensity at r due to the region at ρ is then:

$$\frac{\rho}{r}\frac{d\rho}{\phi(\rho)\sin\alpha},$$

and the total flux F:

$$F(r)=\int_0^r \frac{\rho}{r}\frac{d\rho}{\phi(\rho)\sin\alpha},$$

inserting $\phi(\rho)=\phi_0\rho^{-s}$ and $\rho=r\cos\alpha$:

$$F(r)=\frac{r^{s+1}}{\phi_0}\int_0^{\pi/2}(\cos\alpha)^{s+1}\,d\alpha.$$

For small values of r, the Earth lies within the scattered distribution whatever the position of P on the circle SPE, but when r is large there are two regions contributing to the integral. The observations at about $15R_\odot$ are regarded as the most accurate, and give a relation between ϕ_0 and s. The other observations (Fig. 5) are consistent with a value of s between 2 and 3. The function $F(r)$ is

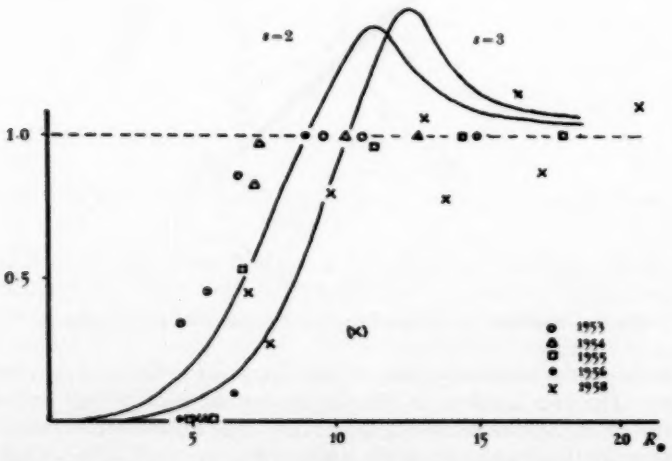

FIG. 7.—*The expected variation of integrated flux from the radio star according to the simple scattering model and the observations at 38 Mc/s.*

plotted for these two values of s in Fig. 7 together with available measurements at 38 Mc/s. This mechanism produces a reduction of integrated intensity at distances, where this is observed, but it also requires an enhancement outside the effective occultation radius. This is not observed at 38 Mc/s but has been reported at higher frequencies (Blum and Boischot 1958, Slee 1959).

Such an enhancement must occur on any theory that does not involve absorption because the flux falling on the corona inside the occultation radius cannot disappear. However, the enhancement is very sensitive to a departure from spherical symmetry in the corona; if the scattering law is somewhat dependent on heliographic latitude, the enhancement can disappear for observations close to the equator, but will then appear in excess when the occultation happens near the polar regions. This could explain the different results obtained at different frequencies.

References

Alfvén, H., 1941. *Ark. Mat. Astr. Fys.*, **27A**, No. 25.
Alfvén, H., 1956. *Tellus*, **8**, 1.
Astronomer Royal, 1927, *Mem. R.A.S.*, **64**, 363.
Babcock, H. D., 1959, *Ap. J.*, **130**, 364.
Babcock, H. W., and Babcock, H. D., 1955, *Ap. J.*, **121**, 349.
Blackwell, D. E., 1956, *M.N.*, **116**, 56.
Blum, E. J., and Boischot, A., 1958, *I.A.U. Symp.* No. 9, 282.
Chandrasekhar, S., 1952, *M.N.*, **112**, 475.
Chapman, S., 1957, *Smithson. Contr.*, **2**, 1.
Conway, R. G., 1956, *Obs.*, **76**, 106.
Gold, T., 1955, *M.N.*, **115**, 340.
Gold, T., 1956, *I.A.U. Symp.* No. 6, 275.
Hewish, A., 1955, *Proc. Roy. Soc.* A, **228**, 238.
Hewish, A., 1958, *M.N.*, **118**, 534.
Hulst, H. C. van de, 1950, *B.A.N.*, **11**, 150.
Jaeger, C de, 1959, *Handb. der Physik LII*, 465.
Machin, K. E., and Smith, F. G., 1951, *Nature*, **168**, 599
Machin, K. E., and Smith, F. G., 1952, *Nature*, **170**, 319.
Michard, R., 1954, *Ann. d'Ap.*, **17**, 429.
Parker, E. N., 1958, *Ap. J.*, **128**, 664.
Saito, K., 1958, *Publ. Astr. Soc. Jap.*, **10**, 49.
Slee, O. B., 1959, *Austr. J. Phys.*, **12**. 134.
Vitkevitch, V. V., 1951, *Dokl. Akad. Nauk. U.S.S.R.*, **77**, 585.
Vitkevitch, V. V., 1955, *Dokl. Akad. Nauk. U.S.S.R.*, **101**, 429.
Vitkevitch, V. V., 1958, *I.A.U. Symp.*, No. 9, 275.

STELLAR GROUPS, VII.
THE STRUCTURE OF THE HYADES GROUP

Olin J. Eggen

(Communicated by the Astronomer Royal)

(Received 1959 November 13)

Summary

From a detailed examination of all stars with known proper motion and radial velocity, approximately 200 stars and binary systems, in addition to the known members of the Hyades and Praesepe clusters, have been selected as probable members of the Hyades group. The (M_V, $B-V$)-diagram for less than 50 per cent of these stars for which accurate magnitudes and colours are available shows (1) that evolution in the group has reached stars with $M_V \approx +2^m$, (2) a well-defined Hertzsprung gap ($B-V = +0^m{\cdot}35$ to $+0^m{\cdot}95$) between $M_V = +0^m{\cdot}5$ and $+1^m{\cdot}5$ with the prototype variable δ Scu and the peculiar stars β CrB and γ Cap on the blue edge of the gap, and (3) that, in common with most well-observed clusters, there are at least two group members still on or near the main sequence well above the break-off point —α CVn and γ Cen. A comparison between the group and trigonometric parallaxes shows no large systematic error in the latter and confirms the high weight usually given the determinations made at the Allegheny Observatory.

The space distribution of the group members indicates that (*a*) there are probably many undiscovered members near the Sun in the Southern Hemisphere and (*b*) the group may be elongated in the direction of galactic rotation. The correlation between the velocity of the individual group members perpendicular to the galactic plane and their distance from that plane indicates that this motion may be uncoupled from that in the plane.

More than 50 per cent of the stars selected as group members have at least one known companion. The sixteen main sequence binaries with known orbital elements are found to deviate more from the normal mass–luminosity relation than the two giant systems in the group, α Aur and γ Cen. There are several eclipsing binaries among the group members but complete data are available for only TX Cnc, in the Praesepe cluster, and Z Her. The primary component of Z Her may be a normal main sequence star but the companion is a late-type subgiant which is evolutive.

---

1. *Members of the Hyades group.*—In the first paper of this series (Eggen 1958a, Paper I) and a subsequent note (Eggen 1959a) the probability that the space motion of the Hyades cluster is shared by an equal number of non-cluster stars as well as by the Praesepe cluster was discussed. There seems to be little doubt that these stars form a moving group with a diameter of at least 200 parsecs. If the space motion vectors are designated as U (directed away from the galactic centre), V (in the direction of galactic rotation) and W (toward the North galactic pole), the size and direction of the group's space motion is such as to place it in the (U, V)-plane near the edge of the (U, V)-distribution of the older population I stars (Eggen 1960a, Paper VI). This circumstance has made it possible to detect the presence of the group by the "convergent-point" method (Paper I). However, since the majority of the older population I are moving

in nearly the same direction with only slightly reduced speed, the convergent-point method of selecting group members will not entirely eliminate non-members, especially since the acceptance tolerances on the radial velocity and proper motion criteria of the method have to be made large enough to allow for inevitable observational errors. Furthermore, the convergent-point method fails to allow for the probability that the W-motion may be partly, or even completely, uncoupled from that in U and V.

A preferable method of selecting group members would, of course, be in computing space motion vectors for a large number of stars and then selecting those that have a common motion with the Hyades. This has been done for the few classes of objects for which homogeneously accurate estimates of the parallax are available—photometric parallaxes of late-type main sequence stars (Eggen 1958b, Paper III), dynamical parallaxes of binary stars (Eggen 1959c), photometric parallaxes of peculiar and metallic-line A-type stars (Eggen 1959b) and photometric parallaxes of dwarf A-type and giant M-type stars (Eggen 1960b, Paper VI)—and in all cases the existence of a Hyades group was apparent.

In lieu of accurate luminosity estimates, there are two additional criteria available for judging group membership of stars selected by the convergent-point method: (1) the observed ultra-violet excess and (2) the $(M_V, B-V)$-diagram. Since the Hyades cluster stars show as strong a metallic-line spectrum as observed in the nearby stars, they have been used to define the standard $(U-B, B-V)$-relation (Sandage and Eggen 1959). The field stars of types later than about F0 show an ultra-violet excess, $\delta(U-B)$, of up to $0^m{\cdot}25$ from this relation and, since we can assume that the Hyades group and cluster stars are coeval and, therefore, probably have the same abundance of heavy elements, the presence of an ultra-violet excess might be used to eliminate non-group members. However, interstellar absorption and the presence of undetected companions can also cause an observed ultra-violet excess and for this reason, and because (*a*) very few candidates for group membership have been observed in the ultra-violet and (*b*) it is desirable eventually to test the assumption that group and cluster stars obey the same $(U-B, B-V)$-relation, I have not used this criterion in selecting the stars discussed here. Eventually a form of narrow band photometry such as that described by Strömgren (1950) may be more useful than the observed $\delta(U-B)$ in deciding on group membership for any particular star.

The form of the $(M_V, B-V)$-diagram for the group is well established by the Hyades and Praesepe cluster members and the few well observed field stars for which there seems to be no doubt of group membership. Therefore I have adopted the following procedure in selecting the probable group members listed in Table I. The predicted position angle of the proper motion, θ_c, and the radial velocity, ρ_c, on the assumption of group membership, were computed (with the Hollerith 602A computer of the Nautical Almanac Office) for every star for which an observed radial velocity and proper motion are available. All stars for which $\theta_o - \theta_c < 50^\circ$ and $\rho_o - \rho_c < 20$ km/sec were selected and space motion vectors computed (with a desk calculator) for a range of reasonable values of the parallax using the spectral type only as a guide. If, for any value of the parallax, the resulting values of (U, V) could be matched with those of the Hyades cluster, $(U, V) = (+40, -18)$, within ± 3 km/sec in both coordinates the star was accepted as a candidate for membership in the group—the W-velocity

was completely disregarded and no star was removed from the list of candidates on the basis of the W-velocity alone. The group parallax was then computed for these candidates from the relation $\pi_g = 4{\cdot}74\,\mu/45 \sin\lambda$, where λ is the angular distance of the candidate from the convergent point of the Hyades cluster motion: R.A. $= 6^h\,18^m{\cdot}5$, Dec. $= +7^\circ{\cdot}6$. The group parallax derived in this way was used to avoid any prejudice in the resulting values of (U, V). Using the luminosity computed from the group parallax, each star was plotted in a (M_V, Sp.T.)-diagram for the Hyades and Praesepe clusters and accepted as a member if it fell within about 1 magnitude of any sequence of that diagram. In practice it was found that of the stars for which a (U, V)-match with the Hyades was possible, only about two dozen were subsequently rejected because of position in the (M_V, Sp.T.)-diagram and many of these were early B-type or supergiant stars with small and uncertain proper motions. A few additional stars for which the observational data are extremely weak were also eliminated even though the available weak data indicate that they are probably group members. It should be noted that the group parallax, π_g, computed as described above, is dependent only upon the observed proper motion; and although the resulting total space motion will be that of the group, any variation that may exist in the ratio U/V from star to star or dependence of U or V on distance may be masked. This point will be discussed further in Section 3.

The group stars, other than known members of the Hyades (Bueren 1951) and Praesepe (Klein Wassink 1927) clusters selected by the procedure outlined above are listed in Table I. The table contains the following information:

Wilson No.: The number in the radial velocity catalogue (Wilson 1953).

Name: Alternative identification.

V_E, $B-V$, $U-B$: The two-decimal magnitudes and the colours are photoelectrically determined values and are taken from a great variety of sources; a few are previously unpublished determinations made with the McClean refractor at the Cape Observatory. The one-decimal magnitudes are visual estimates. A few determinations of $U-B$, made with the Cape refractor, are given in parentheses.

Sp.: Spectral type on the MK-system when available, taken from a variety of sources, or the Mount Wilson system (Wilson 1953). A few types are from the HD. The types of both components of a binary are given when available.

ρ, Q: The radial velocity and its quality taken from the General Catalogue (Wilson 1953); a few additional values have also been included.

μ_α, μ_δ, S: The mean proper motion and its source. The proper motion of most of the stars is large enough so that the differences between various systems (e.g. N30, GC, FK3) have little effect in the present discussion. The catalogues consulted in forming the mean values are as follows:

1. GC.
2. N30.
3. FK3 and supplements.
4. Greenwich astrographic zones.
5. Yale zone catalogues.
6. Second Greenwich catalogue for 1925.
7. Cape photographic catalogues.
8. A. Reitz, *Annals Lund Obs.*, No. 14, 1957.
9. J. Robertson, Washington Zodiacal Catalogue, 1940.
10. First Greenwich catalogue for 1950 —unpublished.
11. Cin. Pub. No. 20.
12. G. van Herk, *Leiden Annals*, 18, 1957.

A plus sign in the "S" column indicates that published Cape, Washington or Pulkova or unpublished Greenwich positions have been used to improve the GC proper motion.

Notes: The notes at the end of the table contain references mainly to visual and spectroscopic binaries.

TABLE I

Hyades group members

W	Name	V_E	$B-V$	$U-B$	Sp	ρ	Q	μ_α	μ_δ	S
		m	m	m				s	"	
39/40	ADS 48	8·23	+1·44	+1·24	dMo	+	2·0 b	+0·874	−0·162	1
70	ADS 102	6·2			A3	+	0·8 b	+0·107	−0·030	1+, 4
93	HD 691	8·7			dG5	−	3·4 a	+0·205	+0·040	1, 5
120	HR 46	5·4			gM4	−	1·7 b	+0·055	+0·006	1+, 5
208	9 Cet	6·40	+0·67	(+1·72)	dG2	−	6·8 b	+0·390	+0·064	1+
220	HD 2025	8·0			dK6	+	5·9 b	+0·668	+0·088	1+
248	HD 2358	6·6			A5	−	4·0 c	+0·081	+0·008	1+
459	HD 4747	7·11	+0·86		dG7	+	5·0 b	+0·515	+0·112	1+
462/3	HR 203/1	5·6			gFo	+	5·9 a	+0·084	−0·006	1
473	HD 4741	8·2			dG7	+	4·4 b	+0·157	+0·009	1+, 4
500	HD 5153	7·17	+0·94		K3V	+	8·0 c	+0·615	+0·040	1+
565	HR 278	6·5			A4	+	6·0 c	+0·085	+0·003	1+, 4
595	HR 289	6·4			A3	+	3·0 c	+0·088	−0·010	1, 6
624	HR 309	6·4			A3	+11·0 c		+0·105	−0·023	1+, 6
651	78 Psc	6·25	+0·40	−0·01	F5IV	+14·0 c		+0·200	−0·129	1, 2, 3
680	θ Cas	4·32	+0·17	+0·11	A7V	+	9·4 b	+0·228	−0·019	1, 6
726	HR 370	4·94	+0·56		F8V	+11·5 a		+0·695	+0·187	1, 2
781	+12°168	9·2			dK3	+10·0 c		+0·406	+0·020	5
...	HD 8391	7·01	+0·30		Fo IV	+	4·2 b	+0·115	+0·031	1, 7
787	HD 8389	7·89	+0·91	(+2·03)	dKo	+30·6 b		+0·476	−0·032	5
790	47 And	5·5			Am	+13·0 c		+0·078	−0·019	1, 3, 6
805	δ Cas	2·67	+0·14	+0·10	A5V	+	6·7 b	+0·297	−0·047	1, 2, 3
810	HR 410	6·2			dF5	+16·9 b		+0·233	−0·084	1, 6
820	HR 415	6·3			F5	+14·5 b		+0·164	−0·011	1, 6
827	ω And	4·86	+0·36		F4 IV	+10·8 b		+0·350	−0·104	1, 2, 3
846	HD 9070	8·2			dG5	+11·8 b		+0·225	−0·007	1
851	HR 428	6·2			A2	+	9·0 c	+0·080	−0·010	1+, 4
921	UV Cet	12·0			dM6e	+29·0 b		+3·27	+0·55	
934	HR 476	5·5			sg A9	+17·4 b		+0·124	−0·038	1, 6
1116	ADS 1613	7·8			dG5	+16·3 b		+0·164	−0·056	6
1117	HD 12402	6·5			K1 III	+16·2 b		+0·060	0·000	1, 5
1244	20 Ari	5·8			dF3	+26·0 b		+0·174	−0·063	1, 5
1412	HR 733	6·46	+0·28		dA9	+25·0 b		+0·086	+0·034	1+
1530	HD 16855	6·7			A2	+20·0 c		+0·083	−0·022	1, 6
1533	+18°339	8·6			dK4	+27·0 c		+0·430	−0·023	1, 5
1553	μ Cet	4·25	+0·31	+0·05	Fo IV	+28·8 b		+0·283	−0·030	1, 2, 3
1617	HD 17922	7·0			F8	+25·5 b		+0·214	−0·098	1, 6
1627/8	ADS 2218	7·8			dK2, Mo	+32·7 b		+0·266	−0·186	1
1646	+28°503	9·0			dG9	+22·7 b		+0·193	−0·056	1, 5
1649	47 Ari	5·8			dF4	+28·5 b		+0·232	−0·029	1, 2, 3
1675	ζ For	5·6			sg A9	+27·0 c		+0·178	+0·092	1+
1695	ADS 2316	7·5			dF7	+35·0 c		+0·094	−0·005	1+
1741	κ Per	3·75	+1·03		Ko III	+28·8 a		+0·182	−0·156	1, 6
1756	δ Ari	4·33	+1·03		K2 III	+25·0 a		+0·152	−0·007	1, 2, 3
1763	HR 981	5·7			Fo III	+	3·0 c	+0·076	+0·074	1, 2

TABLE I—*continued*

Hyades group members

W	Name	V_E	$B-V$	$U-B$	Sp	ρ	Q	μ_α	μ_δ	S
		m	m	m		"		"		
1835	HD 20600	8·0			dGo	+33·5	b	+0·097	−0·025	8
1854	HR 1001	6·2			dF5	+24·7	b	+0·190	−0·067	1, 6
1906	HD 21531	8·37	+1·34	(+2·36)	dMo	+31·3	b	+0·518	+0·343	1, 5
1945	κ Ret	4·69	+0·38		dF2	+12·0	a	+0·378	+0·375	1, 2, 3
1987	−48°1011	8·57	+1·30		K5 V	+22·0	b	+0·394	+0·330	7
1989	HD 22328	7·6			dF5	+34·6	b	+0·095	−0·043	1, 9
2201	γ Hyi	3·35	+1·64	+1·96	M2 III	+15·5	a	+0·051	+0·114	1, 2, 3
2252	43 Per	5·28	+0·41	0·00	F5 IV	+26·7	a	+0·096	−0·130	1, 6
2285	HD 25153	7·7			dF6	+39·5	b	+0·055	−0·017	8, 10
2376	ADS 3017	8·6			Go IV	+32·6	b	+0·054	−0·037	8
2564	43 Eri	3·97	+1·50		gM I	+24·1	a	+0·058	+0·052	1, 2, 3
2639	HR 1401	6·0			A5	+ 9·9	a	+0·030	−0·081	1, 3
2834	HD 30589	7·9			dGo	+40·0	c	+0·081	−0·025	1+
2872	HR 1554	5·9			F2	+38·0	c	+0·048	−0·035	1, 9
2961	HR 1594	6·3			dF6	+16·7	b	+0·073	−0·343	1
3063	HR 1668	5·6			dF3	+33·4	b	+0·064	−0·150	1, 6
3121	α Aur	0·05	+0·80		G8 III + F	+30·2	a	+0·083	−0·426	1, 2, 3
3220	HD 34987	8·7			dF9	+38·0	c	+0·036	−0·065	1, 5
3469	22 Cam	6·9			dF5	+25·5	b	+0·018	−0·134	1, 6
3482/3	ADS 4239	8·4			gF5, F7	+41·3	b	+0·044	−0·054	1
3694	HR 2094	5·28	+0·31		Fo V	+26·3	a	−0·015	+0·244	1+
3806	39 Aur	5·9			dA8	+34·1	b	−0·034	−0·147	1, 6
3889/90	41 Aur	5·9			Ao	+35·0	b	+0·024	−0·056	1, 6
4505	HR 2556	6·2			G7	+30·7	b	−0·025	−0·068	1, 6
4598/9	ADS 5669	6·6			dF8, G8	+19·4	b	−0·080	−0·260	1+
4644/5	ADS5746	6·0			A2, A2	+27·0	c	−0·015	−0·068	1, 6
4652	HR 2666	5·3			A2	+27·9	b	−0·019	+0·065	1, 2, 3
4656	HR 2672	5·1			A2	+25·1	b	−0·058	+0·141	1+
4664	HD 53532	8·1			dG6	+38·9	b	−0·096	−0·078	1, 5
4708	Ross 986	11·65	+1·65		dM5e	+39·0	d	−0·53	−0·99	11
4812	HD 56578	6·8			dFo	+36·9	b	−0·055	+0·040	1+
5425	18 Pup	5·51	+0·46		dF7	+37·7	b	−0·246	+0·052	1, 2
5561	HD 71053	7·9			dF9	+28·0	c	−0·088	−0·029	5
5641	35 Cnc	6·58	+0·67	+0·25	dF5	+36·0	c	−0·040	−0·012	1, 9
...	HD 74558	6·94	+0·25		A7 III	+18·0	c	−0·097	+0·067	1
5751	γ Cnc	4·73	0·00	+0·03	A1 V	+28·7	b	−0·106	−0·044	1, 2, 3
5873	HR 3546	5·9			gF3	+25·9	b	−0·082	−0·050	1, 6
5874	HD 76318	8·2			dF2	+26·8	b	−0·055	−0·025	8
5912	HR 3588	5·17	+0·25		Fo III	+18·0	a	−0·095	+0·049	1
5914	10 UMa	3·96	+0·42	+0·06	F5 V	+26·4	a	−0·437	−0·255	1, 2, 3
6030	ADS 7251	6·99	+1·43		Mo V	+10·0	a	−1·560	−0·638	1, 6
6047	HD 79765	6·9			dFo	+30·5		−0·162	−0·022	1, 2, 9
...	HR 3752	5·76	+0·16		A2 V	+12·0	c	−0·130	+0·055	1
6213	9 Leo	6·6			dF8	+31·4	b	−0·103	−0·024	1, 5
6241	Ross 85	10·6			dM2	+19·0	c	−0·76	−0·09	7
6327	HR 3916	6·32	+0·55		dG1	+23·0	d	−0·286	+0·085	1+
6351/2	ADS 7589	7·6			dF8, G3	+28·4	a	−0·230	−0·019	1
6545	HR 4062	5·54	+0·38		A2	+ 3·0	c	−0·126	−0·044	1+, 2
6546/7	ADS 7762	7·7			dF5, F8	+15·8	a	−0·120	−0·053	1, 6
6563	α Ant	4·25	+1·48		gMo	+13·3	b	−0·077	+0·007	1, 2, 3
6643	ADS 7871	7·9			dF6	+14·3	b	−0·096	−0·002	1, 12
6754	HR 4253	5·7			gG6	+15·3	b	−0·085	+0·010	1+
6967	HR 4409	5·25	+0·99		gKo	+ 4·3	a	−0·116	+0·018	1, 2

TABLE I—*continued*

Hyades group members

W	Name	V_E	$B-V$	$U-B$	Sp	ρ	Q	μ_α	μ_δ	S
		m	m	m				s	"	
7030	HR 4453	5·37	+0·10		A2	+	9·0 c	−0·090	+0·021	1+
7064	HR 4476	5·44	+1·23		gK2	−	1·0 a	−0·080	+0·017	1+
7136	HD 102357	6·8			F6	+	7·5 b	−0·075	0·000	1, 5
7146	HR 4531	5·9			dA6	+	9·0 c	−0·122	−0·001	12
7162	HR 4543	6·2			A3	+	6·9 b	−0·133	+0·005	1, 3
7202	HD 103676	6·9			Fo	+	9·8 b	−0·156	0·000	1, 5
7235	θ Cru	4·29	+0·27		A5	−	2·4 a	−0·146	−0·005	1
7272/4	ADS 8434	7·5			dF8, G1	+	5·8 a	−0·184	−0·026	1, 6
7397	HR 4694	6·18	+0·29		dA8	+	8·0 c	−0·140	+0·015	1, 5
7491	HR 4746	6·3			Fo	−	12·0 c	−0·092	−0·003	1, 9
...	HD 109200	7·12	+0·82		Ko V	+	0·3 b	−0·537	−0·306	1+
7553	Wolf 424	12·20	+1·70		dM6e	−	5·0 c	−1·86	+0·20	11
7616/7	HR 4821/2	5·27	+0·42	+0·10	dF1, F6	−	12·6 a	−0·123	+0·007	1, 9
7619	γ Cen	2·16	−0·02	0·00	Ao III	−	5·0 a	−0·190	−0·011	1, 2, 3
7625	HR 4827	6·03	+0·39	(+1·59)	dF2	−	2·8 b	−0·181	+0·007	1+
7631	HR 4831	4·62	+1·13		gK3	−	11·7 a	−0·132	−0·041	1
7679	30 Com	5·83	+0·02	+0·05	A2 V	+	1·4 b	−0·098	+0·017	1, 2
7698/9	ADS 8690	7·7			A2, F2	−	13·5 a	−0·077	+0·002	1, 6
7709	38 Vir	6·1			dF6	−	7·1 b	0·260	−0·005	1, 3, 9
7732	α CVnB	5·60	+0·34	−0·03	Fo V	−	3·1 b	−0·235	+0·050	1, 2, 3
7733	α CVnA	2·89	−0·12	−0·32	Ap	−	3·3 b	−0·235	+0·050	1, 2, 3
7759	HR 4926	6·1			dF4	+	0·8 b	−0·226	+0·053	1
7760	+13°2618	9·85	+1·47		dM2e	−	11·0 c	−0·69	0·00	11
7998	HR 5085	5·4			Ao	−	7·0 c	−0·081	+0·036	1, 2, 3
8032	HD 117878	7·1			A4	−	17·0 c	−0·074	−0·007	1, 9
8040	ζ Vir	3·37	+0·10		A3 V	−	13·2 b	−0·286	+0·036	1, 2, 3
8055	HR 5120	5·4			A2	−	9·5 b	−0·092	+0·012	1+
8121	1 Cen	4·20	+0·38		F2 III	−	21·8 b	−0·460	−0·149	1, 2, 3
...	HD 121141	7·18	+0·34		F2 V	−	16·0 c	−0·108	−0·035	1+
8470	HD 127506	8·70	+1·13		dK5	−	12·0 c	−0·480	+0·203	8
8581	ADS 9378	7·30	+0·46		dF5	−	21·1 b	−0·079	+0·045	1, 12
8637	HR 5542	6·38	+0·56		dG1	−	26·9 b	−0·323	−0·035	1, 2
8648	HR 5553	6·06	+0·83		dK1	(−40)	d	−0·453	+0·209	1
...	HD 132301	6·57	+0·46		F5 V	−	21·9 b	−0·194	−0·133	1+
8744	HD 134319	8·48	+0·63		dG5	−	4·3 b	−0·130	+0·100	1+, 4
8748/9	ADS 9507	6·8			dG5, G5	−	34·4 a	−0·181	+0·024	1
8825	ADS 9555	8·1			dGo	−	29·0 c	−0·115	+0·050	1, 5
8863	−7°4003	10·56	+1·61	+1·20	dM5	−	30·0 b	−1·32	−0·04	11
8940	β CrB	3·65	+0·27	+0·12	Fop	−	18·7 a	−0·183	+0·082	1, 2, 3
8961/2	HR 5756	6·1			dA5	−	35·0 c	−0·075	−0·035	1, 9
9100	31 Ser	5·72	+0·09	+0·06	A2 V	−	34·2 b	−0·063	+0·031	1+
9216	ι Nor	4·64	+0·25		A5 V	(−20)	d	−0·120	−0·086	1+
9273	HD 144839	7·2			F2	−	30·0 c	−0·087	+0·027	10
9387	HR 6072	4·03	+1·10		gKo	−	29·2 a	−0·155	−0·051	1, 2, 3
9413	η UMi	5·06	+0·24		dA8	−	9·5 b	−0·083	+0·250	1, 2, 3
9420	ξ CrB	4·54	+1·00		Ko III	−	28·9 b	−0·097	+0·108	1, 2, 3
10175	ξ Ser	3·54	+0·26		Fo IV	−	42·8 a	−0·043	−0·063	1, 2, 3
10205	ω Dra	4·77	+0·38		F5 IV	−	14·0 a	+0·002	+0·323	1, 2, 3
10927	λ Sgr	2·77	+1·06		K2 III	−	43·3 a	−0·045	−0·185	1, 2, 3
11094	HR 7013	6·0			A3	−	16·0 c	+0·013	+0·082	1, 2, 3
11112	ζ Pav	4·02	+1·14		gK3	−	17·0 a	+0·003	−0·160	1, 2, 3
11143	δ Scu	4·60	+0·34		F3 III-IV	−	45·3 b	+0·009	0·000	1, 2, 3
11193/4	ϵ^1 Lyr	4·9			A3	−	32·0 a	+0·010	+0·058	1, 6

TABLE I—*continued*

Hyades group members

W	Name	V_E	$B-V$	$U-B$	Sp	ρ	Q	μ_α	μ_δ	S
		m	m	m						
11195/6	ϵ^2 Lyr	4·6			A3	−27·0	c	+0·010	+0·058	1, 6
11228	111 Her	4·30	+0·15		A3 V	−44·6	b	+0·069	+0·117	1, 2, 3
11384	θ Ser A	4·59	+0·15	+0·09	A5 V	−44·0	b	+0·042	+0·032	1, 2, 3
11385	θ Ser B	4·99	+0·20	+0·07	A7	(−54)	c	+0·042	+0·032	1, 2, 3
11388	R Lyr	3·5–4·5	+1·60		M5 III	−28·3	a	+0·023	+0·079	3, 6
11435	HD 176377	6·6			dGo	−39·5	b	+0·051	+0·194	1
11595	HR 7263	6·2			dF3	−39·7	b	+0·046	+0·068	1+
11853	χ Sgr	5·10	+0·20		A5	−41·8	b	+0·051	−0·057	1+
12320	γ Sgr	4·00	+1·52		gMo	−32·8	a	+0·060	+0·025	1, 2, 3
12374/5	ADS 13256	7·0			dF4, F6	−42·5	a	+0·085	+0·032	1+
12585	HR 7723	6·5			Am	−37·0	c	+0·046	+0·030	1, 5
12954	HD 197039	6·8			dF6	−32·5	b	+0·082	+0·049	1+
12957	HR 7914	6·48	+0·64		dG2	−37·0	b	+0·119	+0·303	1
13078	56 Cyg	5·2			A5	−21·0	c	+0·120	+0·133	1, 2
13081	ADS 14355	6·8			gF2	−28·6	b	+0·049	+0·034	1
13140	HR 8010	6·3			sg G6	−30·6	a	+0·063	+0·006	1+
13163	HD 199580	7·9			dG9	−19·4	b	+0·223	+0·217	1, 6
13172	HR 8035	5·8			gG7	−20·7	b	+0·103	+0·072	1, 6
13192	ADS 14528	8·2			dG7	−37·9	b	+0·243	+0·025	5
13265	HR 8061	5·66	+0·58	(+1·68)	G3 IV	−10·0	b	+0·440	−0·335	1, 2
13269	ADS 14638	7·11	+0·90	(+2·00)	dK1	−37·0	c	+0·385	−0·028	1, 5
13496	HR 8220	5·7			dF2	−24·4	a	+0·122	+0·076	1
13504	HD 204734	8·8			dKo	− 9·7	b	+0·218	+0·179	1
...	HD 205067	7·61	+0·65		G2 V	−26·6	b	+0·208	−0·073	1+
13603	γ Cap	3·70	+0·33		Fop	−31·2	a	+0·187	−0·021	1, 2, 3
13639	HR 8293	6·2			A8+A8	−25·0	a	+0·078	−0·010	1, 9
13868/9	ξ Cep	4·30	+0·35		Am	− 6·7	a	+0·200	+0·088	1+
13936	HR 8435	6·1			gKo	−18·1	b	+0·068	+0·005	1, 9
14105	34 Peg	5·8			dF5	−17·8	b	+0·294	+0·050	1+
14162	39 Peg	6·3			Fo	−18·9	b	+0·157	+0·028	1+
14212	ADS 16111	7·5			dF6, F7	− 4·5	b	+0·090	+0·051	1+, 5
14242	11 Lac	4·40	+1·32		K3 III	−10·0	a	+0·094	+0·112	1, 6
14303	HD 215578	8·0			gG8	−20·7	b	+0·037	+0·011	1
14306	HR 8666	5·8			dA8	−10·2	b	+0·140	+0·031	1, 6
14354	HR 8696	6·1			gG3	+ 1·8	b	+0·110	+0·043	1, 6
14408	HR 8748	4·69	+1·40		K4 III	+ 2·9	a	+0·095	+0·031	1, 2, 3
14417	HR 8735	6·4			F2	−13·9	b	+0·090	−0·003	1, 9
14479	83 Aqr	5·55	+0·29		dFo	−13·0	c	+0·123	+0·016	12
14495	HR 8788	6·1			dF4	−12·0	b	+0·220	+0·060	1+
14594	ADS 16642	7·61	+0·66	(+1·74)	dG4	−16·5	b	+0·175	+0·029	1
14627	96 Aqr	5·55	+0·39	(+1·60)	dFo	− 9·2	b	+0·198	−0·015	1, 9
14662	97 Aqr	5·6			A3	−12·0	d	+0·107	+0·022	1
14688	HR 8901	5·55	+1·06		gK1	−19·3	b	+0·085	−0·023	1+
14690	υ Peg	4·38	+0·61	+0·13	F8 IV	−11·1	b	+0·188	+0·040	1, 2, 3
14713	13 And	5·7			Ao	− 9·0	c	+0·089	+0·016	1, 6
14772	ADS 16830	6·7			Go	− 7·1	b	+0·263	+0·030	1+, 5
14781	14 Psc	6·0			A2	− 2·8	b	+0·104	−0·006	1, 9
14838	HR 8977	6·3			F5	− 0·2	b	+0·233	+0·025	1, 6
14900	20 Psc	5·49	+0·94	(+2·01)	gG8	− 6·9	b	+0·091	+0·010	1, 2, 3
15000	+45°4378	9·5			dMo	+ 4·5	b	+0·563	−0·031	1

NOTES TO TABLE I

39/40	$\Delta m = 0^m.00$
70	$\Delta m = 0^m.18$
120	ADS 180, 12^m 3″
462/3	ADS 683, $\Delta m = 0^m.0$
500	Sp. B, with no orbit
595	ADS 862, $\Delta m = 1^m.5$. Bright star is Sp. B, no orbit.
624	Sp. B, no orbit
787	11^m K6 40″, binary
790	Double lined Sp. B, no period
827	ADS 1152, 12^m 2″ binary
851	Sp. B, no orbit
921	Flare star. Visual binary with $\Delta m = 0^m.5$.
1116	AB, 0″.2 with $\Delta m = 0^m.2$. AB–C, 0″.7 with $\Delta m = 3^m$. See Section 4.
1627/8	$\Delta m = 2^m.24$.
1695	$\Delta m = 1^m.0$
1763	8^m 15″. Sp. B, no orbit
2252	Sp. B. P = 30^d, double lines
2376	$\Delta m = 1^m.0$, binary
2639	ADS 3267, 13^m 40″ binary
3121	ADS 3841, see Section 4. Has cpm with the H component, which is itself binary
3482/3	$\Delta m = 0^m.4$, binary
3889/0	ADS 4773, $\Delta m = 0^m.83$ binary
4598/9	$\Delta m = 1^m.08$, binary
4644/5	$\Delta m = 0^m.1$, binary
4652	Sp. B. with double lines, no period
4708	Sp. B. with range of 110 km/sec, no period
4812	Optical companion to HR 6724
5912	11^m 24″, binary. Spectral type by Evans, Menzies and Stoy (1957); from the luminosity and colour we might expect the spectrum to be similar to that of β CrB, Fop.
5914	$\Delta m = 2^m.07$, see Section 4.
6030	$\Delta m = 0^m.0$, binary
HR 3752	10^m 8″ binary
6351/2	$\Delta m = 0^m.78$ binary
6546/7	$\Delta m = 0^m.5$ binary
6643	$\Delta m = 2^m.0$, see Section 4.
6947	10^m 11″ binary
7030	$\Delta m = 0^m.0$ binary
7162	ADS 8320, $\Delta m = 4^m$ binary
7146	ADS 8311, $\Delta m = 5^m$ binary
7235	Sp. B. with double lines, $P = 24^d$
7272/4	$\Delta m = 0^m.81$ binary
7553	$\Delta m = 0^m.2$ binary
7616/7	ADS 8627, $\Delta m = 0^m.03$ binary. A is Sp. B with $P \sim 44^d$ and B is double lined Sp. B. with $P \sim 1^d.5$
7619	$\Delta m = 0^m.04$, see Section 4.
7698/9	$\Delta m = 0^m.51$ binary
7732/3	ADS 8706
8055	ADS 8966, $\Delta m = 0^m.95$ binary
8121	Sp. B., $P = 10^d$
8581	$\Delta m = 0^m.14$, see Section 4
8648	Sp. B., no period
8748/9	$\Delta m = 0^m.20$ binary
8825	$\Delta m = 2^m$ binary
8940	Sp. B., $P = 10$ years
8961/2	ADS 9681, $\Delta m = 2^m.5$ binary. A is Sp. B. with double lines, no period. B is Sp. B. with a range of 85 km/sec, no period

NOTES TO TABLE I—*continued*

9216	$\Delta m = 0^m.00$, also 8″.5 physical companion 11″, see Section 4
10175	Sp. B., $P = 2^d$
10205	Sp. B., $P = 5^d$
11143	Prototype variable
11193/6	ADS 11635, a quadruple system. $\Delta m(AB) = 1^m.10$, $\Delta m(CD) = 0^m.24$
11384/5	ADS 11853, binary
11388	Irregular variable
12374/5	$\Delta m = 0^m.50$ binary. A is Sp. B.
12585	ADS 13543, $\Delta m = 3^m$ binary
13081	$\Delta m = 3^m$ binary
13140	ADS 14430, $\Delta m = 1^m.39$ binary
13192	$\Delta m = 3^m$ binary
13269	$\Delta m = 3^m$ binary
13639	Sp. B., $P = 6^d$
13868/9	ADS 15600, $\Delta m = 2^m.03$ binary
14105	ADS 15935, $\Delta m = 5^m$ binary
14212	$\Delta m(AB-D) = 0^m.96$, $\Delta m(AB) = 0^m.0$. AB is Sp. B., no period
14303	Forms ADS 16254 with optical companion
14317	ADS 16317, $\Delta m = 1^m.20$ binary
14479	ADS 16497, see Section 4
14495	Sp. B., no period
14594	$\Delta m = 0^m.29$ binary
14627	ADS 16676, $\Delta m = 4^m$ binary. A is Sp. B. with range of 77 km/sec, no period
14662	ADS 16708, see Section 4
14713	Sp. B. with range of 70 km/sec, no period
14772	12^m 13″ binary

The group parallaxes and the resulting luminosities and space motion vectors are listed in Table II.

2. *The $(M_V, B-V)$-diagram.*—Unfortunately, accurate colours and magnitudes are available for less than 50 per cent of the approximately 200 stars and binary systems listed in Table I. The available colours and luminosities are plotted in Fig. 1 which also includes the standard Hyades main sequence (Sandage and Eggen 1959) and the individual Hyades (crosses) and Praesepe (plus signs) cluster members with $M_V < +2^m$.

The following are the most noteworthy features of Fig. 1.

(1) Evolution has apparently reached group members with $M_V \approx +2^m.5$. The three stars above the main sequence at $M_V \approx +2^m.5$ and $B-V \approx +0^m.38$ are known binaries. Also, the few stars falling slightly above the main lower sequence are mostly known or suspected spectroscopic binaries or have faint visual companions.

(2) At the present time stars in the interval $M_V = +0^m.5$ to $+1^m.5$ are evolving across the Hertzsprung gap ($B-V = 0^m.35$ to $+0^m.95$) to the region of the late G-type giants. Two stars are apparently in the process of crossing the gap; a member of the Praesepe cluster and υ Peg (Wilson No. 14690).

(3) The prototype variable δ Scu (Eggen 1956a) is probably a member of the group but, unfortunately, it is very near the apparent convergent point of the group motion, and the velocity is almost entirely in the radial direction. The proper motion is therefore very small (0″.009/yr) and the group parallax is nearly indeterminate. An uncertainty of about $0^m.75$ in the luminosity of δ Scu, obtained from a consideration of both the group parallax and the relatively well determined trigonometric parallax (0″.020 Allegheny, 0″.019 McCormick and 0″.020 Yale) is indicated in the figure. The position of δ Scu

TABLE II

Parallaxes, luminosities and space motion vectors of Hyades group members

W	π_g (0".001)	M_V	U	V km/sec	W
		m			
39/40	90	+ 8.00	+40	−19	−15
70	11	+ 1.4	+40	−17	−17
93	22	+ 5.4	+42	−17	+ 2
120	6	− 0.7	+41	−18	− 2
208	41.5	+ 4.50	+41	−17	+ 5
220	71	+ 7.3	+41	−17	− 8
248	8.5	+ 1.3	+40	−17	− 7
459	55	+ 5.80	+42	−16	− 3
462/3	9	+ 0.4	+40	−21	− 5
473	17	+ 4.4	+40	−19	− 0
500	65	+ 6.23	+41	−19	− 4
565	9	+ 1.3	+40	−19	+ 6
595	9.5	+ 0.8	+40	−21	− 3
624	11.5	+ 1.7	+41	−16	− 5
651	23.5	+ 3.10	+39	−19	− 2
680	25	+ 1.32	+42	−17	0
726	76	+ 4.34	+40	−19	− 9
781	45	+ 7.5	+41	−18	− 1
HD 8391	13	+ 2.58	+40	−18	− 3
787	52	+ 6.47	+41	−21	−24
790	9	+ 0.3	+39	−19	− 8
805	33	+ 0.26	+38	−20	− 1
810	26	+ 4.3	+41	−19	−14
820	18	+ 2.6	+43	−17	− 2
827	40	+ 2.87	+38	−20	− 7
846	23.5	+ 5.0	+41	−20	+ 1
851	9	+ 1.0	+39	−18	+ 4
921	39.0	+15.7	+42	−18	−19
934	14.5	+ 1.3	+41	−17	− 4
1116	20	+ 4.3	+39	−20	− 5
1117	7	+ 0.7	+41	−17	− 3
1244	22	+ 2.5	+40	−19	−11
1412	12	+ 1.86	+40	−18	− 8
1530	10	+ 1.7	+42	−16	+ 5
1533	55	+ 7.3	+42	−16	− 1
1553	37	+ 2.09	+40	−20	− 5
1617	29.5	+ 4.4	+42	−18	− 3
1627/8	43	+ 6.0	+42	−17	−16
1646	25	+ 6.0	+39	−21	+ 1
1649	31.5	+ 3.3	+42	−17	− 1
1675	24.5	+ 2.5	+42	−17	− 4
1695	15	+ 3.4	+40	−19	−10
1741	30	+ 1.14	+42	−17	−11
1756	20	+ 0.84	+39	−15	+ 5
1763	11.5	+ 1.0	+40	−18	− 4
1835	15	+ 4.0	+41	−18	− 5
1854	25.5	+ 3.2	+42	−16	+ 8
1906	84	+ 8.00	+43	−16	− 3
1945	57.5	+ 3.49	+41	−20	− 2
1987	60	+ 7.46	+40	−21	− 4
1989	16	+ 3.6	+40	−20	− 6
2201	13.5	− 1.00	+39	−19	−15
2252	20	+ 1.79	+41	−17	− 8
2285	11	+ 3.0	+41	−18	− 6
2376	11	+ 3.8	+39	−18	− 4
2564	10.5	− 0.93	+37	−19	− 2
2639	10	+ 1.0	+37	−19	−10
2834	21.5	+ 4.5	+42	−17	0
2872	12.5	+ 1.4	+40	−18	+ 1
2961	40	+ 4.3	+38	−18	−10
3063	25.5	+ 2.6	+42	−18	− 3
3121	68	− 0.80	+39	−17	− 9
3220	17	+ 4.9	+38	−18	− 4
3469	18.5	+ 3.2	+39	−17	− 5
3482/3	22.5	+ 5.2	+41	−17	0
3694	29.5	+ 2.70	+41	−18	− 8

TABLE II—*continued*

W	π_g (0″·001)	M_V m	U	V km/sec	W
3806	(22·5)	+ 2·7	+41	−17	−13
3889/0	10	+ 0·9	+40	−17	+ 7
4505	11	+ 1·4	+40	−17	− 7
4598/9	31	+ 4·1	+42	−17	− 6
4644/5	10	+ 1·0	+38	−18	− 3
4652	9	+ 0·1	+43	−17	− 2
4656	19	+ 1·5	+42	−16	− 7
4664	26	+ 5·2	+41	−17	−10
4708	220	+13·38	+43	−16	− 5
4812	13	+ 2·4	+38	−18	−12
5425	45	+ 3·78	+39	−20	−11
5561	(12·5)	+ 3·4	+39	−17	−17
HD 74558	13	+ 2·50	+42	−17	− 5
5751	16	+ 0·75	+39	−20	− 8
5873	13	+ 1·5	+40	−18	− 6
5874	(8)	+ 2·7	+39	−18	−10
5912	12	+ 0·55	+41	−16	−14
5914	70	+ 3·19	+40	−16	− 4
6030	(163)	+ 8·05	+41	−16	−22
6047	25	+ 3·9	+41	−16	− 2
HR 3752	14·5	+ 1·57	+41	−17	−18
6213	15	+ 2·5	+42	−19	+ 1
6241	(80)	+10·1	+42	−18	−17
6327	36	+ 4·10	+41	−20	− 7
6351/2	31	+ 5·2	+42	−16	− 2
6545	14	+ 1·27	+41	−17	− 9
6546/7	15	+ 3·6	+39	−20	− 1
6563	8·5	− 1·10	+39	−20	−13
6643	11	+ 3·1	+39	−18	− 8
6754	9·5	+ 0·6	+41	−17	− 4
6967	12·5	+ 0·64	+41	−18	− 6
7030	10	+ 0·37	+40	−21	+ 1
7064	8·5	+ 0·09	+42	−16	− 2
7136	8	+ 1·4	+41	−20	− 3
7146	13	+ 1·5	+39	−20	0
7162	14·5	+ 2·0	+39	−19	− 3
7202	16·5	+ 3·0	+41	−21	+ 2
7235	15·5	+ 0·24	+40	−18	− 9
7272/4	20	+ 4·0	+39	−21	+ 2
7397	15	+ 2·06	+42	−17	+ 4
7491	9·5	+ 1·2	+41	−18	−14
HD 109200	(55)	+ 5·82	+40	−20	−28
7553	220	+13·9	+42	−16	−11
7616/7	13	+ 0·84	+42	−16	− 8
7619	20	− 1·33	+42	−18	− 3
7625	19	+ 2·42	+40	−19	− 2
7631	14·5	+ 0·42	+42	−17	−18
7679	10·5	+ 0·93	+41	−17	+ 2
7698/9	8	+ 2·2	+40	−21	−11
7709	27·5	+ 3·3	+40	−20	− 5
7732	26	+ 2·67	+41	−17	− 7
7733	26	− 0·04	+41	−17	− 7
7759	24·5	+ 3·0	+41	−16	+ 3
7760	75	+ 9·23	+39	−21	− 7
7998	9·5	+ 0·3	+40	−16	− 8
8032	8·5	+ 1·7	+39	−21	− 9
8040	32	+ 0·90	+41	−18	− 1
8055	10	+ 0·4	+40	−17	+ 8
8121	55	+ 2·90	+41	−17	−12
HD 121141	12	+ 2·58	+43	−18	− 4
8470	58	+ 7·52	+40	−19	− 7
8581	10·5	+ 2·40	+41	−20	− 5
8637	43	+ 4·55	+43	−15	+ 3
8648	(85)	+ 5·71	+42	−16	−21
HD 132301	28	+ 3·81	+43	−16	− 5
8744	18	+ 4·76	+39	−17	+ 2
8748/9	28	+ 4·0	+40	−21	− 9
8825	15	+ 4·0	+38	−21	+ 6

TABLE II—*continued*

W	π_g (0″·001)	M_V m	U	V km/sec	W
8863	(175)	+11·78	+40	−20	+ 1
8940	24	+ 0·55	+38	−21	+ 7
8991/2	12·5	+ 1·6	+41	−20	− 8
9100	11	+ 1·23	+42	−18	− 3
9216	18	+ 0·92	+38	−21	+ 6
9273	14	+ 2·9	+37	−22	+ 2
9387	20	+ 0·54	+41	−17	+18
9413	28	+ 2·30	+41	−17	−12
9420	21	+ 1·15	+41	−18	− 1
10175	33	+ 1·03	+40	−18	− 5
10205	35	+ 2·49	+41	−16	−10
10927	50	+ 1·26	+40	−22	+ 2
11094	9	+ 0·8	+41	−19	− 8
11112	18·5	+ 0·36	+40	−19	+ 1
11143	(20)	(+ 1·10)	+42	−19	+ 1
11193/4	8·5	− 0·4	+43	−17	− 2
11195/6	8·5	− 0·7	+40	−17	− 3
11228	32·5	+ 1·86	+43	−19	− 8
11384	23	+ 1·40	+42	−18	− 3
11385	23	+ 1·80	+42	−18	− 3
11388	12	−1·1, −0·1	+40	−18	− 4
11435	35	+ 4·3	+41	−21	− 2
11595	17	+ 2·4	+41	−18	− 7
11853	22	+ 1·70	+43	−18	− 1
12320	12	− 0·60	+38	−17	−12
12374/5	18	+ 3·3	+42	−21	− 7
12585	9	+ 1·3	+41	−20	− 8
12954	15·5	+ 2·8	+41	−17	− 2
12957	49·5	+ 4·95	+40	−18	+15
13078	21·5	+ 1·9	+41	−17	− 1
13081	8	+ 1·3	+41	−18	− 5
13140	10	+ 1·3	+39	−18	− 7
13163	38	+ 5·8	+40	−16	− 2
13172	15	+ 1·7	+42	−16	− 7
13192	41	+ 6·3	+44	−16	+ 2
13265	60	+ 4·55	+41	−17	− 9
13269	62·5	+ 6·09	+41	−18	+ 3
13496	18	+ 2·0	+42	−19	− 2
13504	30	+ 6·2	+41	−19	− 4
HD 205067	30	+ 5·00	+41	−19	− 3
13603	26·5	+ 0·82	+40	−19	0
13639	10	+ 1·2	+41	−16	− 6
13868/9	23	+ 1·11	+42	−18	−10
13936	8	+ 0·6	+41	−16	− 8
14105	32	+ 3·3	+44	−16	− 6
14162	18	+ 2·6	+40	−20	− 5
14212	11	+ 2·7	+39	−20	− 1
14242	10·5	− 0·50	+38	−19	−12
14303	4·5	+ 1·2	+40	−21	+ 4
14306	16	+ 1·8	+38	−19	− 7
14354	12·5	+ 0·6	+43	−16	+ 5
14408	10·5	− 0·21	+41	−18	− 5
14417	10	+ 1·4	+40	−22	− 5
14479	13·5	+ 1·20	+41	−18	− 4
14495	25	+ 3·1	+42	−16	0
14594	19·5	+ 4·06	+41	−17	+ 2
14627	22	+ 2·26	+38	−20	− 7
14662	12	+ 1·0	+41	−19	+ 1
14688	10	+ 0·55	+42	−17	+ 8
14690	20·5	+ 0·94	+41	−20	0
14713	10	+ 0·7	+39	−22	− 2
14772	28·5	+ 4·0	+41	−19	− 4
14781	11	+ 1·2	+39	−21	−10
14838	25	+ 3·3	+41	−16	− 6
14900	10	+ 0·49	+40	−18	− 2
15000	59	+ 8·4	+40	−16	−11

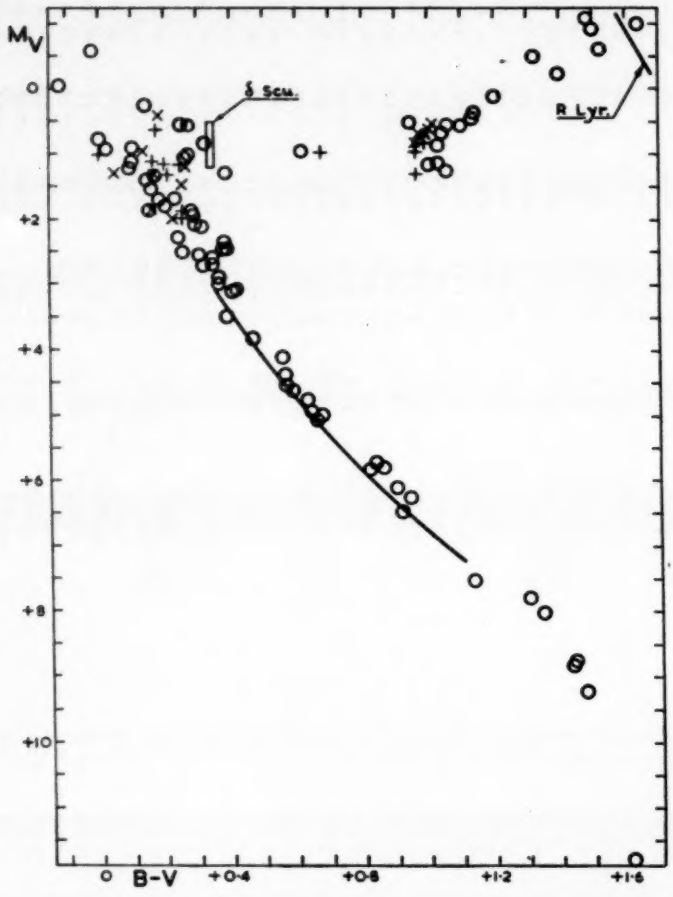

FIG. 1.—*(M_V, $B-V$)-diagram for the stars in Table I with known values of ($B-V$). The standard Hyades main sequence is also shown as well as known members of the Hyades (crosses) and Praesepe (plus signs) clusters with luminosities brighter than $+2^m$. The estimated uncertainty of the luminosity of δ Scu, because of its position near the apparent convergent point of the group motion, is shown by the open bar.*

at the blue edge of the Hertzsprung gap confirms a previous conclusion (Eggen 1957) that this type of variable may be the older type I counterpart of the RR Lyrae stars in the disk and halo populations. The δ Scu variables are sometimes associated in a sequence with another group of ultra-short period intrinsic variables, typified by CY Aqr, AI Vel and SX Phe (Smith 1955) but these objects are undoubtedly members of the disk population (Eggen 1960a, Paper V) and are related to the δ Scu variables only in that they fall in the same region of instability in the (M_V, $B-V$)-diagram.

(4) The semi-regular variable R Lyr, period $\approx 46^d$, is among the reddest and intrinsically brightest group members. Several of the other M-type giant

members have also been found to show small and erratic variations in magnitude. The actual path traced in the $(M_V, B-V)$-diagram during the light variation of R Lyr is unknown because the variation in $B-V$ has not been determined.

(5) Nearly every well observed cluster has been found to have a few stars on or near the main sequence well above the break-off point. The two outstanding examples of this kind in the Hyades group (brighter than $M_V = 0^m$) are the equal components of γ Cen (A0 III) and the peculiar A-type spectrum variable α CVn. The existence of stars in this part of the $(M_V, B-V)$-diagram is unexplained by the evolutionary theory unless the stars are (*a*) "late-evolvers" because of some anomaly in constitution or structure, (*b*) in an advanced stage of evolution and are returning to the main sequence from the M-type giants or (*c*) representative of a second generation of group members created long after the main body of stars.

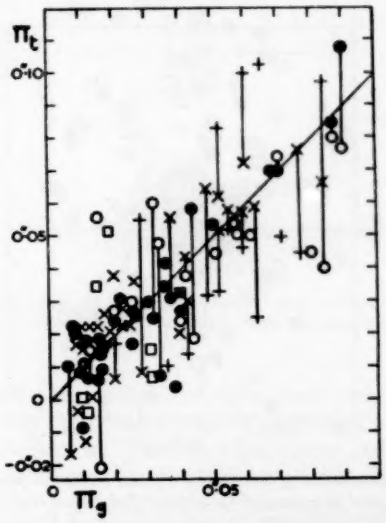

FIG. 2.—*A comparison between the trigonometric and group parallaxes for about 75 per cent of the available material. Values of the absolute trigonometric parallax from various observatories are indicated as follows: Allegheny (filled circles), Yale (crosses), McCormick (open circles), Cape (plus signs), and Greenwich (open squares). Trigonometric values pertaining to the same star are connected by a line. The diagonal line in the figure represents a one-to-one correlation between the two types of parallax.*

(6) No significance can be placed on the obvious gaps in the lower main sequence until colour observations are available for more of the group members in Table I.

Trigonometric parallaxes, mainly from the Cape, Yale, McCormick, Allegheny and Greenwich Observatories, are available for many of the stars listed in Table I. A comparison between the individual trigonometric values, π_t, and the group parallaxes, π_g, is shown in Fig. 2. The trigonometric values pertaining to the same star are connected by straight lines and the origin of the individual values are as follows: Yale (crosses), Cape (plus signs), McCormick (open circles), Allegheny (filled circles) and Greenwich (open squares). There is no obvious systematic error in the run of trigonometric parallaxes; the high

weight usually assigned to the Allegheny determinations seems to be justified. To avoid crowding, only a representative 75 per cent of the available material is shown in Fig. 2.

3. *Space distribution of Hyades group members.*—The spatial distribution of the Hyades group members in Table I is shown in Figs. 3 and 4 where the Sun is at the origin, $(X, Y)=(0,0)$. Fig. 3 contains the objects that are within 20 parsecs of the galactic plane (open circles), between 20 and 30 parsecs from the plane (filled circles) and between 30 and 40 parsecs (crosses). The approximate boundary of the Hyades cluster, which is within 20 parsecs of the galactic plane, is shown as a large open circle. Fig. 4 includes the stars more than 40 parsecs above (filled circles) or below (open circles) the galactic plane. The Praesepe cluster, which lies 80 parsecs above the plane, is shown in Fig. 4 as a large filled circle.

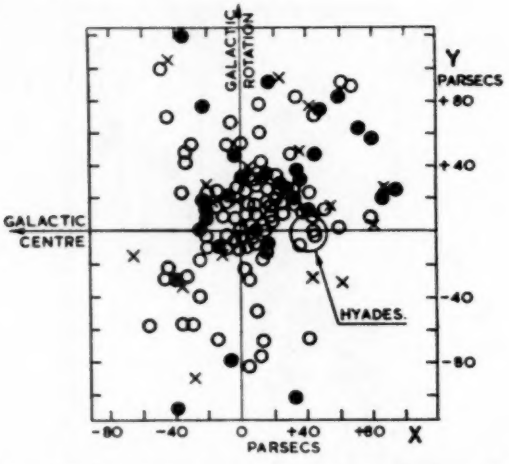

FIG. 3.—*The space distribution of the stars in Table I within 20 parsecs of the galactic plane (open circles), between 20 and 30 parsecs of the plane (filled circles) and between 30 and 40 parsecs of the plane (crosses). The approximate boundary of the known Hyades cluster is indicated by a large open circle; the Hyades cluster is within 20 parsecs of the plane.*

Fig. 3 indicates that (*a*) the group is roughly elongated in the direction of galactic rotation and (*b*) the majority of the group members precede the Sun in the direction of galactic rotation. However, selection effects probably seriously affect the spatial distributions shown in Figs. 3 and 4. This is particularly true of the apparent scarcity of members seen from the Sun in the direction opposite to that of galactic rotation, since this represents a region in the southern hemisphere between $\alpha \approx 8^h - 12^h$. An evaluation of the effect of observational selection on the extent of the group as shown in Figs. 3 and 4 is more difficult. For example, stars nearly 90° or 270° from the apparent convergent point of the group motion are more likely to be included in Table I because the total group motion will then be reflected in the proper motion and, therefore, there is a higher probability that they have been included on observational programmes.

The effects of selection can be largely removed if we regard only those stars in Table I that are brighter than visual magnitude $5^m.5$, since all stars brighter than this limit have been included on both radial velocity and proper motion

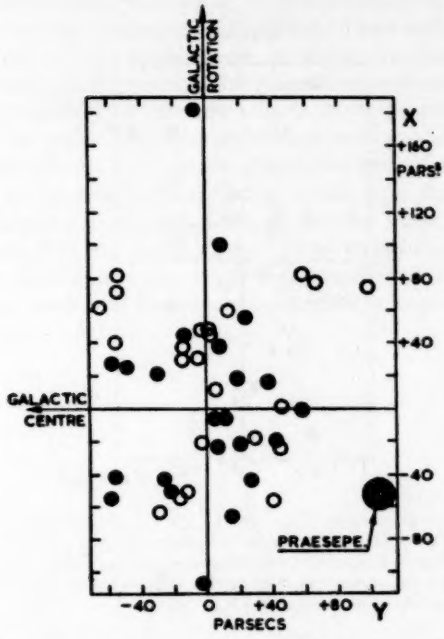

FIG. 4.—*The space distribution of the stars in Table I that are more than 40 parsecs above (filled circles) or below (open circles) the galactic plane. The Praesepe cluster, which is 80 parsecs above the plane, is shown as a large filled circle.*

programmes. The spatial distribution of these stars is shown in Fig. 5 where those within 25 parsecs of the galactic plane are indicated by open circles, those between 25 and 50 parsecs of the plane by filled circles and the remaining stars by crosses. It is obvious from Fig. 5 that the concentration of stars preceding the Sun in the direction of galactic rotation, shown in Fig. 3, is the result of observational selection and that many group members remain to be found in the southern hemisphere. However, the elongation of the group in the direction of galactic rotation appears to be real. The arrow shown in Fig. 5 indicates the direction of the solar motion with respect to the group; the length of the arrow represents the displacement relative to the Sun of the group members in 5×10^5 years. The distribution of group members above and below the galactic plane (including the Sun) can be seen in Fig. 6 (discussed below).

The correlation between the distance from the galactic plane, $|Z|$, and the space motion vector perpendicular to that plane, $|W|$, of the group members in Table I is shown in Fig. 6; stars now above the plane are indicated by filled circles, those below by open circles. The distribution of the values of W is shown in Fig. 7 where the continuous curve represents the computed error curve that gives the best fit to the normal points (filled circles); the median value of W is $-4{\cdot}5$ km/sec.

The full significance of Figs. 6 and 7 can be discussed only when an accurate estimate of the extent of the Hyades group becomes available. However, if the motion perpendicular to the plane, W, is more or less independent of the

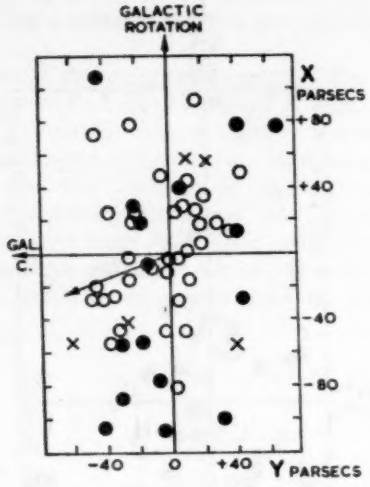

FIG. 5.—*The space distribution of the stars in Table I brighter than visual magnitude 5·5. Stars within 25 parsecs of the galactic plane are shown as open circles, those between 25 and 50 parsecs from the plane as filled circles, and those more than 50 parsecs from the plane as crosses. The arrow indicates the direction of the solar motion with respect to the group; the length of the arrow represents the amount of this motion in* 5×10^5 *years.*

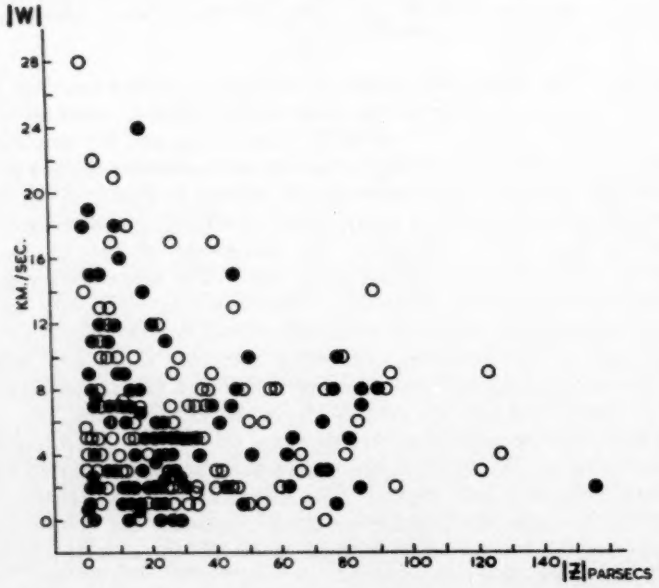

FIG. 6.—*The correlation between the space motion perpendicular to the galactic plane,* $|W|$, *and the distance from that plane,* $|Z|$, *for the stars in Table I. Filled circles refer to stars now above the plane, open circles to those below.*

U- and *V*-vectors of the space motions of the group members, the distribution of $|W|$ with $|Z|$ shown in Fig. 6 is that to be expected. Stars with small values of Z either never leave the vicinity of the plane, in which case they have low values of W or they are now falling through the plane from various distances from it and therefore show values of W directly related to the maximum distance they have travelled to the plane. The relationship between the distance from the plane and the W velocity is, of course, dependent upon the component of the galactic force field at right angles to the plane (Oort 1932, Woolley 1957). The extension of the Hyades group perpendicular to the plane and the observed values of W indicate that the component of force in the Z-direction is greater than that found by Oort and closer to the determination made by Woolley, but a more quantitative result will be better made when a larger number of stellar groups are available for analysis.

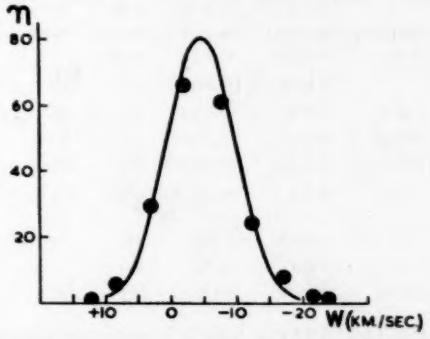

FIG. 7.—*The computed error curve giving the best fit to the observed distribution of the W-vectors which are represented by normal points (filled circles). The median value of W is −4·5 km/sec.*

Woolley (1959) has shown that deviation of 1 to 2 km/sec/100 pcs may result from the small differences in the eccentricities of the galactic orbits that are necessary to keep together isoperiodic groups of widely separated stars. However, as discussed in Section 1, the procedure used here of computing the group parallax from the proper motions may mask this effect. Also, the more distant group members are apparently faint and the observational data, particularly the proper motions, are therefore usually of low weight. When colours of more of the lower main sequence group members are available, the "rocking" (or "rolling") effect predicted by the distance–eccentricity relation can perhaps best be looked for in space motions computed with the aid of photometric parallaxes.

4. *Visual binaries.*—The incidence of binary stars in Table I is very high. 50 per cent of the listed stars have at least one companion and there are many multiple systems. In fact, it was the attempt to explain the existence of these multiple systems, some of which are almost small clusters, that led to the present series of investigations of stellar groups (Eggen 1950).

It has been known for some time that the visual binaries in the Hyades *cluster* show a mass–luminosity relation that deviates from that found for field stars (Kuiper 1937). Periods and semi-major axes, a, for six visual binaries in the cluster are now available and are listed in the first section of Table III. An

TABLE III

Hyades group visual binaries with known orbits

ADS	V_E	$B-V$	M_V	M_B	Mass	P (yrs)	a	π_g	Δm
	m	m	m	m			"	(0".001)	m
3135 A	7·23	+0·52	+4·22	+4·17	0·74 ⊙	90·0	0·545	25	1·04
B	8·27	+0·69	+5·26	+5·19	0·54				
3169 A	7·30	+0·52	+4·29	+4·23	0·80	487	1·715	25	1·19
B	8·49	+0·73	+5·48	+5·41	0·56				
3210 AB	8·28	+0·68	+5·35	+5·28	0·42	28·56	0·23	26	0·10
3248 AB	7·34	+0·53	+4·25	+4·20	1·70	40·4	0·425	24	0·30
3475 AB	7·51	+0·54	+4·38	+4·33	1·04	16·25	0·195	24	0·00
3483 A	6·49	+0·47	+3·58	+3·52	0·85	105·57	0·755	30	1·61
B	8·10	+0·73	+5·49	+5·42	0·55				
102 AB	6·9	...	+2·1	+2·0	3·1	288	0·88	11	0·18
1613 AB	8·5	...	+5·0	+4·95	0·85	12·71	0·13	20	0·1
10 UMa A	4·10	+0·39	+3·33	+3·28	0·90	22·2	0·63	70	2·07
B	6·17	+0·71	+5·40	+5·33	0·58				
7871 AB	8·6	...	+3·0	+2·95	1·15	215	0·52	11	0·5
ε Nor AB	5·39	+0·23	+1·67	+1·45	6·2	26·4	0·37	18	0·0
9378 AB	8·05	+0·46	+3·15	+3·10	1·9	87·7	0·325	10·5	0·14
16497 AB	6·30	+0·29	+1·95	+1·83	3·4	22·0	0·20	13·5	0·03
16708 AB	5·6	...	+1·4	+1·1	5·4	63·2	0·42	12	0·0
6841 A	0·70	...	−0·14	−0·5	3·0	0·285	0·0536	68	0·25
B	0·95	...	+0·11	0·0	2·9				
γ Cen AB	2·91	−0·02	−0·58	−1·6	6·3	84·5	0·895	20	0·04

additional binary, μ Ori (ADS 4617), which is sometimes assigned to the cluster, is omitted here because it is very near the convergent point of the apparent cluster motion and the group parallax is therefore nearly indeterminate. The orbital elements of the binaries discussed here have been taken from the extensive double star literature, except those for ADS 3210, which are unpublished values by D. Jones, and ADS 3475, for which I have derived new elements. The values of a in every case are adjusted to the "standard observers" in a manner previously described (Eggen 1956b); the available values of the magnitude differences between the components have also been discussed in the same reference and were used to derive the individual magnitudes and colours of the components of ADS 3135, 3169 and 3483.

Unfortunately, astrometric determinations of the mass ratios of the components of the binaries in the cluster have not been made. For the three pairs with observed values of Δm less than $0^m{\cdot}5$ I have discussed the mean component. For the remaining stars the mass ratio was obtained from the assumption that the stars obey the mass–luminosity relation (Eggen 1956b); the small error that might be introduced by this assumption has negligible effect on the results derived here. The bolometric magnitudes, M_B, in Table III were obtained from the values of M_V by applying the bolometric corrections previously derived (Eggen 1956b).

The second section of Table III contains an additional eight binaries that are listed in Table I as non-cluster members of the group and are known, from the group parallax, to consist of main sequence, or near main sequence, components.

In all but one case the components of each pair are so nearly equal that the mean component will be discussed here; the exception is 10 UMa, for which the individual magnitudes and colours have been derived, using the known difference in visual magnitude, from the observed magnitude and colour of the combined light.

The values of M_B and of the logarithms of the masses of the stars in the first two sections of Table III are plotted in Fig. 8; the filled and open circles represent, respectively, the primary and secondary components, and the half-filled circles indicate those pairs for which the mean components are described in the table. The continuous line in Fig. 8 represents the mass–luminosity relation, $M_B = +4^m{\cdot}79 - 7{\cdot}8 \log (\text{mass})$ (Eggen 1956b), which will here be called the normal relation. In addition to the pairs in Table III the components of the intrinsically faint binary, Wilson No. 921, of which one component is the flare star UV Cet, are also shown in Fig. 8. The orbital

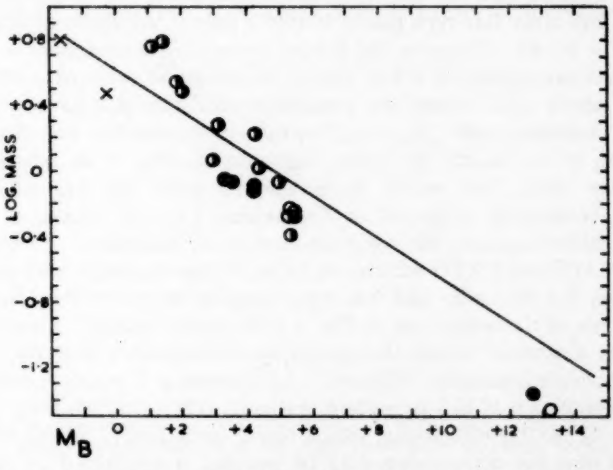

FIG. 8.—*The "normal" mass–luminosity relation is represented by the straight line. The primary components of main sequence Hyades group binaries are shown as filled circles and the secondary components as open circles; half-filled circles represent those systems in which the mean component has been discussed in the text. The crosses represent two giant systems in the group.*

elements, mass and bolometric corrections are those recently derived by van de Kamp (1959) and received after the preparation of Table III. The weakest datum for UV Cet is the bolometric correction, but since this must certainly be greater than 1^m, and a correction of 0^m would be required to place the components on the normal mass–luminosity relation, the deviation of UV Cet from this relation is certain.

It is apparent from Fig. 8 that the deviation for the normal mass–luminosity relation, suspected for the cluster members, is confirmed by the non-cluster group members. Furthermore, this deviation is not merely a matter of a systematic error in the computed group parallaxes since the two relations seem to intersect, within the rather large scatter, near $M_B \approx +4^m{\cdot}5$. This deviation and the unexpectedly large scatter in the individual mass determinations near $M_B \approx +5^m$ are unexplained and will be more fully discussed, in connection with the mass–luminosity relations for other moving groups, in a later paper.

In addition to the main sequence binaries discussed above there are two giant binaries in the Hyades group, γ Cen and α Aur (ADS 3841). These systems are described in the third section of Table III and the mean components are plotted in Fig. 8 as crosses.

From the interferometric and radial velocity observations of α Aur, Wright (1954) found a parallax, $0''.068$, which is identical to that found from the group motion; the well determined mean trigonometric value is $0''.072$. There is a difference of opinion on the nature of this system; Struve and Kung (1953) consider it to consist of an F-type and a G-type giant, both of which may be peculiar, while Wright regards the components as normal luminosity class III stars of types Go and G5. The available spectroscopic and photometric data are discussed by Franklin (1959). A visual magnitude difference of $0^m.25$ has been adopted in Table III with the later type component being also the brighter; the masses are those determined by Wright from the interferometric and spectroscopic orbits. The luminosity of the bright component, $M_V = -0^m.1$, would fit in with the run of the other late-type giants in Fig. 1 only if the spectral type was near K3 ($B-V = +1.2$). However, the fainter component would then be an A-type star to make the combined colour match the observed value of $+0^m.80$. The observed, nearly equal masses are consistent with stars that have evolved from the main sequence near $M_V = +2^m$ which is reasonable for the late-type component, if we accept the giant sequence in Fig. 1 as representing an evolutionary track, but which is inconsistent with the luminosity of the early-type component unless it is "returning" to the region of the main sequence after completing the red giant stage in its evolution. We might adopt the types Go III and G8 III without violating the spectroscopic and photometric observations but the early- and late-type components would then both lie well above the run of the other stars in Fig. 1 with similar colour. Also, by analogy with Z Her described below, the possibility of anomalous evolution of one or both components cannot be forgotten. In conclusion it is only possible to say that the explanation of this important system is still not satisfactory and *if* it is a member of the Hyades group, which seems quite likely, Struve and Kung's conclusion that the components may be peculiar is confirmed by the present results.

Unless we can invoke the possibility that the components are "returning" to the region of the main sequence, the system of γ Cen is nearly as inexplicable as that of α Aur. The equal components are classified as A0 III and although the masses fall on the normal mass–luminosity relation they correspond to main sequence stars with M_V near $+1^m$ in the Hyades group. It is interesting that the two highly evolved systems in the Hyades group appear, within reasonable limits, to follow the normal mass–luminosity relation, whereas the systems consisting of components on or near the main sequence generally deviate from that relation.

5. *The eclipsing binaries TX Cnc and Z Her.*—The W Ursae Majoris-type variable TX Cnc is known to be a member of the Praesepe cluster. The group parallax and the total light place the system $0^m.5$ above the main sequence at $B-V = +0^m.63$. Therefore the system can be resolved into stars with the following luminosities and colours: (A) $M_B = +4^m.6$, $B-V = +0^m.60$; (B) $M_B = +5^m.2$, $B-V = +0^m.70$. Popper (1948) finds individual masses of $1.5\odot$ and $0.8\odot$ but both the mass ratio and the individual masses derived

from spectroscopic observations of the components of contact systems may be suspect. However, the masses and bolometric luminosities given above place both stars near the intersection of the normal and Hyades group mass–luminosity relations and well within the scatter of the individual visual binaries of the Hyades group; the mass and luminosity of the mean component deviates very little from the normal relation.

The eclipsing system Z Her has a period of almost exactly 4 days. Popper (1956), from two-colour photometry and coudé spectroscopic observations, has derived the following description of the system:

	V_E	$(B-V)$	Mass ($\odot=1$)	R ($\odot=1$)	Sp.
	m	m			
A	7·72	0·48	$1{\cdot}22\pm0{\cdot}06$	$1{\cdot}6\pm0{\cdot}1$	F4
B	8·59	0·91	$1{\cdot}10\pm0{\cdot}04$	$2{\cdot}6\pm0{\cdot}2$	K0

The systemic radial velocity is $\gamma=-46{\cdot}0$ km/sec and the well-determined proper motion is $\mu_\alpha=-0''{\cdot}022$, $\mu_\delta=+0''{\cdot}060$. The group parallax, derived from the proper motion, is $0''{\cdot}018$, which leads to $(U, V, W)=(+44, -18, +1)$.

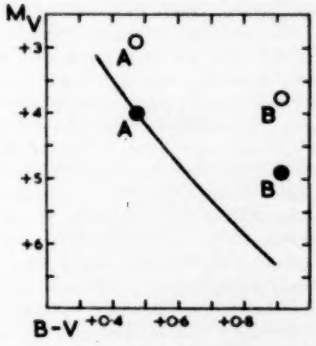

FIG. 9.—*The position of the A- and B-components of Z Her in the $(M_V, B-V)$-diagram derived from parallaxes of $0''{\cdot}018$ (filled circles) and $0''{\cdot}010$ (open circles).*

The resulting luminosities of the two components are shown as filled circles in Fig. 9. The F-type component is a normal main sequence star—Roman (1956) has classified the system as F4 V at maximum light—but the late-type companion falls about $1^m{\cdot}5$ above the main sequence. Since subgiants in this part of the $(M_V, B-V)$-diagram would be expected only after $>2\times10^{10}$ years (Hoyle 1959, Eggen 1960a, Paper V) the companion to Z Her may have undergone a forced evolution of the type described by Huang and Struve (1957). The mass of the bright component places that star slightly below the normal mass–luminosity relation in Fig. 8 and agrees well with the run of the Hyades group main sequence stars. The mass of the fainter component is also approximately that which might be expected for a Hyades group member with its derived luminosity, indicating that the star may have evolved from the main sequence with very little change in luminosity but with a large increase in radius. From the effective temperatures of the components, derived from the spectral types, and by applying a surface-brightness criterion, Popper derived a parallax of $0''{\cdot}010$ for the system. The resulting positions of the stars in the $(M_V, B-V)$-diagram are shown in Fig. 9 as open circles. The resulting values of $(U, V, W)=(+49, -15, +8)$

are not consistent with the motion of the Hyades group unless the observed systemic radial velocity is too large by some 6–8 km/sec; the observed value is based on two nearly identical determinations from independent investigations separated by about 35 years. Since it seems unlikely that the group parallax would accidentally place the primary component on the main sequence, membership in the group seems well established and the luminosities indicated by filled circles in Fig. 9 are probably nearly correct even though the system is fairly near the convergent point of the apparent group motion. Popper also found that the H and K emission lines of the secondary component gave the same systemic velocity as the absorption lines, which gives weight to a previous conclusion (Eggen 1955) that part of the evidence for intra-system calcium clouds in some eclipsing systems is inconclusive.

There are several additional eclipsing binaries, including TT Hya, TX Leo and RS CVn, which may also be members of the Hyades group but the available data are not as complete as those for TX Cnc and Z Her. Both RS CVn and TT Hya may be similar to Z Her.

Royal Greenwich Observatory,
Herstmonceux Castle:
1959 *November* 5.

References

Bueren, H. G. van, 1951, *B.A.N.*, No. 432.
Eggen, O. J., 1950, *Ap. J.*, **112**, 169.
Eggen, O. J., 1955, *Pub. A.S.P.*, **67**, 315.
Eggen, O. J., 1956 a, *Pub. A.S.P.*, **68**, 238.
Eggen, O. J., 1956 b, *A.J.*, **61**, 361.
Eggen, O. J., 1957, *A.J.*, **62**, 45.
Eggen, O. J., 1958 a, *M.N.*, **118**, 65.
Eggen, O. J., 1958 b, *M.N.*, **118**, 560.
Eggen, O. J., 1959 a, *Obs.*, **79**, 143.
Eggen, O. J., 1959 b, *Obs.*, **79**, 197.
Eggen, O. J., 1959 c, *Obs.*, **79**, 206.
Eggen, O. J., 1960 a, *M.N.*, **120**, 430.
Eggen, O. J., 1960 b, *M.N.*, **120**, 448.
Evans, D. S., Menzies, A., and Stoy, R. H., 1957, *M.N.*, **117**, 534.
Franklin, K. L., 1959, *Ap. J.*, **130**, 139.
Hoyle, F., 1959, *M.N.*, **119**, 124.
Huang, S. S. and Struve, O., 1957, *Occ. Notes R.A.S.*, **3**, 161.
Klein Wassink, W. J., 1927, *Groningen Pub.*, No. 41.
Kuiper, G., 1937, *Ap. J.*, **86**, 166.
Oort, J., 1932, *B.A.N.*, No. 238.
Popper, D. M., 1948, *Ap. J.*, **108**, 490.
Popper, D. M., 1956, *Ap. J.*, **124**, 196.
Roman, N. G., 1956, *Ap. J.*, **123**, 246.
Sandage, A. R. and Eggen, O. J., 1959, *M.N.*, **119**, 278.
Smith, H. J., 1955, *A.J.*, **60**, 179.
Strömgren, B., 1950, *Trans. I.A.U.*, **7**, 404.
Struve, O. and Kung, S. M., 1953, *Ap. J.*, **117**, 1.
Van de Kamp, P., 1959, *A.J.*, **64**, 236.
Wilson, R. E., 1953, *Papers of the Mt Wilson Obs.*, VIII.
Woolley, R. v. d. R., 1957, *M.N.*, **117**, 198.
Woolley, R. v. d. R., 1959, *Vistas in Astronomy*, III (in press).
Wright, K. O., 1954, *Pub. Dom. Astroph. Obs.*, **10**, No. 1.

STELLAR GROUPS, VIII.
THE STRUCTURE OF THE SIRIUS GROUP

Olin J. Eggen

(Communicated by the Astronomer Royal)

(Received 1959 December 7)

Summary

One hundred stars with (U, V)-loci that pass within 4 km/sec of $(U, V)=(-14{\cdot}2, -0{\cdot}4)$ are assigned to the Sirius group. The most noteworthy features of the resulting $(M_V, B-V)$-diagram are (*a*) the main sequence of the Sirius group is displaced from that of the Hyades group, ΔM_V (Sirius-Hyades) $= +0^{m}{\cdot}2$, and the main sequence stars with $+0^{m}{\cdot}3 \leq B-V < +0^{m}{\cdot}6$ show an ultra-violet excess of $\delta(U-B)=+0^{m}{\cdot}04$ with respect to the Hyades stars, (*b*) the small amplitude, short period light and velocity variable, δ Del, is a group member with luminosity and colour similar to those found for the prototype variable δ Scu in the Hyades group, (*c*) the presence of bluer main sequence stars and brighter G-type giants in the Sirius group indicates that this group is younger than the Hyades group, and (*d*) there are probably very many undiscovered group members near the Sun. The spatial distribution of the group members gives some indication of elongation in the direction of galactic rotation but because of the smallness of the motion and the resulting incompleteness of the group membership, no definite conclusion can be drawn. The mass-luminosity relation for the visual binaries in the group with $M_V > +3^{m}$ deviates from the normal relation in the same way as the Hyades group binaries in this luminosity range; the Sun is one magnitude fainter than Hyades and Sirius group members of the same mass. The binaries with components brighter than $M_V = +3^{m}$, including the eclipsing binaries β Aur and α CrB, indicate that there may not be a unique mass-luminosity relation for group stars of this luminosity.

---

1. *Members of the Sirius group.*—The first paper of this series (Eggen 1958, Paper I) contained a list of 70 stars selected, by the convergent point method, as members of the Sirius group. Many of these stars have in the past been assigned to the "Ursa Major stream" which appears to share the motion of 6 bright, and 6 fainter, stars in the region of Ursa Major—the so-called "Ursa Major nucleus cluster". Since the Hyades cluster is used to define the motion of the Hyades group (Eggen 1960b, Paper VII), by analogy it might appear reasonable to define the motion of the extended Ursa Major stream by that of the nucleus cluster. However, the position and direction of motion of the nucleus cluster stars cause difficulties in fixing the apparent convergent point of their motion (cf. Petrie and Moyls 1953) and, therefore, the well-determined proper motion, radial velocity and parallax of Sirius, which is known to be a member of the group, were used to define the group motion.

In the previous paper (Paper VII) it was found that the *W*-motions (perpendicular to the galactic plane) of the Hyades group stars may be uncoupled from the *U*- (away from the galactic centre) and *V*- (in the direction of galactic

rotation) motions. Therefore the convergent point method of selecting group members discriminates against members whose W-motion differs from that of the Hyades cluster, which defines the group motion. Also, because in the convergent point method the group parallax of each member is computed from the *size* of the proper motion, that parallax will be in error if any of the W-motion is reflected in the observed proper motion and if the W-motion deviates from that of the Hyades stars. The motion criteria for membership in the Hyades group was therefore based on the U- and V-motions alone; those stars for which a (U, V)-match with the Hyades cluster stars, $(U, V) = (+48, -18)$, was possible within ± 3 km/sec in both coordinates were selected as possible members. The median W-motion of the Hyades group members, ~ -4 km/sec, is only a small fraction of the total space motion, 45 km/sec, of the group. On the other hand, the median W-motion of the Sirius group contains a large percentage of the total motion and so a somewhat different procedure than that described for the Hyades group has been used here in selecting possible members.

The space motion vectors of Sirius, relative to the Sun, are as follows:

$$U = -14{\cdot}2 \text{ km/sec};$$
$$V = -\ 0{\cdot}4 \text{ km/sec};$$
$$W = -11{\cdot}8 \text{ km/sec};$$

all vector motions discussed here have been computed to the nearest 0·1 km/sec but are rounded-off to units of 1 km/sec in Table II. The small total space motion of Sirius and group members compared to that of the Hyades group makes the likelihood of including spurious members comparatively greater. This disadvantage is only partly compensated by the fact that the Sirius group motion relative to the Sun is diametrical to that of the bulk of the older population I stars (Eggen 1960a, Paper VI) and lies in the (U, V)-plane near the circumference of the limiting ellipse for that population.

Fig. 1 shows a section of the (U, V)-plane containing Sirius (filled circle). Space motion vectors have been computed, assuming 3 values of the parallax, for (*a*) the stars in Roman's (1949) combined list of all stars assigned at various times to the Ursa Major stream, and (*b*) approximately 500 additional stars selected from the General Catalogue of Radial Velocities (Wilson 1953). The resulting (U, V)-loci of three probable members of the Sirius group are illustrated in Fig. 1 where the points corresponding to various values of the parallax are also indicated. Those stars whose (U, V)-loci pass within 4 km/sec of the point representing Sirius are considered as possible members of the group and the group parallax is taken to be that value which corresponds to the shortest distance between $(U, V) = (-14{\cdot}2, -0{\cdot}4)$ and the (U, V)-locus of the star. This procedure has the advantages that (*a*) the resulting group parallax depends upon both the observed radial velocity and the proper motion, and (*b*) no restriction is placed on the value of W. The dependence of the computed parallax of a group member on the accuracy of the (U, V)-values for Sirius is also apparent in Fig. 1. For example, combined errors in the proper motion, radial velocity and parallax of Sirius that might produce an error of 1 km/sec in U would have relatively little effect on the computed parallax of β Aur but would cause an error of 15 per cent in that of δ Del.

The 100 possible members of the Sirius group chosen in this way are listed in Table I with the following information :

W: Number in Wilson's (1953) radial velocity catalogue.

Name: Alternative identification.

V_E, $B-V$, $U-B$: Magnitudes and colours mainly by Johnson and Knuckles (1957), Stoy (1953), Naur (1955), and Eggen (1955, and unpublished). No colours are available for a few of the stars; the values of $(U-B)_C$ determined with the Cape refractor are given in parentheses.

Sp: Spectral types on the MK system are mainly by Roman (1949), Slettebak (1954, 1955) or de Vaucouleurs (1957); the remaining are mainly from the radial velocity catalogue (Wilson 1953).

μ_α, μ_δ, S: The proper motion and its source. The references consulted in forming the mean values are as follows:

1. GC.
2. N30.
3. FK3 and supplements.
4. Second Greenwich Catalogue for 1925.
5. G. van Herk, *Leiden Annals*, **18**, 1957.
6. J. Robertson, *Washington Zodiacal Catalogue*, 1940.
7. Yale Zone Catalogues.

Notes: The notes pertain mainly to known companions.

The group parallaxes are listed in Table II together with the resulting luminosities and space motions.

TABLE I

Probable members of the Sirius group

W	Name	V_E	$B-V$	$U-B$	Sp	ρ Q	μ_α	μ_δ	S
		m	m				s	s	
164	σ And	4·53	+0·05	+0·06	A2 V	− 8·0 b	−0·067	−0·038	1, 2
228	44 Psc	5·8:	+0·80	...	gG5	− 4·1 b	−0·016	−0·012	1+, 2, 3
378	μ Phe	4·58	+0·97	...	G8 III	+16·5 a	−0·022	+0·001	1, 2, 3
408	HR 196	5·5	...	...	A2	− 8·5 b	−0·026	+0·004	1, 4
*1019	HD 11131	6·79	+0·63	(+1·71)	dG1	− 2·5 b	−0·137	−0·088	1+
1021	χ Cet	4·62	+0·34	+0·02	F2 V	− 0·9 b	−0·153	−0·088	1, 2, 3
*1106	48 Cas	4·50	+0·18	...	A4 V	− 5·0 c	−0·064	+0·009	1
*1222	HR 647	6·06	+0·40	−0·07	F5 V	− 8·1 b	−0·064	−0·056	1, 5
*1463	υ Cet	4·86	+0·86	+0·53	G5 III	+ 5·0 a	−0·030	−0·021	1, 2, 3
1616	υ Hyi	4·77	+1·36	...	gK4	+ 4·7 a	−0·030	−0·022	1, 2
2197	HR 1195	4·11	+0·96	...	gG8	+ 2·0 a	−0·051	−0·047	1, 2, 3
*2546	ξ Eri	5·17	+0·08	+0·08	A2	− 6·3 c	−0·049	−0·054	1, 2, 3
2871	2 Aur	4·77	+1·41	+1·58	K3 III	−16·5 a	−0·026	−0·008	1, 2, 4
3046	β Eri	2·80	+0·13	+0·10	A3 III	− 8·0 c	−0·094	−0·080	1, 2, 3
*3566	γ Lep B	6·15	+0·94	+0·74	dK5	− 9·7 a	−0·288	−0·372	1, 2, 3
*3567	γ Lep A	3·60	+0·47	−0·03	F6 V	− 9·7 a	−0·288	−0·372	1, 2, 3
3663	χ' Ori	4·41	+0·59	+0·06	G0 V	−13·5 a	−0·187	−0·084	1, 6
*3730	β Aur	1·90	+0·03	+0·06	A2 IV	−18·2 a	−0·051	−0·004	1, 2, 3
*4050	δ Col	3·81	+0·88	...	gG6	− 2·6 a	−0·028	−0·056	1, 2
*4079	RR Lyn	5·64	+0·24	+0·12	Am	−12·7 a	−0·019	+0·018	1, 4
*4392	α CMa	−1·46	−0·01	−0·06	A1 V	− 7·6 a	−0·537	−1·210	1, 2, 3
4993	ι CMa	4·60	+1·23	...	K2 III	−15·4	0·000	−0·023	1+, 2, 3
5317	HR 3131	4·62	+0·08	+0·09	A3 V	−12·0 c	−0·008	−0·047	1, 2, 3
*5899	α Cnc	4·22	+0·18	...	Am	−13·8 b	+0·034	−0·035	1, 2, 3
5935	υ Cnc	5·46	−0·03	−0·10	Ap	−15·1 b	−0·002	−0·009	1, 2
*5947	α Vol	4·02	+0·15	...	Am	+ 4·9 b	+0·004	−0·102	1+, 2, 3
*6050	HR 3676	5·7	...	...	A1	−12·1 a	+0·019	+0·006	1, 2, 3
*6154	23 UMa	3·66	+0·33	+0·10	Fo IV	− 9·5 b	+0·109	+0·024	1, 2, 3
6404	21 LMi	4·48	+0·18	+0·08	A7 V	−17·8 b	+0·054	−0·001	1, 3
*6440	34 Leo	6·44	+0·46	+0·02	F6 V	−16·0 b	+0·037	−0·040	1, 6
6478	ζ Leo	3·44	+0·30	+0·20	Fo III	−15·0 b	+0·017	−0·013	1, 2, 3

TABLE I—*continued*

W	Name	V_E	$B-V$	$U-B$	Sp	ρ	Q	μ_α	μ_δ	S
		m	m							
6614	37 UMa	5·16	+0·34	−0·01	F1 V	−12·3	a	+0·067	+0·034	1, 2, 3
*6705	μ Vel	2·67	+0·90	...	G5 III	+ 6·9	a	+0·072	−0·053	1, 2, 3
6809	β UMa	2·36	−0·02	+0·02	A0 V	−12·0	a	+0·083	+0·028	1, 2, 3
6812	61 Leo	4·73	+1·62	...	K5 III	−13·5	a	+0·015	−0·037	1, 3
6892	δ Leo	2·55	+0·13	+0·12	A4 V	−20·6	b	+0·144	−0·137	1, 2, 3
6985	τ Leo	4·95	+1·00	+0·80	G8 II	− 9·1	a	+0·017	−0·016	1, 2, 3
7119	ζ Crt	4·74	+0·96	+0·76	G5 III	− 4·6	a	+0·035	−0·038	1, 2, 3
7177	γ UMa	2·44	0·00	+0·01	A0 V	−12·9	a	+0·094	+0·005	1, 2, 3
7276	α Crv	4·03	+0·31	−0·02	F2 IV	+ 4·4	a	+0·083	−0·050	1+
...	HD 109011	8·09	+0·93	+0·64	K2 V	−12·4	b	+0·104	−0·004	7
7337	δ UMa	3·29	+0·09	+0·07	A3 V	−12·9	b	+0·104	+0·003	1, 2, 3
*7590	HR 4803	5·45	+0·33	+0·02	F2 V	− 0·9	a	+0·075	−0·097	1+
7630	HD 110463	8·27	+0·95	+0·76	K3 V	− 6·3	b	+0·130	−0·008	1, 4
7659	34 Vir	6·0	...	...	A3	− 3·0	c	+0·038	−0·023	1+
7675	29 Com	5·70	+0·01	+0·07	A2 V	− 7·0	b	+0·029	−0·031	1+, 3
7678	HR 4867	5·85	+0·46	−0·04	F6 V	−12·0	b	+0·110	−0·006	1, 4
7714	41 Vir	6·26	+0·27	+0·05	A7 p	−10·0	c	+0·054	−0·032	1+, 2
7722	ε UMa	1·76	−0·02	+0·03	Ap	− 9·3	a	+0·113	−0·011	1, 2, 3
*7762	78 UMa	4·93	+0·36	+0·01	F2 V	−10·4	b	+0·117	−0·014	1, 2
*7825	HD 114260	7·19	+0·73	(+1·82)	dG7	− 8·8	b	+0·113	−0·030	1, 4
*7958/9	ζ UMa	2·04	+0·02	+0·04	A2 V, Am	− 9·0	a	+0·122	−0·027	1, 2, 3
7966	80 UMa	4·01	+0·15	+0·08	A5 V	− 7·5	a	+0·120	−0·024	1, 4
8035	78 Vir	4·94	+0·04	0·00	Ap	− 8·0	a	+0·041	−0·030	1, 2
8177	HR 5214	6·65	+0·11	+0·07	A4 V	−12·3	b	+0·031	−0·017	1, 4
*8325	κ Boo B	6·69	+0·39	−0·04	F2 V	−15·6	a	+0·064	−0·013	1, 4
*8328	κ Boo A	4·54	+0·20	+0·14	A7 IV	−15·6	a	+0·064	−0·013	1, 4
8344	HR 5343	5·98	+0·26	+0·05	Am	0·0	c	+0·043	−0·040	1+
8383	HR 5373	6·33	+0·05	+0·05	A2 V	−10·5	b	+0·023	−0·018	1, 4
8531	HR 5473	6·0	...	...	A8	− 7·9	b	+0·052	−0·030	1+
*8537	ζ Boo	3·78	+0·04	+0·05	A2 III	− 4·6	b	+0·050	−0·026	1, 5
*8553	HR 5492	6·25	+0·41	−0·01	F2 III	− 6·3	b	+0·070	−0·037	1, 4
8747	45 Boo	4·92	+0·44	−0·03	F5 V	− 7·3	b	+0·182	−0·173	1, 2, 3
*8909	η Cr B	4·98	+0·58	+0·04	G2 V	− 6·8	a	+0·134	−0·192	1, 5
*8990	α Cr B	2·23	−0·02	−0·02	A0 V	+ 1·7	a	+0·118	−0·094	1, 2, 3
9054	19 Ser	6·01	+0·90	+0·61	G5 III	+ 3·4	a	+0·023	−0·020	1+
*9094	β Ser A	3·67	+0·06	+0·07	A2 IV	− 0·8	b	+0·066	−0·049	1, 2, 3
*9095	β Ser B	9·95	+0·99	+0·81	dK3	− 0·8	b	+0·066	−0·049	1, 2, 3
...	β Ser CD	8·07	+0·66	...	Go	− 0·8	b	+0·066	−0·049	1, 2, 3
*9376	ν Cr B	5·78	+0·07	+0·10	A3 III	+ 2·0	c	+0·016	−0·024	1, 3
*9448	ζ Tr A	4·86	+0·54	...	dGo	+ 8·5	a	+0·205	+0·102	1, 2, 3
*9677	52 Her	4·80	+0·09	+0·04	Ap	0·0	a	+0·022	−0·063	1, 4
*9747	56 Her	6·08	+0·92	+0·62	G5 III	+ 1·1	a	+0·011	−0·026	1
10058	HR 6481	5·69	+0·06	+0·10	A3 III	+11·2	b	+0·010	−0·035	1+
*10916	HR 6917	5·83	+0·05	+0·09	A2 V	+ 8·5	a	+0·015	−0·024	1, 2, 3
*11082	HR 6993	5·75	+0·08	+0·06	A2	+12·4	a	+0·009	−0·024	1, 3
*11218	5 Aql AB	5·66	+0·17	+0·08	Am	+17·0	c	+0·009	−0·024	1+
*11426	10 Aql	5·90	+0·26	...	Ap	+14·5	a	−0·005	−0·050	1, 2
11674	59 Dra	5·12	+0·30	−0·01	F2 V	− 4·0	a	+0·044	−0·122	1, 3
11855	HR 7382	5·9	...	...	gG5	− 0·1	b	+0·012	−0·030	1, 4
11988	HR 7451	5·72	+0·47	−0·01	F8 V	+ 1·2	b	+0·026	−0·193	1, 4
*12789	ρ Cap	4·77	+0·35	...	F2 III	+18·4	b	−0·016	−0·023	1, 2, 3
12981	β Pav	3·44	+0·14	+0·05	A5 IV	+ 9·8	b	−0·039	+0·016	1, 2, 3
*12987	δ Del	4·5	+0·34	...	F2 III	+ 9·3	a	−0·024	−0·044	1, 2, 3
*13628	76 Cyg	6·10	+0·06	+0·06	A2	+ 3·0	d	−0·014	−0·047	1, 4
*13854	HR 8407 AB	5·60	−0·40	−0·10	Ao	− 1·2	b	−0·018	−0·032	1, 4
*13866	32 Aqr	5·32	+0·22	+0·14	g A8	+20·4	a	−0·021	−0·044	1, 2
13931	π Peg	4·30	+0·45	+0·18	F5 II-III	+ 2·0	b	−0·017	−0·020	1, 2, 3
*14359	γ Ps A	4·42	−0·02	...	A0 V	+16·5	b	−0·035	−0·024	1, 2
...	HD 217595	7·22	+0·43	...	F5 V	+20·5	b	−0·018	−0·008	1+

Notes to TABLE I

No.

1019 The $U-B$ was determined with the Cape refractor and shows an excess of $\delta(U-B)_C = +0^m\cdot02$ (Eggen 1959a).

1106 ADS 1598, see Section 4.

1222 ADS 1709, see Section 4.

1463 ADS 1971, $9^m\,8^s$.

2546 The discordant velocity determination from Yerkes Observatory has been omitted.

2566/7 ADS 4334.

Notes to TABLE I—*continued*

3730 Spectroscopic and eclipsing binary, luminosity corrected for equal components before plotting in Fig. 1; see Section 5.
4050 Sp. B., $P=870^{d}$.
4079 Spectroscopic and eclipsing binary; see Section 5.
4392 ADS 5423; see Section 4.
5899 ADS 7115, 11^{m} 11″.
5947 Sp. B with double lines; luminosity corrected for equal components before plotting in Fig. 1.
6050 Sp. B., $P=16^{d}$.
6154 ADS 7402, 9^{m} 23″.
6440 ADS 7674, $\Delta m=0^{m}\cdot5$. There are few observations of this pair, which was discovered in 1905 ($\theta=290°$, separation=0″·22) and was too close in 1949–51 for van Biesbroeck to separate with the 82-inch reflector.
6705 Visual binary, 7^{m} 2″.
7590 ADS 8612, 12^{m} 2″.
7762 ADS 8739, see Section 4.
7825 $\delta(U-B)C=+0^{m}\cdot02$ (Eggen 1959a).
7958/9 ADS 8891, $\Delta m=1^{m}\cdot66$; the bright component is also an interferometric double; see Section 4.
8325/8 ADS 9713; the fainter component is Sp. B, no period.
8537 ADS 9343, $\Delta m=0^{m}\cdot02$, luminosity corrected for equal components before plotting in Fig. 1; see Section 4.
8553 ADS 9357, $\Delta m\approx 1^{m}\cdot5$.
8909 ADS 9617, $\Delta m=0^{m}\cdot26$; luminosity corrected for equal components before plotting in Fig. 1; see Section 4.
8990 Spectroscopic and eclipsing binary; see Section 5.
9094/5 ADS 9778; CD is ADS 9766.
9376 ADS 9990, 3 companions all fainter than 10^{m}.
9448 Sp. B., $P=13^{d}$.
9677 ADS 10227, 10^{m} 1″·5; the companion is itself double, see Section 4.
9747 ADS 10259, 10^{m} 18″.
10916 Sp. B., $P=10^{d}$.
11082 Sp. B., $P=?$
11218 ADS 11667, Δm (AB)=$1^{m}\cdot59$, C is 11^{m} 27″.
11426 Although shown as filled circle in Fig. 1 (metallic-line), this star is actually a " peculiar " star with the latest known A-type.
12989 ADS 13887, 10^{m} 2″.
12987 δ Scuti-type variable (Eggen 1956).
13628 Sp. B. with range of 43 km/sec, no period.
13854 ADS 15578, $\Delta m\approx 2^{m}$, separation of 0″·5, little observed.
13866 Sp. B., $P=8^{d}$.
14359 Visual binary, 8^{m} 4″.

TABLE II

Parallaxes, luminosities and space motions of stars in Table I

No.	π_g (0″·001)	M_V	U	V	W	No.	π_g (0″·001)	M_V	U	V	W
		m	km/sec					m	km/sec		
164	28	+1·77	−15	−3	− 1	4392	375	+1·41	−14	0	−11
228	7	0·0:	−14	−2	0	4993	16	+0·62	−15	+1	− 7
378	9	−0·65	−13	+2	−16	5317	14	+0·35	−16	+2	−12
408	10	+0·5	−14	0	+ 3	5899	33	+1·81	−14	+2	− 6
1019	50	+5·28	−15	0	− 4	5935	10	+0·46	−11	+1	−11
1021	56	+3·36	−14	+2	− 5	5947	27	+1·18	−14	0	−12
1106	25	+1·49	−12	+3	− 3	6050	13	+1·3	−13	+1	− 7
1222	22·5	+2·72	−14	−1	−14	6154	49	+2·11	−14	−1	0
1463	8	−0·62	−13	+4	−18	6404	50	+2·98	−14	+2	−12
1616	12·5	+0·26	−14	+2	− 3	6440	26	+3·51	−15	+2	−11
2197	19	+0·50	−14	+1	−10	6478	12	−1·16	−14	+1	−10
2546	23	+1·98	−14	0	− 9	6614	40	+3·17	−13	+2	− 7
2871	15	+0·65	−17	0	− 7	6705	30	+0·06	−14	0	−10
3046	30	+0·19	−14	+1	−16	6809	42	+0·48	−13	+2	− 7
3566	130	+6·72	−15	+4	−12	5812	12·5	+0·22	−13	−1	−15
3567	130	+4·17	−15	+4	−12	6892	90	+2·32	−15	+2	−17
3663	(101)	+4·43	−13	+3	− 9	6985	8	−0·53	−14	+2	− 9
3730	23	−1·29	−16	+1	−14	7119	16	+0·76	−14	+1	− 8
3836	70	+5·96	−12	0	−12	7177	42	+0·56	−13	+1	−10
4050	17	−0·04	−14	0	−11	7276	33	+1·62	−14	+3	− 8
4079	18	+1·92	−13	0	− 8	HD 10911	40	+6·10	−14	+1	− 9

TABLE II—*continued*

No.	π_g (0″.001)	M_V	U	V km/sec	W	No.	π (0″.001)	M_V	U	V km/sec	W
		m						m			
7337	44	+1·51	−14	0	− 9	9054	9·5	+0·89	−14	+2	− 8
7590	30	+2·84	−14	−1	−12	9094	23	+0·48	−14	+2	−14
7630	50	+6·77	−12	+3	− 5	9095	23	+6·76	−14	+2	−14
7659	14	+1·7	−14	+1	− 5	β Ser CD	23	+4·88	−14	+2	−14
7675	13	+1·27	−14	−2	−10	9376	9	+0·55	−14	−1	− 6
7678	43	+4·02	−14	0	−10	9448	95	+4·75	−12	+2	− 7
7714	19·5	+2·70	−14	+4	−13	9677	21	+1·41	−14	−2	− 4
7722	44	−0·02	−13	+2	− 8	9747	8·5	+0·73	−13	−4	− 8
7762	45	+3·20	−14	+1	− 9	10058	18	+1·92	−15	+2	0
7825	46	+5·50	−14	+4	−18	10916	7·5	+0·21	−15	+4	−11
7875	42	+4·96	−14	+1	− 7	11082	12	+1·15	−14	+1	− 7
7958/9	42	+0·16	−14	+2	− 8	11218	15	+1·54	−18	+2	− 4
7966	43	+2·18	−13	+3	− 7	11426	20	+2·41	−17	+2	− 4
8035	13·5	+0·59	−13	+4	−15	11674	40	+3·13	−12	+4	−10
8177	11	+1·86	−14	0	−14	11855	8	+0·4	−14	0	−14
8325	19	+3·08	−14	+1	−17	11988	53	+4·34	−15	+2	−10
8328	19	+0·91	−14	+1	−17	12789	25	+1·76	−17	+2	− 8
8344	18	+2·26	−14	−1	− 6	12987	19	+0·9	−14	0	− 4
8383	8·5	+0·98	−14	−2	−13	13628	13·5	+1·75	−14	+1	−10
8531	13	+1·6	−14	+4	−18	13854	11·5	+0·90	−14	−2	− 5
8537	14·5	−0·42	−13	+4	−13	13866	15	+1·20	−18	+4	−17
8553	28·5	+3·53	−13	+1	− 7	13931	9·5	−0·82	−14	0	−14
8747	61	+3·85	−14	+2	−15	14359	26	+1·49	−14	+2	−16
8909	65	+4·04	−13	−4	−12	HD 217595	22	+3·83	−12	−3	−16
8990	45	+0·50	−14	+2	− 7						

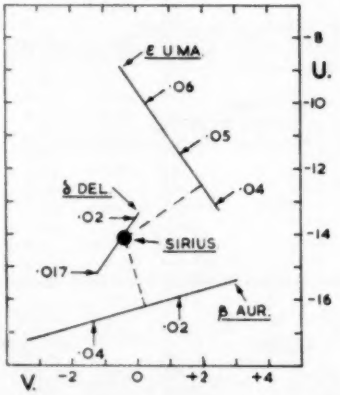

FIG. 1.—*A section of the (U, V)-plane containing Sirius (filled circle) at (U, V)=(−14·2, −0·4). Points corresponding to various values of the parallax for three probable members of the group, β Aur, δ Del and ε UMa, are indicated on the (U, V)-loci of these stars. The parallax corresponding to the shortest distance between (U, V)=(−14·2, −0·4) and the (U, V)-locus, indicated by the dashed line, is taken to be the group parallax.*

This list of members is not only very incomplete, even for the stars with known proper motion and radial velocity, but also it undoubtedly contains several spurious members. All stars brighter than visual magnitude 5·5 have been included on radial velocity and proper motion programmes and the completeness of Table I to this limit is affected only by the errors of observation. However, very few fainter stars more distant than about 50 parsecs will be included because of the small total space velocity of the group, $V_t = 18{\cdot}4$ km/sec (Sirius), with respect to the Sun. The parallax of a group member is related to the proper

motion by the expression $\mu \approx 4\pi \sin\lambda$, where λ is the angular distance of the star from the apparent convergent point of the group motion. Even in the most favourable case, when $\sin\lambda = 1$, a group member more distant than 50 parsecs will have $\mu < 0''.1$ and relatively few stars with such small motions have been included on radial velocity programmes.

It is obvious that the group parallax of stars near (or 180° from) the convergent point is nearly indeterminate because the space motion is then almost completely in the radial direction. However, it should also be noted that the present procedure causes the same situation to arise in the special cases where the proper motion is mainly reflected in the W-motion. For example, the dependence of (U, V, W) for χ' Ori (W 3663) on π_g is as follows:

π_g	U	V	W
$0''.100$	-13.1	$+3.0$	-9.4 km/sec
$0''.200$	-12.5	$+3.6$	-3.9 km/sec

The group parallax in this case is nearly indeterminate and the well-determined trigonometric parallax is given in parentheses in Table II.

The difficulty in assigning individual stars to membership in the Sirius group on the basis of a motion criterion alone can be emphasized in the following way.

(i) A catalogue has been compiled of 400 stars brighter than visual magnitude 5 and (*a*) with spectral types between B5 and F6, (*b*) of luminosity class III, IV, or V—the two-dimensional Mt Wilson system has been used for a few stars—and (*c*) with reliable radial velocities.

(ii) The (U, V)-locus for each star has been computed from the assumption that the luminosity is within $\pm 0^m.5$ of that given by the calibration of the luminosity classes (Keenan and Morgan, cf. Hynek 1951).

(iii) The (U, V)-values for the AV, Ap and Am stars were shown in Paper VI (Fig. 2) to lie in a very restricted region of the (U, V)-plane with few stars other than those in the Sirius group having negative values of both U and V—that is, that are following the Sun in their motion in the direction of galactic rotation.

(iv) The (U, V)-loci for those stars of the 400 mentioned above, which follow the Sun in the direction of galactic rotation, are shown in Fig. 2. These include:

(*a*) The AV, Ap and Am stars (solid lines) most of which were included in the previous discussion (Paper VI, Fig. 2).

(*b*) The luminosity class III and IV stars (broken lines).

(*c*) The stars assigned to the Sirius group in Table I are indicated by crosses at the (U, V)-values given in Table II. The large circle is centred on the (U, V)-value for Sirius and has a radius of 4 km/sec. From the distribution of the crosses it appears that (*a*) too large a tolerance has been placed on the V-motions, (*b*) there is a larger dispersion in the V- than in the U-motions of group members, or (*c*) the procedure of taking the group parallax as that value which corresponds to the point on the (U, V)-locus closest to $(U, V) = (-14.2, -0.4)$ is incorrect. The latter possibility arises because the majority of the (U, V)-loci for these stars lie more nearly parallel to the U-axis than to the V-axis so that adopting the minimum length of the normal to the loci passing through $(U, V) = (-14.2, -0.4)$ tends to minimize the dispersion of the U-motions.

It is interesting to note that only one or two stars with spectral type between B5 and A0 have negative values of both U and V.

(v) The possibility of including spurious members in the Sirius group is obvious in Fig. 2. All stars whose (U, V)-loci cut the circle around the (U, V)-value for Sirius are candidates for membership if the motion criterion alone is used. On the other hand, any estimate of the luminosity that is accurate to, say, one magnitude in most cases restricts the (U, V)-locus to a very limited region of the (U, V)-plane and permits the star to be assigned to a definite group with some accuracy.

(vi) The Sirius and Hyades (Paper VII) groups both lie near the edge of the (U, V)-distribution for a pure sample of older Population I—that is, the AV, Ap and Am stars—and, therefore, the members of these groups are the easiest to isolate in that population. However, when older stars, represented by the broken lines in Fig. 2, are included this advantage is no longer held by the two groups but is transferred, for the stars in Fig. 2, to the group with $(U, V) = (-25, -3)$. This group, which we will call the α Ophiuchi group, will be discussed in detail in a later paper. Moreover, when a selection of stars that contains still older objects is considered—such as spectral types later than F5 (Paper III) or subgiants (Paper V)—the (U, V)-dispersion becomes even larger and such high velocity groups as the ζ Herculis, 61 Cygni and γ Leonis groups become the easiest to isolate. For the same reason it is obvious that the probability of including spurious members in, say, the Sirius group is greater for stars of type later than about F5 than it is for main sequence A-type stars.

(vii) It should be noted that the (U, V)-loci shown in Fig. 2 assume that there is no error in the observed radial velocities or proper motions. Uncertainties in the observed components of the motions will broaden the loci but the broadening due to errors in the proper motion will be dependent upon the parallax and will give fan-shaped loci with increasing width for decreasing parallax.

(viii) There are at least three other groups in addition to the Sirius group in Fig. 2. Five of the stars may share the motion of Procyon, which is indicated by the crossed circle. The apparent group near $(U, V) = (-8, +5)$ is that numbered 7 in Paper VI. The values of $(U, V) = (-25, -3)$ for the α Ophiuchi group were determined by treating the loci as "Sumner-lines" and obtaining a "fix" by minimizing the sum of the squares of the lengths of the normals to the loci.

2. *The* $(M_V, B-V)$*-diagram.*—The colours and luminosities of the stars in Tables I and II are displayed in Fig. 3 where the main sequence defined by the Hyades cluster stars (Sandage and Eggen 1959) is also shown. This diagram is more open that that previously found (Paper I), mainly because of the inclusion of many stars as group members by the procedure used here that were excluded by the convergent point method. The most noteworthy features of Fig. 3 are the following:

A. The most obvious feature of the $(M_V, B-V)$-diagram for the Sirius group members is the apparent displacement of the main sequence from that of the Hyades cluster stars. If we omit known binaries (crosses) and the one star slightly above the main sequence at $B-V = +0^{m}.92$, an eighth magnitude object for which only a photographic proper motion is available, the average displacement of the stars redder than $B-V = +0^{m}.4$ is M_V (Sirius group) $- M_V$

(Hyades group) $= +0^{m}\cdot2$. This displacement is also reflected in the $(U-B, B-V)$-relation for the Sirius group stars, compared with those in the Hyades group, shown in Fig. 4. Here the "standard" relation, derived from the Hyades cluster members, is shown as a continuous curve; the extension for $B-V < +0^{m}\cdot35$, as indicated by the main sequence Hyades group members (Paper VII), is shown as a dotted curve. The main sequence, or near main sequence, members of the Sirius group are indicated by open circles, the metallic-line and peculiar A-type stars by crosses, and the G- and K-type giants by filled circles; the two stars indicated by open boxes will be discussed below.

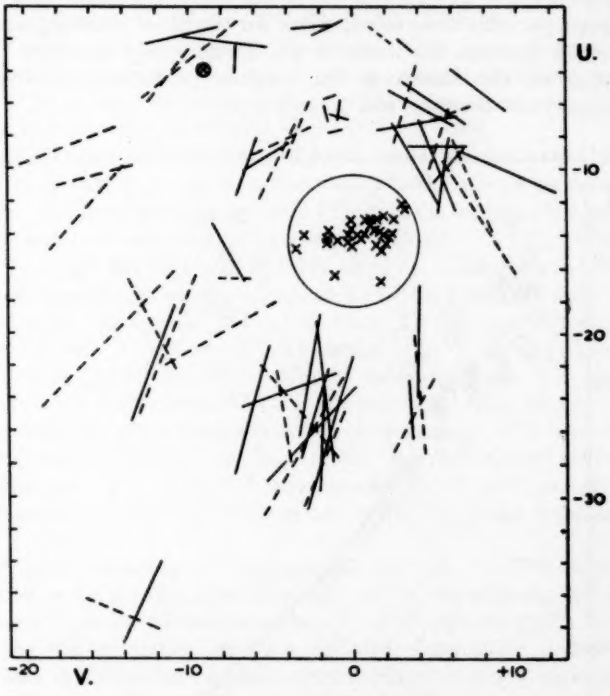

FIG. 2.—*The (U, V)-loci for AV, Ap, and Am stars (continuous lines) and B8 to F5 stars of luminosity class III or IV (broken lines) brighter than visual magnitude 5·0. The crosses represent members of the Sirius group and the large circle is centred on the (U, V)-value for Sirius and has a radius of 4 km/sec. The crossed circle represents the accurately known position of Procyon.*

The main sequence stars bluer than $B-V = +0^{m}\cdot2$ appear to have the same $(U-B, B-V)$-relation as the Hyades stars in the colour range common to both groups. However, the Sirius group members with $+0^{m}\cdot3 \leqslant B-V \leqslant +0^{m}\cdot6$ definitely depart from the standard relation and show an average ultra-violet excess, $\delta(U-B)$, of $+0^{m}\cdot04$. If this excess is interpreted as due to line-blanketing (Sandage and Eggen 1959, Table IV) the expected ΔM_{V} (Sirius–Hyades) is $+0^{m}\cdot3$; the agreement with the observed value is excellent

in view of the preliminary nature of the blanketing theory. In testing the theory with known subdwarfs near the Sun, Sandage and Eggen found that $\delta(U-B)\approx 0$ for subdwarfs redder than $B-V\approx +0^{m}\cdot 8$. This same result is obtained for the red dwarfs in the Sirius group and indicates that the "blanketing line" in the $(U-B, B-V)$-diagram lies along the intrinsic $(U-B, B-V)$-relation for these stars. Unfortunately, values of $(U-B)$ are not available for the few known dwarfs in the Sirius group with $+0^{m}\cdot 6 < B-V < +0^{m}\cdot 8$. Two stars in this interval, W 1019 and W 7825, have values of $B-V=+0^{m}\cdot 63$ and $+0^{m}\cdot 73$, respectively, and the ultra-violet colours, $(U-B)_{C}$, obtained with the Cape refractors give $\delta(U-B)_{C}=+0^{m}\cdot 02$ for both. Adopting the rough relation (Eggen 1959a), $\delta(U-B)=1\cdot 5\,\delta(U-B)_{C}$, the resulting values of $\delta(U-B)$ are in good agreement with those found above for the bluer main sequence objects. The ultra-violet excesses for some of the Sirius group members (cf. χ^{1} Ori, Eggen 1959a) are also shown by the 6-colour photometry of Stebbins and Whitford (1945) and Stebbins and Kron (1956).

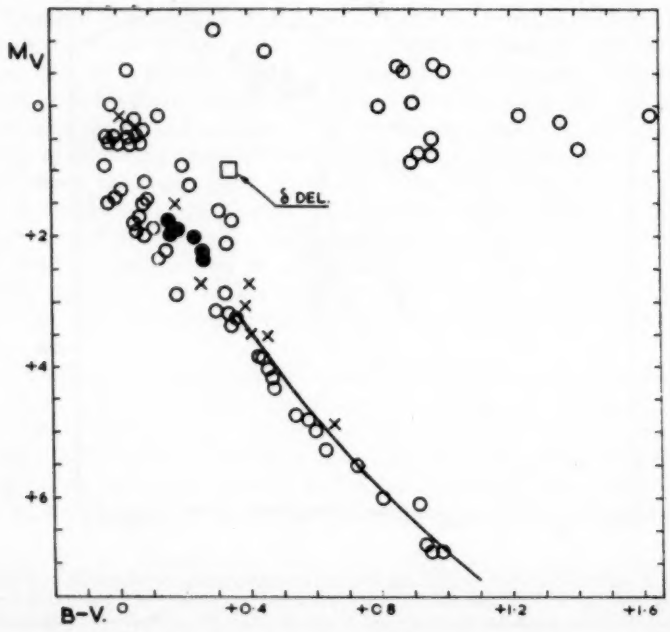

FIG. 3.—*The $(M_V, B-V)$-diagram for the Sirius group members. The continuous curve represents the main sequence of the Hyades cluster stars, the crosses represent known binaries with companions bright enough to affect materially the observed colour and magnitude, and the filled circles represent metallic-line stars. The δ Scuti-type variable, δ Del, is shown as an open box.*

B. The metallic-line stars in the group (filled circles), like those in galactic clusters (Eggen 1957, 1959b) populate a restricted region of the $(M_V, B-V)$-diagram on the red side of the A-type main sequence stars. Wilson No. 11426 (10 Aql), although classified as A4p and "of a later A type than most of the magnetic stars" (Babcock 1958), falls among the metallic-line stars in Fig. 3

and is represented there by a filled circle. The wide binary W 7958/9 (ζ UMa) consists of a main sequence A-type star, which is itself a binary (Section 4), and a fainter, metallic-line star; the observed luminosity and colour of the system are indicated in Fig. 3 by a cross at $M_V = +0^m{\cdot}16$ and $B-V = +0^m{\cdot}02$. Since the visual magnitude difference in the wide pair is $1^m{\cdot}66$, the metallic-line component falls in the centre of the region populated by the metallic-line stars at $M_V = +2^m{\cdot}03$. The colour of this component is, therefore, probably near $B-V = +0^m{\cdot}20$, leaving $B-V \approx 0^m{\cdot}0$ and $M_V = +1^m{\cdot}12$ for the equal components of the bright star. If evolution of A-type main sequence stars is accompanied by increasing colour, then we are led to the conclusion that ζ UMa B ($M_V = +2^m$) is in a more advanced stage of evolution than the two intrinsically brighter stars ($M_V = +1^m$) that form ζ UMa A.

It seems reasonable to interpret the metallic-line stars as representing a definite stage in the evolution of A-type main sequence dwarfs but whether they have evolved from main sequence objects of the same or of lower luminosity may only be settled with a knowledge of the stellar masses.

C. The small amplitude, short period light and velocity variable δ Del (Eggen 1957) has a luminosity very similar to that found for the prototype variable δ Scu (Paper VII). The five stars lying between δ Del and the region of the metallic-line stars are, in order of decreasing luminosity: κ Boo A (F2 IV), 32 Aqr (gA8), α Crv (F2 IV), ρ Cap (F2 III), and 23 UMa (F0 IV). The observed line-widths of three of these stars (κ Boo A, ρ Cap, and 23 UMa) indicate values of $V_r \sin i$ between 115 and 150 km/sec (Slettebak 1954, Herbig and Spalding 1955) while those for two of the metallic-line stars give $V_r \sin i \approx 70$ km/sec; the value for δ Del is 35 km/sec. The available determinations of $V_r \sin i$ for the group members are shown on a $(M_V, B-V)$-diagram in Fig. 5; the few values available for late-type giant members are all < 25 km/sec. The axes of rotation may be randomly distributed or there is no close correlation between main sequence luminosity and rotational velocity and Fig. 5 gives no obvious clue to the main sequence origins of δ Del or any of the non-main sequence stars in the figure.

D. The dense clumping of A-type stars near $M_V = +0^m{\cdot}5$ contains such diverse objects as the peculiar stars α Cnc and 78 Vir, the eclipsing variable α CrB and several A0–A3 stars of luminosity class V. Although the group membership represented by the objects in Table I is obviously incomplete, it does not seem likely that this fact alone can explain such a relatively heavy concentration of stars with a sharp cut-off near $M_V = +0^m{\cdot}6$ at the edge of an $\sim 0^m{\cdot}5$ gap in the main sequence.

E. The two stars represented in Fig. 4 by open boxes are ζ Leo ($M_V = -1^m{\cdot}2$, $B-V = +0^m{\cdot}30$) and π Peg ($M_V = -0^m{\cdot}8$, $B-V = +0^m{\cdot}45$). The large ultraviolet deficiencies for these stars may be connected with the fact that at least one of them, π Peg, is known to be a shell star (Greenstein 1953).

F. The distribution in the $(M_V, B-V)$-diagram of the G- and K-type giant members of the Sirius group differs markedly from the orderly sequence from $B-V = +0^m{\cdot}95$, $M_V = +1^m$ to $B-V = +1^m{\cdot}6$, $M_V = -0^m{\cdot}5$ found for the Hyades giants (Paper VII). Although this difference may be partially caused by the inclusion of spurious members in the Sirius group, especially in the case of the small proper motion stars redder than $B-V = +1^m{\cdot}2$, there is undoubtedly a real difference in the spread of luminosity for the G-type giant members in the

two groups. This difference is also reflected in the colour–spectral type relation for the giants in the two groups since those with colour near $+0^{m}.95$ are classified K0 III in the Hyades and G5 III in the Sirius group. Group membership of individual giant stars in the Sirius group can ultimately be tested through independent luminosity determinations such as those of Wilson and Bappu (1957).

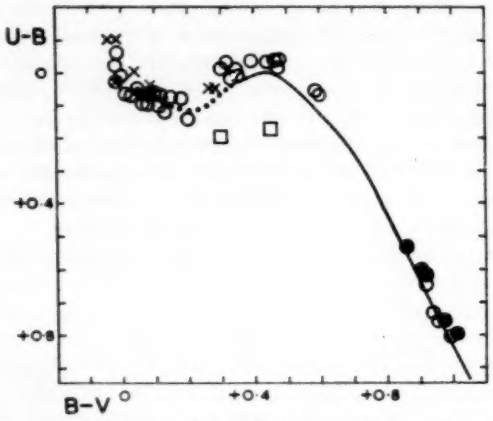

FIG. 4.—*The $(U-B, B-V)$-relation for group stars not known to be binaries. The standard relation, for the Hyades cluster stars, is shown as a continuous curve with an extension indicated by the Hyades group stars shown as a dotted curve. Metallic-line and peculiar A-type stars are shown as crosses, G- and K-type giants as filled circles, and the bright F-type giants, ζ Leo and π Peg, as open boxes.*

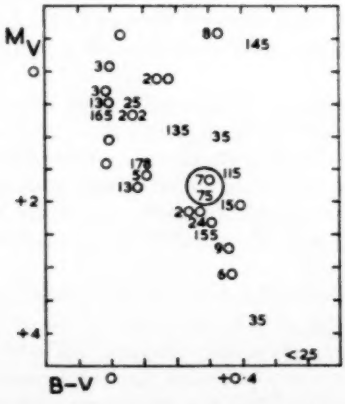

FIG. 5.—*Available estimates of $V_r \sin i$, in km/sec, for group stars marked on a $(M_V, B-V)$-diagram. The values for two metallic-line stars are circled.*

G. A comparison between the schematic $(M_V, B-V)$-diagrams for the Hyades (hatched) and Sirius (unhatched) groups is shown in Fig. 6. The few Hyades (crosses) and Sirius (open circles) group members falling outside the enclosed areas are also indicated in the figure. Although the effects of evolution on the

main sequence stars are apparent to about the same luminosity in both groups ($M_V \approx +3^m$) the presence of bluer main sequence stars and brighter G-type giants in the Sirius group indicates that, on the basis of the evolutionary theory (Sandage 1958), this is the younger group.

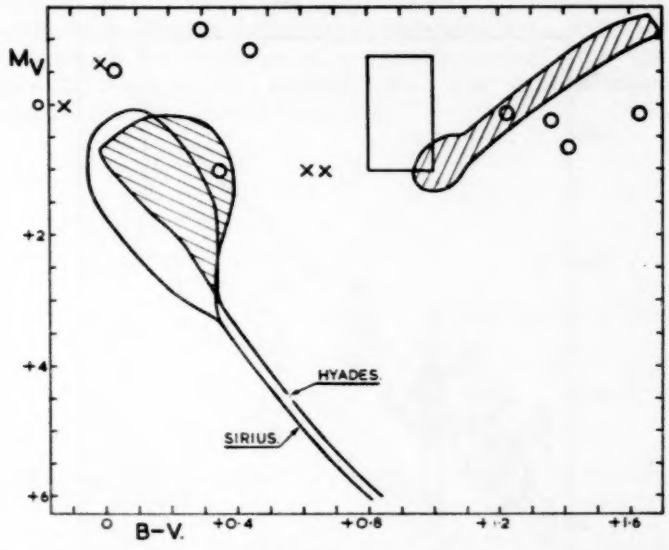

FIG. 6.—*A comparison of the schematic* (M_V, $B-V$)*-diagrams for the Hyades (hatched) and Sirius (unhatched) groups. A few Hyades (crosses) and Sirius (open circles) group stars falling outside the enclosed areas are also shown.*

H. The large number of blue stars brighter than $M_V = +2^m$ compared to the relatively small number populating the lower main sequence indicates that, for any assumed luminosity function based on known galactic clusters, we can predict a very large number of undiscovered main sequence Sirius group members of G-type and later. In this connection the following M-type dwarfs are possible group members selected from Vyssotsky's (cf. 1956) spectrophotometric survey; the radial velocities of these stars are based almost entirely on one spectrogram for each star by Dyer (1954) and the proper motions are all uncertain:

BD/AC	vis. mag.	Sp	ρ km/sec	μ_α	μ_δ	π_g
				"	"	"
+16°2708	10·5	dMo	+ 5	+0·30	−0·14	+0·11
+22°2302	9·5	dM2	−20	+0·15	−0·04	+0·08
+22°214−219	9·5	dMo	− 7	−0·10	−0·21	+0·05
+23°2124	9·8	dK8	+ 3	−0·08	−0·10	+0·04
+30°1367	9·5	dMo	− 5	+0·09	−0·22	+0·08
+36°2393	9·6	dM2	+ 6	+0·30	−0·06	+0·11
+39°2675	9·2	dK8	− 8	+0·10	−0·10	+0·04
+55°1519	10·0	dM2	−10	+0·25	+0·08	+0·08
+63°965	9·1	dMo	− 6	+0·08	+0·01	+0·05

The spectra of all these stars show H and K lines in emission and the first three show emission lines of hydrogen.

The comparison between the group parallaxes and the trigonometric determinations is shown in Fig. 7. The trigonometric values are from the Allegheny (filled circles), McCormick (open circles), Cape (plus signs), Yale (crosses)

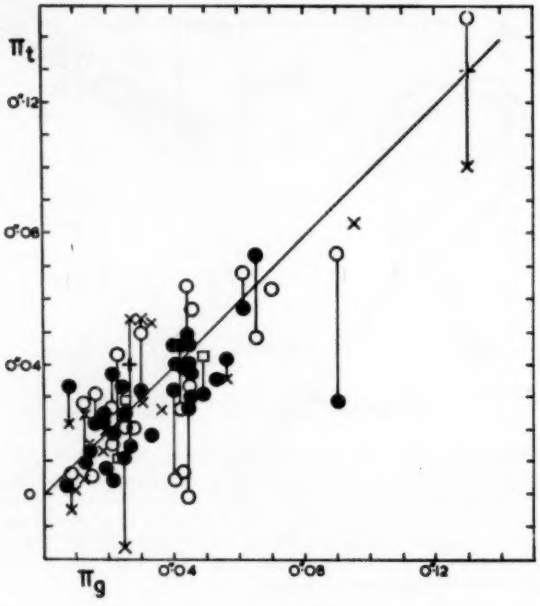

FIG. 7.—*The correlation between the group and trigonometric parallaxes. The observatories represented are Allegheny (filled circles), McCormick (open circles), Yale (crosses), Cape (plus signs) and Greenwich (boxes). Determinations by more than one observatory for the same star are connected by straight lines. The one-to-one correlation is represented by the 45° line. The large deviation for the Allegheny determination at $\pi_g = 0''.090$ is for δ Lec.*

and Greenwich (boxes) Observatories; values by more than one observatory for the same star are connected by a straight line. The large deviation of the Allegheny determination at $\pi_g = 0''.09$ is for δ Leo.

3. *Spatial distribution of group members.*—The spatial distribution of the stars in Table I is shown in Figs. 8 and 9. The stars within 25 parsecs (crosses) and between 25 and 50 parsecs (circles) of the galactic plane (including the Sun) are shown in Fig. 8, whereas those more than 50 parsecs above (filled circles) and below (open circles) the plane are shown in Fig. 9. Although, like the Hyades group (Paper VII), the distribution shown in Fig. 8 indicates that the Sirius group may be elongated roughly in the direction of galactic rotation, this result depends on only a few distant stars, and, because of the smallness of the proper motions and the resulting incompleteness in the known membership of the group, no conclusion on this point can yet be reached. Seventy-five per cent of the stars, including all but one of those represented by the clump of crosses near the Sun ($X, Y = 0, 0$) in Fig. 8, are above the galactic plane.

4. *Visual binaries.*—Eight visual binaries, including the interferometric pair ζ UMa Aa, among members of the Sirius group have known orbits. The orbital periods and semi-major axes adjusted to the "standard observers" (Eggen 1956), and group parallaxes of these systems are listed in Table III together with the resulting values of the mass and luminosity. Astrometric determinations of the mass-ratio have been used in determining the individual masses in three systems, but the magnitude difference between the components of the other four is small enough to permit the discussion of a mean component; the white dwarf companion of Sirius is not discussed here. The apparent magnitude of ADS 10227BC may be uncertain by $\sim 0^{m}.5$.

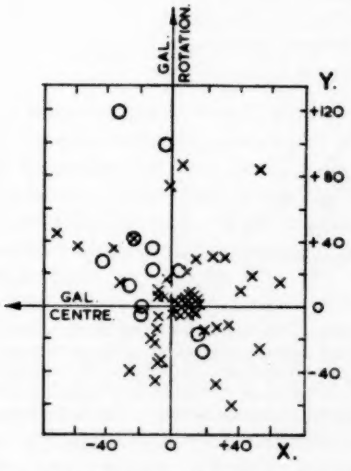

FIG. 8.—*The space distribution of the group members. Stars within 25 parsecs of the galactic plane (through the Sun) are shown as crosses and those between 25 and 50 parsecs of this plane by open circles. The Sun is at (X, Y)=(0, 0).*

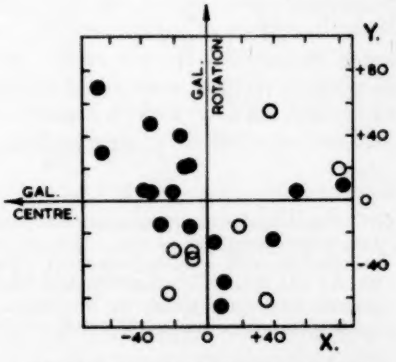

FIG. 9.—*Space distribution of stars more than 50 parsecs above (filled circles) and below (open circles) the galactic plane.*

TABLE III

Visual binaries with known orbital elements in the Sirius group

ADS	Wilson	Name	*P* (years)	*a*	π_g (0."001)	M_V	Mass (⊙=1)
1598A	1106	48 Cas	60	0."680	25	+1·7	3·0
B						+3·4	2·6
1709AB	1222	—	144·7	0·91	22·5	+3·6	1·5
5423A	4392	α CMa	50·0	7·765	375	+1·4	2·5
8739A	7762	78 UMa	115·7	1·286	45	+3·3	1·2
B						+5·7	0·6
8891Aa	7958	ζ UMa	0·056	0·0115	42	+1·1	3·1
9343AB	8537	ζ Boo	126	0·60	14·5	+0·3	2·2
9617AB	8909	η CrB	41·6	0·888	65	+4·8	0·75
10227BC	9677	52 Her	51	0·29	21	+6·1	0·5

The masses and visual luminosities in Table III are plotted in Fig. 10; the visual luminosities are used here to avoid the difficulty with bolometric corrections. The mass–(visual) luminosity relation taken from a previous discussion (Eggen 1956), and here called the "normal relation", is shown in the figure as a full curve. The brighter components of the systems are plotted in the figure as open circles, fainter components as filled circles and mean components as half-filled circles. The two components of ADS 1598 and 10227BC are connected by straight lines.

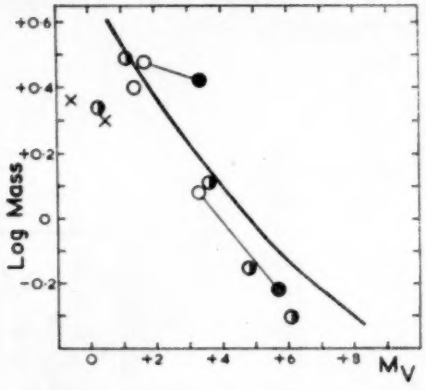

FIG. 10.—*Masses and luminosities of group binaries. The continuous curve is the normal mass-(visual) luminosity relation. Open circles represent primary components of visual binaries and filled circles the secondary components. The half filled circles are mean components for visual binaries with a small magnitude difference between the components. Straight lines connect components of the same system; the unconnected open circle represents Sirius. The two crosses represent the bright component of α CrB and the mean component of β Aur.*

The deviation from the normal relation of the group stars with $M_V = +3^m$ to $+6^m$ is very similar to that found previously (Paper VII, Fig. 8) for the Hyades group binaries. In fact, a mean mass–luminosity relation for the stars of both groups with luminosities in this range indicates that the Sun, $M_V = +4^m.8$, is almost exactly one magnitude fainter than group stars of the same mass.

Among the brighter stars, three fall near the normal relation—the bright component of 48 Cas, the mean component of ζ UMa Aa, and Sirius—but the mean component of ζ Boo is nearly two magnitudes brighter, and the secondary of 48 Cas nearly two magnitudes fainter, than predicted by that relation.

Two additional, little observed binaries in the group deserve attention; W 6440 (ADS 7674), which is in rapid motion, and W 13854 (ADS 15578).

5. *The eclipsing binaries β Aur, α CrB and RR Lyn.*—Of the three known eclipsing variables in the group, double lines have been observed only in the spectra of β Aur. The two components are of equal mass, $2.3 \odot$ (Popper 1959), and equal luminosity, $M_V = -0^m.54$, and are the brightest members for which a mass determination is available; the mean mass and luminosity are represented in Fig. 10 by a cross.

In a discussion of photoelectric observations with a red-sensitive photocell of the single-lined binary α CrB, Kron and Gordon (1953) found a 4^m difference between the components at λ7230. The secondary component is probably a

G-type dwarf so that the visual magnitude difference is $<4^m$. The visual luminosity of the secondary is then $M_V > +4^m{\cdot}5$ and, from the run of the mass–luminosity relation for the group stars in Fig. 10, the mass is $<0{\cdot}8\odot$. The mass function, $0{\cdot}063\odot$, given by Kron and Gordon, then yields a mass of $\leqslant 2\odot$ for the bright component; the upper limit for this mass is shown in Fig. 10 as a cross.

Stebbins and Huffer (1931) have published a light curve ($\lambda 4500$) of the single-lined binary RR Lyn. A new solution of this curve, based on an assumed value of 0·6 for the limb darkening coefficient of both components, gives the following elements:

$$i = 86^\circ{\cdot}5 \pm 0^\circ{\cdot}4 \text{ (p.e.)} \qquad a_1 = 9{\cdot}2 \times 10^6 \text{ km}$$
$$k = 0{\cdot}075 \pm 0{\cdot}006 \qquad L_1 = 0{\cdot}63 \pm 0{\cdot}04$$
$$r_1 = 0{\cdot}075 \pm 0{\cdot}006 \qquad L_2 = 0{\cdot}37 \pm 0{\cdot}04.$$
$$r_2 = 0{\cdot}071 \pm 0{\cdot}004$$

The mass function, $0{\cdot}31\odot$ (Harper 1915), and the normal mass–luminosity relation are satisfied by masses of $2{\cdot}3\odot$ and $1{\cdot}7\odot$ for the primary ($M_V = +2^m{\cdot}2$) and secondary ($M_V = +2^m{\cdot}8$), respectively. More definite information about the masses of these stars is especially desirable because the brighter component is a metallic-line star. If the luminosity difference derived from the light curve is correct the secondary component might be detectable by modern spectroscopic observations.

The masses and luminosities of both Sirius and Hyades group binaries give a strong indication that for $M_V < +3^m$ there is not a unique mass–luminosity relation. Although the deviation of the fainter component of 48 Cas ($M_V = +3^m{\cdot}4$) from the normal relation in Fig. 10 could be explained as either an error in the mass function, 0·3 instead of 0·43 (Kent 1950), or by the assumption that this star is itself double ($\text{mass}_1 \approx \text{mass}_2 \approx 1{\cdot}3\odot$), the nearly equal masses of β Aur, ζ Boo and, probably, α CrB, all giving large deviations from the normal relation, are unlikely to be the result of erroneously assuming that they are group members.

Royal Greenwich Observatory,
Herstmonceux Castle, Hailsham,
Sussex:
1959 *November* 28.

References

Babcock, H. W., 1958, *Ap. J., Supp.* No. 30.
de Vaucouleurs, A., 1957, *M.N.*, **117**, 449.
Dyer, E. R. Jr., 1954, *A.J.*, **59**, 221.
Eggen, O. J., 1955, *A.J.*, **60**, 131.
— 1956, *A.J.*, **61**, 361.
— 1957, *A.J.*, **62**, 45.
— 1958, *M.N.*, **118**, 65.
— 1959a, *M.N.A.S.S.A.*, **18**, 91.
— 1959b, *Obs.*, **79**, 197.
— 1960a, *M.N.*, **120**, 448, Paper VI.
— 1960b, *M.N.*, **120**, 540, Paper VII.
Greenstein, J., 1953, *Ap. J.*, **117**, 269.
Harper, I. W., 1915, *Pub. Dom. Obs.*, **2**, 127.
Herbig, G. H., and Spalding, J. F., 1955, *Ap. J.*, **121**, 118.

Hynek, J. A., 1951, *Astrophysics*, London.
Johnson, H. L., and Knuckles, C. F., 1957, *Ap. J.*, **126**, 113.
Kent, J. T., 1950, *A.J.*, **55**, 243.
Kron, G. E., and Gordon, K. C., 1953, *Ap. J.*, **118**, 55.
Naur, P., 1955, *Ap. J.*, **122**, 182.
Petrie, R. M., and Moyls, B. N., 1953, *M.N.*, **113**, 239.
Popper, D., 1959, *Ap. J.*, **130**, 130.
Roman, N. G., 1949, *Ap. J.*, **110**, 205.
Sandage, A. R., 1958, *Stellar Populations*, Spec. Vat., **5**, 41.
Sandage, A. R., and Eggen, O. J., 1959, *M.N.*, **119**, 278.
Slettebak, A., 1954, *Ap. J.*, **119**, 146.
— 1955, *Ap. J.*, **121**, 653.
Stebbins, J., and Huffer, C. M., 1931, *Pub. Washburn Obs.*, **15**, part 4.
Stebbins, J., and Whitford, A. E., 1945, *Ap. J.*, **102**, 1.
Stebbins, J., and Kron, G. E., 1956, *Ap. J.*, **125**, 440.
Stoy, R. H., 1953, *Cape Mimeogram* No. 1.
Wilson, O. C., and Bappu, M. K. Vainu, 1957, *Ap. J.*, **125**, 661.
Wilson, R. E., 1953, *General Catalogue of Stellar Radial Velocities*, Papers of the Mount Wilson Obs. **8**.
Vyssotsky, A. N., 1956, *A. J.*, **61**, 201.

A SURVEY OF RADIO STARS AT A FREQUENCY OF 38 MC/S

G. R. Whitfield

(Communicated by F. Graham Smith)

(Received 1959 November 11)

Summary

This paper describes a survey of small diameter radio stars made with an interferometer at 38 Mc/s. The positions and flux densities of 59 radio stars, all of which are confirmed by other surveys, are given in the catalogue.

---

1. *Introduction.*—The determination of the spectra of radio stars requires observations at widely spaced frequencies. This survey, at 38 Mc/s, was intended to be combined with the 2C and 3C surveys (**1, 2**) at 81·5 and 159 Mc/s to determine the spectra of as many stars as possible. The observations were made in 1957. Of the 136 stars observed, 59 are confirmed by other surveys, and are listed in the catalogue. The other 77, mostly weak sources, were rejected.

Some preliminary results have already been used in a determination of the spectral indices of radio sources (**3**); more accurate calibrations have shown that the values of flux density used were too low by a factor of 2. The spectral indices deduced in that paper depend largely on observations at higher frequencies and are almost unaffected by this error.

2. *The aerial system.*—An interferometer was used, with the two aerials spaced 60 wave-lengths East–West. The aerials were dissimilar, one having high directivity in declination and the other in right ascension. When used with a phase-switching receiver (**4**) this arrangement has a much higher resolving power than a conventional interferometer of the same gain. Careful attention must be given to side lobes in such aerials, and a grading of excitation was used which should have reduced the side lobe level to 1½ per cent.

The arrangement of the aerials is shown in Fig. 1. Each point represents a Yagi array of four elements, with a beam width between half-power points of 54°. The Yagis of the East aerial were connected in groups of four by open wire transmission lines, with quarter-wave transformers for grading and matching. The groups were connected by coaxial cables, with stub matching. Twelve of the quarter-wave transformers had variable impedances, for adjustment of the grading. The adjustments were made by measuring the phase and amplitude of the voltage at each Yagi when a signal generator was connected at the centre, and also by conventional impedance measurements.

At the West end, the Yagis were connected by coaxial cables, with resistive attenuators for grading. The beam was swung in declination by introducing

phasing cables in the cable to each Yagi. The phase difference between successive Yagis could be any multiple of $\pi/4$ radians; this interval shifted the beam by slightly more than half the declination beamwidth (a shift of 6° near the zenith).

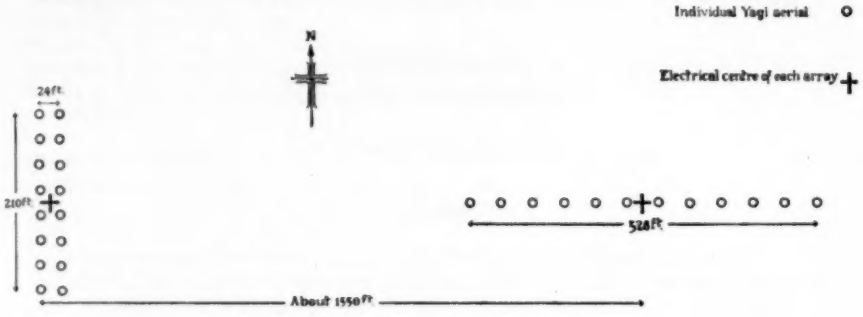

FIG. 1.—*The general arrangement of the aerial.*

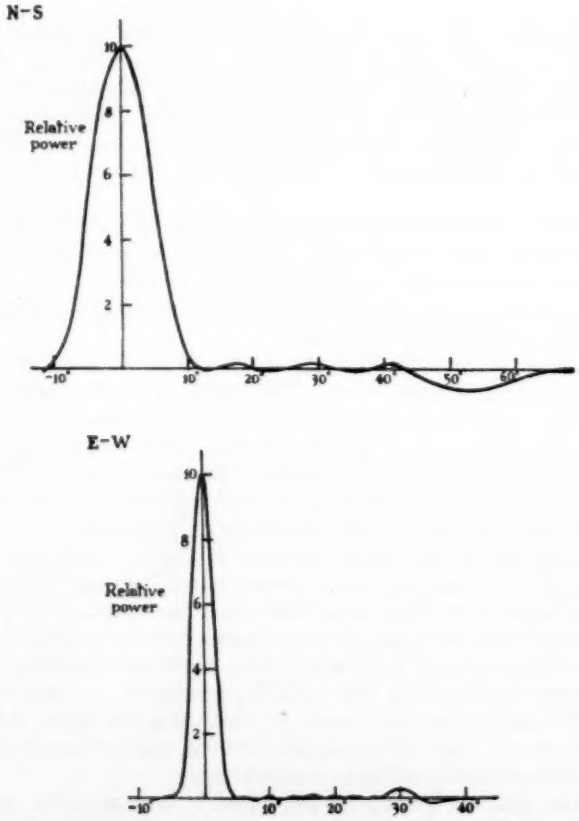

FIG. 2.—*The theoretical polar diagrams, in right ascension and declination, of the whole aerial when pointed at the zenith. The interference pattern due to the separation of the two aerials is not shown; it is a* ***sine wave****, of period 1°, in right ascension, whose envelope is the polar diagram shown.*

The predicted right ascension and declination polar diagrams of the aerial are shown in Fig. 2. The beamwidth per half-power points is $4\frac{1}{2}^\circ$ in right ascension and 12° in declination near the zenith, but is wider in declination at large zenith angles. The observed polar diagrams were similar, but with larger side lobes. In right ascension there was a 5 per cent side lobe close to the main beam, but nothing else above 2 per cent. In declination the side lobe level averaged 5 per cent, and increased in a few months to 8 per cent. These levels are consistent with likely errors in the adjustment of the grading.

The gain of the system was not measured, but was calculated to be 90 (over an isotropic radiator). Measurements of the six most intense sources showed that the gain decreased by 25 per cent from the zenith to the horizon; the flux densities in the catalogue have been corrected for this change.

3. *The Survey.*—The sky was covered in 14 strips of declination by observing for 24 hours at each setting of the aerials. A uniform coverage between declinations -20° and $+80^\circ$ was achieved, except for R.A.'s close to those of the four most intense sources. The performance of the aerial was checked at intervals by repeating one strip, and by observing Cassiopeia A with the East aerial phase-switched against a single pair of Yagis at the West end.

Apart from man-made interference, which was usually easily recognised, the principal difficulty was scintillation. As 1957 was a year of sunspot maximum, scintillation occurred frequently, causing random fluctuation with a time constant from a few seconds to a few minutes in the positions and amplitudes of sources. It was most serious at night, occurring to some extent on 75 per cent of the records, but it also occurred during the day. On about 10 per cent of the nights, when scintillation was very severe, the records were unreadable. But when scintillation was slight, it was difficult to detect except with the most intense sources; to ensure that recordings were not affected, it was necessary to observe each strip more than once.

The method of analysis was similar to that developed by Edge for the 3C survey. The information contained in each record was transferred on to a large sheet of graph tracing paper marked out in right ascension and declination, the position of each interference maximum being marked. The record amplitude was marked at intervals, usually every second lobe. When all the records had been traced, stars could be picked out by their consistent appearance on contiguous strips.

A continuous calibration system was used, power from a noise signal generator being divided and fed into the cables, before the preamplifiers, through attenuating T junctions (fig. 3). This gave a deflection proportional to the overall gain of the preamplifiers and receiver. At intervals the calibration signal was switched off for $\frac{1}{2}$-hour to obtain the zero level, which varied slowly. Observations of the more intense sources were made with attenuators in the aerial cables, before the calibrating T junctions, with the receiver gain unchanged.

These methods gave the relative intensities of all the sources observed. They were converted into absolute flux densities by using the flux densities of the six most intense sources, derived from all available observations (3). The required correction factor changed linearly with declination, implying a corresponding change in the gain of the aerial. A further small correction was applied for diffraction round the edge of one of the large aerial elements of the 2C and 3C interferometer surveys, which lay within the beam of the East aerial at low declinations.

4. *The Catalogue of Radio Stars.*—The catalogue contains all the stars confirmed by both the 2C and 3C surveys, the criterion being agreement of position within two probable errors, after any necessary lobe shifts. Most of these 59 stars are thought to be genuine; but, allowing for lobe shifts, 12 random coincidences would be expected between the 136 stars of the present survey and the 316 stars of the 2C survey brighter than 40×10^{-26} w.m.$^{-2}$ (c/s)$^{-1}$.

The first column gives the number of the star in the present survey†, and the next four columns the right ascension and declination (epoch 1950·0), with their estimated errors; these errors are based on the variations between different records of the same strip of sky, but comparison with the 2C and 3C surveys show that they approximate closely to probable errors. Owing to the skew axis of the interferometer (the same as that of the interferometer used for the 2C and 3C surveys), these errors define a parallelogram whose long axis does not quite lie along the meridian (see **1**).

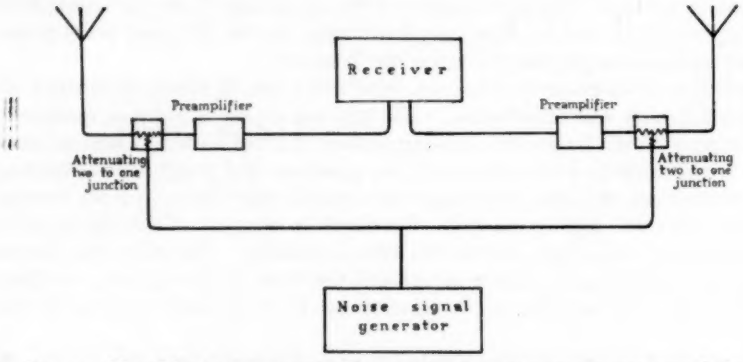

FIG. 3.—*The calibration system used. The noise signal generator was run continuously, but was switched off occasionally to check the zero level.*

It is possible for the wrong lobe of the interference pattern to have been chosen, giving an error in right ascension of one or more periods. Where the 2C and 3C surveys suggest that such a change is necessary, arrows ↑ or ↓ are inserted before the right ascension, the number of arrows indicating the number of lobe shifts required; an arrow pointing upwards indicates a later right ascension. The increment of right ascension corresponding to one lobe is given, as a function of declination, in Fig. 4.

The sixth and seventh columns give the flux density (both polarizations) and its probable error. The value given is that measured with an aerial spacing of 60 wavelengths; where the diameter of the source is known from other surveys, the total flux density has been calculated and is given in brackets. The error quoted is derived mainly from the variations between different records, but includes an allowance for the effects of confusion.

The last column gives the I.A.U. number of the source (**5**) followed by its numbers in the 2C and 3C surveys, chosen as the most complete surveys covering the region of the present survey. Comparison with other surveys has been restricted to the derivation of spectra (**3**).

† It is suggested that stars should be referred to by their 2C or 3C numbers as far as possible.

Seven stars have had their positions changed by re-examination of the records after a comparison with other surveys. These stars are indicated by the symbol* in column 1.

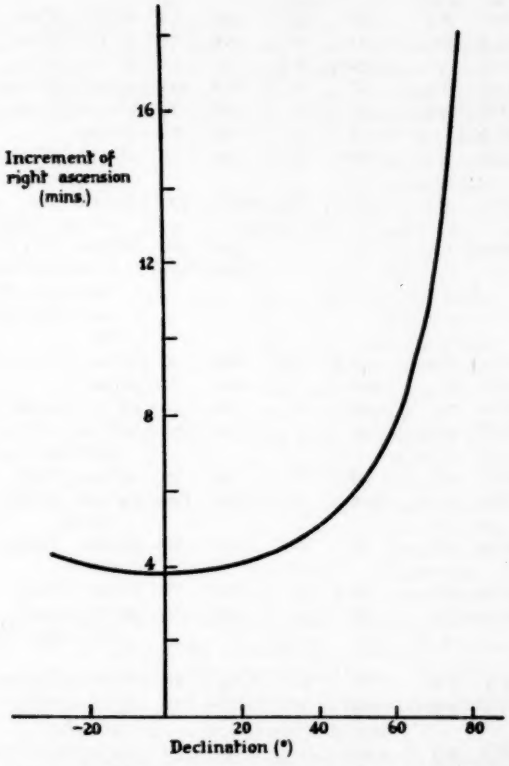

FIG. 4.—*The increment of right ascension corresponding to one lobe shift.*

Catalogue of Radio Sources

No.	Right Ascension			Declination		Flux Density $\times 10^{-26}$ w.m.$^{-2}$ (c/s)$^{-1}$		Notes
	h	m	± (m)	°	± (°)		±	
1	00	23·3	1	64·5	2	550	250	00N6A, 2C34, 3C10. Tycho Brahe Supernova.
2	↓ 00	38·0	0·5	−06·5	2	170	70	2C50, 3C15 and 3C17.
3	↓ 00	46·2	1	51	1	375	200	3C20. Possibly side lobe of Cassiopeia A.
4	↑ 01	02·3	0·4	12	1	335	70	2C94, 3C33.
5	01	32·7	0·4	18	1·5	240	70	3C47.
6	02	18·6	0·5	−02	1	125	70	02S1A, 2C196, 3C63.
7	03	07·7	0·5	17	1	120	70	2C283, 3C79.
8	↓ 03	19·3	1	40	3	560	120	03N4A, 2C296, 3C84, NGC 1275.
9	03	57·0	0·5	10·5	1·5	170	70	2C349, 3C98.

Catalogue of Radio Sources—continued

No.	Right Ascension			Declination		Flux Density $\times 10^{-26}$ w.m.$^{-2}$ (c/s)$^{-1}$		Notes
	h	m	± (m)	°	± (°)		±	
10*		04	02·7	0·5	40	3	130	70	2C361, 3C103.
11	↓	04	15·4	0·5	13	2	210	70	2C374, 3C109.
12*		04	15·6	0·5	39·5	1·5	255	70	2C379, 3C111.
13		04	34·7	0·5	31	1	600	150	04N3A, 2C404, 3C123.
14		05	01·0	0·5	37	1	270	70	2C440, 3C134.
15	↓	05	11·3	1	−18	4	150	70	2C449.
16	↑	↑05	27·0	1	50·5	2	150	70	2C485, 3C147. Confused with Taurus A side lobe.
17		05	31·2	0·3	21·5	0·5	2680	270	Taurus A. 05N2A, 2C481, 3C144. Crab Nebula.
18		↑06	09·5	1	23	1	350 (960)	100 (250)	06N2A, 2C537, 3C157, IC443. Confused with Taurus A side lobe and 2C526. Diameter from Baldwin and Dewhirst (6).
19		07	10·7	0·5	12·5	1·5	205	70	2C625, 3C175.
20		07	20·0	1	−20	5	100	70	2C641.
21*		07	59·4	0·5	14	2	170	70	2C714, 3C190.
22		08	06·8	0·5	43	3	125	70	08N4A, 2C724, 3C196. Very confused record.
23	↓	08	36·8	0·5	18·5	2	85	70	2C749, 3C201.
24		09	16·9	0·3	−09	3	1100	100	09S1A, 2C806, 3C218. Double Galaxy.
25		09	40·4	0·5	16	2	125	70	2C840, 3C225, Confused with 3C228.
26		09	45·9	0·3	09·5	2	350	70	2C843, 3C227.
27	↓	10	02·4	0·3	26	2	300	100	2C855, 3C234. Confused with first order maximum of Virgo A.
28		↑10	04·5	0·8	06	2	170	70	2C866, 3C237 and 2C876, 3C238.
29		10	55·1	0·5	−05	2	170	70	2C951, 3C249. Confused with 3C246.
30		↑11	06·3	0·5	40	1	140	70	3C251 and 3C254.
31		11	13·3	0·5	04	3	110	70	2C977, 3C253.
32		11	35·8	0·5	−11	2	180	70	11S1A, 2C1006.
33		↑11	39·4	0·5	19·5	1	200	70	2C1013, 3C264.
34		11	44·5	0·5	35	2	140	70	2C1012, 3C265.
35		12	28·5	0·3	12·8	0·5	2920	300	Virgo A. 12N1A, 2C1041, 3C274, M87.
36		13	26·1	1	61·5	2	125	70	2C1110.
37	↓	14	15·5	0·5	53	1	150	70	14N5A, 2C1175, 3C295.
38		↑14	16·7	0·5	18·5	1	115	70	3C300.
39	↓	14	54·8	0·5	−09·5	3	155	70	2C1244.
40		14	56·0	1	71	1·5	130	70	3C307. Possibly 2C1248.
41		15	04·0	0·5	29	2	270	100	2C1259, 3C310. Confused with first order maximum of Virgo A.
42	↓	15	15·8	0·5	26·5	1	120	70	2C1273, 3C315. Confused with No. 41.
43		15	16·4	0·5	10	1·5	270	70	2C1281, 3C317. Confused region.
44		16	01·0	0·5	−30	15	70	70	2C1352.
45		↑16	03·3	1	68·5	1	140	70	2C1383, 3C330.
46	↓	16	03·9	0·5	00	2	180	70	2C1359, 3C327.

Catalogue of Radio Sources—continued

No.	Right Ascension			Declination		Flux Density $\times 10^{-26}$ w.m.$^{-2}$ (c/s)$^{-1}$		Notes
	h	m	± (m)	°	± (°)		±	
47	16	26·1	0·5	37·5	1·5	225	70	16N4A, 2C1402, 3C338.
48	16	49·9	0·5	06	1	1570	160	16NoA, 2C1432, 3C348.
49	17	18·8	0·5	−01·5	2	660	70	2C1473, 3C353.
50	↓ 18	57·9	0·5	1·5	1	500	70	2C1607, 3C392. Diameter 2° × 3° at 38 Mc/s (7), so total flux density is much greater than quoted value.
51*	19	03·0	2	81	1	160	70	2C1591.
52	19	58·0	0·3	40° 35′		24600	3000	Cygnus A. 19N4A, 2C1673, 3C405. Position from Smith (8).
53	↓ 20	14·8	0·5	19·5	2·5	250	70	2C1686, 3C409. Confused with Cygnus A.
54	21	22·0	0·5	23	2	180	70	2C1775, 3C433.
55	↑ ↑ 21	56·0	0·5	27	2	90	70	2C1826, 3C441.
56*	22	13·8	0·5	−12·5	3	320	100	2C1843, 3C444.
57*	22	22·7	1	−06	4	80	70	3C446.
58	23	21·1	0·5	58° 32′·1		41500	4000	Cassiopeia A. 23N5A, 2C1890, 3C461. Position from Smith (8).
59*	23	35·8	0·5	26·6		240	70	2C1906, 3C465. Only observed on one strip, due to interference and side lobe of Cassiopeia A. Declination taken from 3C survey.

5. *The reliability of the Survey.*—Any radio star survey, made with a sufficiently sensitive receiver, will be affected by confusion. The effect is negligible for the most intense sources, but increases for the weaker ones. It is first noticeable as a small perturbation in position and amplitude of individual sources; ultimately the individuality of the weakest sources is entirely lost.

An estimate of the effects of confusion can be made by considering the distribution of amplitude on the records. Fig. 5 shows the observed distribution, where $p(s)\,ds$ is the probability that the record amplitude represents a flux density between s and $s+ds$. The median flux density of this distribution is

$$95 \times 10^{-26}\ \text{w.m.}^{-2}\,(\text{c/s})^{-1}.$$

Comparison of the 2C and 3C surveys (9) shows that individual sources can be reliably observed if their flux densities exceed the median by a factor of about 2·5; this suggests that the present survey is reliable down to about

$$250 \times 10^{-26}\ \text{w.m.}^{-2}\,(\text{c/s})^{-1}.$$

There are 26 sources above this level, of which only 4 are not confirmed by the 2C and 3C surveys†. Weaker sources are less reliable, but since the catalogue only includes sources which also appear in the 2C or 3C surveys, the majority are genuine; however, many weak sources are likely to have been missed, and the survey is not complete below 250×10^{-26} w.m.$^{-2}$ (c/s)$^{-1}$.

The record of each individual source is superimposed on the record due to all the other sources; this background has a random amplitude, whose distribution is given in Fig. 5, and random phase. Thus the probable error in the flux density of

† These figures are appropriate to the 136 stars observed, not the 59 in the catalogue.

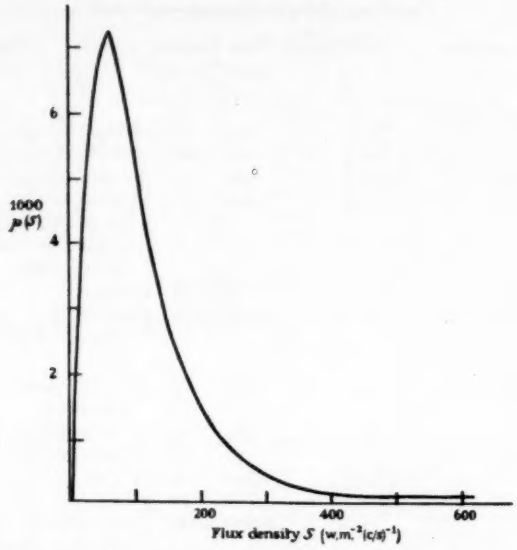

FIG. 5.—*The distribution of record amplitudes obtained from records of strips at 12° and 27° declination. The median amplitude of this distribution corresponds to a flux density of* 95×10^{-26} *w.m.*$^{-2}$ $(c/s)^{-1}$.

a source due to confusion is $1/\sqrt{(2)}$ times the median record amplitude, or about 70 w.m.$^{-2}$ $(c/s)^{-1}$. This is the major source of error for the weaker sources, and is included in the figure given in the catalogue.

This work forms part of a programme of research supported at the Cavendish Laboratory by the Department of Scientific and Industrial Research, to which I am indebted for a maintenance grant. I also have to thank Trinity College for a Coutts Trotter Studentship.

I wish to thank all my colleagues for their advice and assistance, particularly Professor Ryle who suggested this survey, and who, with Dr Scheuer, was responsible for the preliminary design of the aerial.

Mullard Radio Astronomy Observatory,
Cavendish Laboratory,
Cambridge:

1959 *November.*

References

(1) J. R. Shakeshaft, M. Ryle, J. E. Baldwin, B. Elsmore and J. H. Thomson, *Mem. R.A.S.*, **67**, 106, 1955.
(2) D. O. Edge, J. R. Shakeshaft, W. B. McAdam, J. E. Baldwin and S. Archer, *Mem. R.A.S.*, **68**, 37, 1959.
(3) G. R. Whitfield, *M.N.*, **117**, 680, 1957.
(4) M. Ryle, *Proc. Roy. Soc.* A, **211**, 351, 1952.
(5) J. L. Pawsey, *Ap. J.*, **121**, 1, 1955.
(6) J. E. Baldwin and D. W. Dewhirst, *Nature*, **173**, 164, 1954.
(7) J. H. Blythe, *M.N.*, **117**, 652, 1957.
(8) F. G. Smith, *Nature*, **168**, 555, 1951.
(9) D. O. Edge, P. A. G. Scheuer and J. R. Shakeshaft, *M.N.*, **118**, 183, 1958.

NOTICE TO AUTHORS

Presentation of Papers at Meeting

At some meetings of the Society the background and conclusions of selected papers are presented and then discussed. In order to assist the Secretaries in the selection of papers for such meetings, authors are asked to let the Society know, when submitting papers, whether they would be willing to give an account of their paper, if requested.

The attention of authors resident abroad is drawn to the fact that the Society welcomes information about their work. The Secretaries would be happy to consider having such work described at a meeting, in accordance with the author's wishes, either by a Secretary or other Fellow.

Publication of Papers

1. *General.*—It is the aim of the Society to be of the greatest possible service in disseminating astronomical results and ideas to the scientific community with the utmost possible speed. Contributors are accordingly urged to give the most careful consideration to the presentation of their work, for attention to detail will assuredly result in a substantial saving of time.

It is the practice of the Society to seek a referee's opinion on nearly every paper submitted for publication in *Monthly Notices*; experience has shown that frequently the comments of referees have enabled authors to improve the presentation of their work and so increase its scientific value.

2. *Communication.*—Papers must be communicated to the Society by a Fellow. They should be accompanied by a summary at the *beginning* of the paper conveying briefly the content of the paper, and drawing attention to important new information and to the main conclusions. The summary should be intelligible in itself, without reference to the paper, to a reader with some knowledge of the subject; it should not normally exceed 200 words in length. Authors are requested to submit MSS. in duplicate. These should be typed using double spacing and leaving a margin of not less than one inch on the left-hand side. Corrections to the MSS. should be made in the text and not in the margin. By Council decision, MSS. of accepted papers are retained by the Society for one year after publication; unless their return is then requested by the author they are destroyed.

3. *Presentation.*—Authors are allowed considerable latitude, but they are requested to follow the general style and arrangement of *Monthly Notices*. References to literature should be given either in the traditional form of a numbered list at the end of the paper, or as prescribed in *Notes on the Preparation of Papers to be Communicated to the Royal Society*.

4. *Notation.*—For technical astronomical terms, authors should conform closely to the recommendations of Commission 3 of the International Astronomical Union (*Trans. I.A.U.*; Vol. VI, p. 345, 1938). Council has decided to adopt the I.A.U. 3-letter abbreviations for constellations where contraction is desirable (Vol. IV, p. 221, 1932). In general matters, authors should follow the recommendations in *Symbols, Signs and Abbreviations* (London: Royal Society, 1951) except where these conflict with I.A.U. practice.

5. *Diagrams.*—These should be designed to appear upright on the page, drawn about twice the size required in print and prepared for direct photographic reproduction except for the lettering, which should be inserted in pencil. Legends should be given in the manuscript indicating where in the text the figure should appear. Blocks are retained by the Society for 10 years; unless the author requires them before the end of this period they are then destroyed. Enough copies or prints of the diagrams should accompany each manuscript.

6. *Tables.*—These should be arranged so that they can be printed upright on the page.

7. *Proofs.*—Authors are liable for costs of alteration exceeding 5 per cent of composition. It is therefore in their own and the Society's interests to seek the maximum conciseness and simplification of symbols and equations consistent with clarity.

CONTENTS

PAGE

R. d'E. Atkinson, The use of a pentag with a transit-circle 505

C. A. Murray, On the determination of Ephemeris Time: a correction 515

J. S. Mainstone, The calculation of meteor velocities from continuous-wave radio diffraction effects from trails 517

J. A. Högbom, The structure and magnetic field of the solar corona 530

Olin J. Eggen, Stellar groups, VII. The structure of the Hyades group ... 540

Olin J. Eggen, Stellar groups, VIII. The structure of the Sirius group ... 563

G. R. Whitfield, A survey of radio stars at a frequency of 38 Mc/s 581

Printed in London by Taylor & Francis, Ltd., 1960 July